Performance of GFRP Bars for Reinforced Concrete Beams Under Fatigue Loading

Islam Osama Mohamed Nabil Elsayed Nagy

A Thesis
In the Department of
Building, Civil, and Environmental Engineering

Presented in Partial Fulfillment of the Requirements for the
Degree of Doctor of Philosophy (Civil Engineering) at
Concordia University
Montréal, Québec,
Canada

May 2024

CONCORDIA UNIVERSITY

School of Graduate Studies

This is to certify that the thesis is prepared

By: Islam Osama Mohamed Nabil Elsayed Nagy

Entitled: Performance of GFRP Bars for Reinforced Concrete Beams Under Fatigue Loading

and submitted in partial fulfillment of the requirements for the degree of

Doctor of Philosophy (Civil Engineering)

complies with the regulations of the University and meets the accepted standards with respect to originality and quality.

Signed by the final examining committee:

_____ Chair
Dr. Carol Fung

_____ External examiner
Dr. Khaled Sennah

_____ External to program
Dr. Mehdi Hojjati

_____ Examiner
Dr. Ahmed Soliman

_____ Examiner
Dr. Anjan Bhowmick

_____ Thesis supervisor
Dr. Khaled Galal

Approved by _____
Dr. Chunjiang An, Graduate Program Director

_____
Dr. Mourad Debbabi, Dean
Gina Cody School of Engineering and Computer Science

Date of Defence: 2024-05-22

ABSTRACT

Performance of GFRP bars for reinforced concrete beams under fatigue loading

Islam Elsayed Nagy, Ph.D.

Concordia University, 2024

Structural components are susceptible to different types of loading, such as monotonic and cyclic loadings, etc. Fatigue loading is cyclic in nature and falls into two general categories: low-cyclic fatigue and high-cyclic fatigue. Glass fibre-reinforced polymer (GFRP) bars are suitable replacements for steel reinforcement rebars due to their corrosion-resistant characteristics. This characteristic warrants an extended service life for GFRP RC structures. The research investigates the fatigue performance of ribbed GFRP bars in concrete, which is crucial due to the growing use of GFRP as a substitute for traditional steel reinforcements. An experimental program was carefully planned to evaluate the fatigue life of ribbed GFRP bars within concrete beams, including factors such as concrete strength and the degrees of fatigue stress applied. An innovative displacement-controlled testing technique was devised to address the limitations of conventional force-controlled fatigue testing methods. The results demonstrate that ribbed GFRP bars may withstand up to 2 million cycles of fatigue stress, exceeding current code standards and questioning previous empirical data. This research also includes the fatigue characteristics of ribbed GFRP bars during tension-tension fatigue through a detailed review and innovative experiments. The experimental program included the fatigue, the fatigue life and the behaviour of ribbed GFRP bars, classifying them according to the testing protocol. Low-frequency fatigue testing is between 0.03 and 0.04 Hz, and fatigue tests are under higher frequency fatigue testing at 4 Hz. This research identified an optimal gripping mechanism for conducting fatigue tests on GFRP bars and evaluated the feasibility of using conventional universal testing machines for fatigue life assessment, commonly found in many structural laboratories. In addition, the impact of influential factors such as stress ratio is examined through a testing program. Finally, the study expands to present a simplified model based on the Sendeckyj model, but it utilizes a normal distribution to forecast the fatigue life of FRP-RC elements under repeated loading situations. This novel method is used to analyze fatigue data for GFRP, CFRP, and BFRP materials, allowing for the creation of S-N-P curves to be simplified with accurate estimations.

Dedications

To my beloved parents, Amani and Osama,

To my beloved and dear wife Noura,

To my lovely children, Abdelrahman and Laila

To my dear brother, Tarek

Acknowledgments

In the Name of Allah, the Most Compassionate, Most Merciful.

All gratitude and praises are to Allah the Most Gracious, with the blessings of Whom the good deeds are fulfilled.

I want to sincerely appreciate my supervisor, Professor Khaled Galal, for his significant effort in assisting and guiding me during my Ph.D. program. Dr. Khaled Galal consistently offers encouragement and vitality to help us achieve our goals in an intelligent and supportive manner. This research would not have been achievable without his ongoing advice, support, and constructive discussions. Being one of his graduate students was an honour. I want to express my gratitude to my committee members, Dr. Khaled Sennah, Dr. Mehdi Hojjati, Dr. Ahmed Soliman, and Dr. Anjan Bhowmick, for their meticulous evaluation of the thesis and their insightful and helpful feedback.

I want to express my gratitude to postdoctoral fellow Dr. Alireza Asadian for his valuable assistance, productive conversations, and invaluable guidance throughout my Ph.D. studies. This research would not have been possible without his continuous assistance and productive conversations. I want to express my sincere gratitude to my colleague AbdulElah Al-Ahdal. I also want to express my gratitude to my colleagues Mostafa Rabea, Omar Gouda, Omar Elmeligy, Abdelrahman Abdallah, Amgad Mahrous and Abdallah Montaser for their support and valuable assistance during the experimental phase.

Besides, I would like to thank the technical staff of the Structures Laboratory at Concordia University, Alexander McGilton and Alexis Gosselin, as well as the Engineer in Residence, Ricky Gioia, for their support, brainstorming, and innovative ideas during the experimental work. I want to express gratitude to the Research Associate of the Structures Laboratory at Sherbrooke University, Marc Demers, and the Structural Laboratories Manager, Olivier Gauron, for their assistance, testing, collaborative thinking, and creative concepts throughout the experimental process. I also want to thank Concordia's M.Eng. and undergraduate students for their help during the experimental work.

I am grateful to my parents, Amani and Osama, for consistently offering me support and being the driving force behind my accomplishment. I am extremely grateful for their efforts, motivation, and advice. I am deeply appreciative and thankful to my cherished life partner, my wife, Noura. I am immensely grateful to her for her unwavering support, motivation, advice, conversations, and patience. I am grateful to my little heroes, Abdelrahman and Laila, for giving me love. I am also grateful to my brother Tarek, who offered continuous support.

I also acknowledge the funding support from the Natural Sciences and Engineering Research Council of Canada (NSERC), MST Rebar Inc. and Concordia University.

Co-Authorship

This thesis has been prepared in accordance with the regulations of a sandwich (manuscript-based) thesis format. This research presents experimental and analytical carried out solely by Islam Elsayed Nagy. Advice and guidance were provided for the whole thesis by the academic supervisor, Dr. Khaled Galal, and Postdoctoral Fellow, Dr. Alireza Asadian. This thesis consists of the following chapters:

Chapter 3: Elsayed Nagy, I., Asadian, A., and Galal, K. (2024). Fatigue Life and Behaviour of GFRP Reinforced Concrete Beams. Engineering Structures Journal, Elsevier. Accepted, April 2024.

Chapter 4: Elsayed Nagy, I., Asadian, A., and Galal, K. (2024). Tension-Tension Fatigue Behavior of Ribbed Glass Fiber-Reinforced Polymer Bars in Air. Submitted to ASCE Journal of Composites for Construction. October 2023.

Chapter 5: Elsayed Nagy, I., Asadian, A., and Galal, K. (2024). Stress Ratio Effect on the Fatigue Behaviour of Ribbed Glass Fiber-Reinforced Polymer. To be Submitted to Engineering Structures Journal.

Chapter 6: Elsayed Nagy, I., Asadian, A., and Galal, K. (2024). Fitting Fatigue Life Data with a Normal Distribution Probabilistic Model. To be submitted to Engineering Structures Journal.

All authors reviewed the final manuscript and approved of the contents.

Table of Contents

List of Figures

List of Tables

CHAPTER 1

Introduction

1.1 General

The corrosion-resistant characteristics of glass fibre-reinforced polymer (GFRP) reinforcing bars make them a suitable alternative for steel reinforcements in structural applications subjected to harsh environmental conditions, such as bridges and parking garages. Despite many research studies on the performance of GFRP-reinforced concrete (RC) elements under static loading, there are only a few studies on the fatigue behaviour of FRP composite materials in concrete structures. Moreover, there is a scarcity of conclusive experimental data on the fatigue performance of GFRP RC flexural elements.

GFRP bars are composed of two main components, namely, resin and fibre. The main types of glass fibres are E-glass, S-glass and E-CR-glass. Resins fall into two general categories: thermosetting polymers, such as polyester, vinyl-esters and epoxies, and thermoplastic polymers (El-Ragaby 2007). In order to provide stress transfer between GFRP bars and concrete, GFRP bars are produced with different surface profiles, as shown in Fig. 1.1.

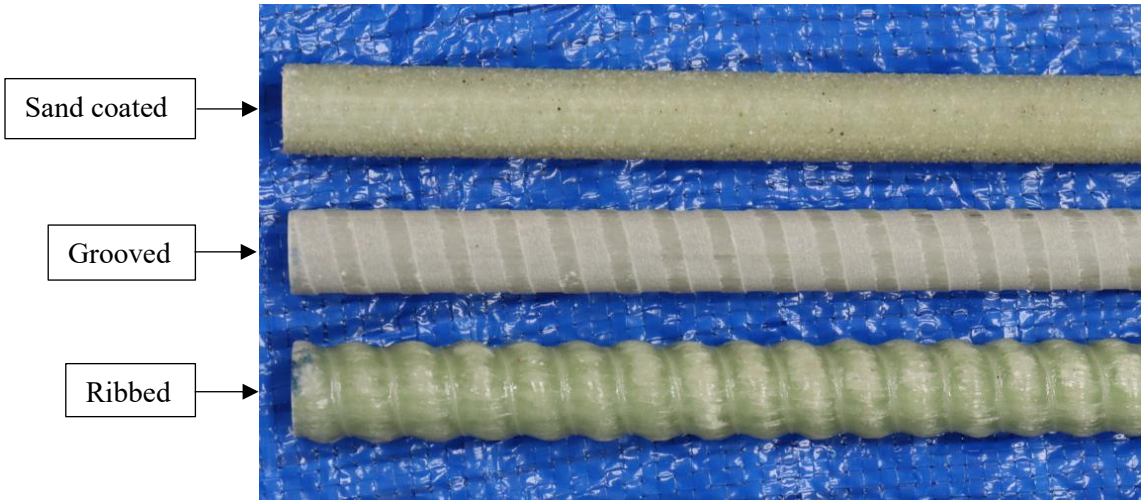

Fig. 1.1. Common types of GFRP bar surfaces

The fatigue of GFRP materials used for aerospace and marine applications has been investigated for many decades. However, the available knowledge does not apply to GFRP materials used in construction because of their inherent differences. These differences arise from

the fabrication process, fibre content, type of resin used, concrete elements and friction between the FRP rebar and the surrounding concrete.

Throughout its fatigue life, a GFRP bar goes through three main stages (Ramakrishnan and Jayaraman 1993; Wu and Yao 2010). In the first stage, the matrix starts cracking. In the second stage, one of two scenarios can occur: the initiated matrix cracks can propagate to matrix interfacial debonding, or the matrix cracks can lead to fibre breakage. Finally, in the third stage, the GFRP bar fails.

The performance of the GFRP bar under fatigue loading has been thoroughly investigated in RC slabs, where the stress developed in the GFRP bar was negligible. Accordingly, the bridge design codes and standards ignore the fatigue effect on GFRP reinforcement deck slabs (ACI 440.1R 2015a; CSA S6 2019). However, limited research has been conducted on other structural elements under fatigue loadings. The validity of the current empirical design equations and limits for fatigue design in the existing codes need to be evaluated. This requires an in-depth understanding of the behaviour of GFRP bars as internal reinforcement in concrete beams and as bars under high-cyclic fatigue loading.

The fatigue life performance of concrete beams reinforced with GFRP bar is considered different from the behaviour of bare bars tested under cyclic fatigue loading. Janus et al. (2021) concluded that the GFRP bar tested in concrete had a higher fatigue life than that tested in the air because the concrete prevented the premature failure of the rebar with no damaged core. On the other hand, Noël and Soudki (2014) concluded that the presence of concrete reduces the fatigue life of rebar. Thus, it is essential to investigate the fatigue behaviour of GFRP, especially as a reinforcement for concrete beams.

The literature survey also showed inconsistent S–N curves drawn previously (Noël and Soudki 2014a; Janus et al. 2019, 2021). Additionally, under the same stress ranges, there is more than an entire order of magnitude difference in the fatigue life from the results of one study to another. This is important because there is a need to propose more accurate and representative fatigue stress limits for GFRP bars to be implemented in the relevant design codes and guidelines. Several important factors that directly affect the fatigue life of GFRP bars have not yet been investigated,

such as the effect of the stress level, range, ratio, loading rate, surface type, and diameter of GFRP bars. Furthermore, a limited number of studies have shown the flexural cracking behaviour, mode of failure, and deflections of concrete beams reinforced with GFRP as flexural reinforcement under static and fatigue loading.

1.2 Problem statement

The last few decades have witnessed many applications of GFRP bars as internal reinforcement in concrete structures, including buildings and bridges. There are several North American codes and standards for the design of GFRP-reinforced concrete (RC) structures: (AASHTO LRFD for GFRP 2018; CSA S6 2019; CSA S806 2021; ACI 440.11 2022). There is a wealth of research on the behaviour of GFRP-RC flexural elements (beams and girders) subjected to static loading. However, there are very few experimental tests on the behaviour of GFRP-RC flexural elements under fatigue loading, which arises from repeated loads, e.g., bridges.

There are very limited studies on the fatigue behaviour of GFRP composite materials in concrete structures. The available literature shows contradictory experimental data and conclusions on the effect of concrete on GFRP bar. Moreover, research is needed to propose fatigue life models for GFRP RC elements. Additionally, a simple probabilistic procedure to analyze fatigue data is important. All probabilistic models are either not representative or hard to apply. Testing high-cyclic rebars are time- and money-consuming, so a low-cyclic fatigue test technique is proposed as an alternative. In addition, experimental results of GFRP-reinforced beams should be obtained and analyzed to form more representative code limits.

1.3 Research Objectives and Scope of Work:

This research aims to:

- Propose a simple fatigue probabilistic model capable of describing the fatigue life at various reliability levels.
- To test GFRP bars under low-cycle fatigue loading, with the objective to interpolate the fatigue life of high-cycle fatigue.

- Test high-cycle fatigue bars to evaluate the fatigue life of GFRP, identify the effect of stress ratio on the fatigue life and identify the fatigue limit.
- Test GFRP reinforced concrete beams to quantify the fatigue life of GFRP as concrete reinforcement.

To achieve the main objectives, the research scope of work includes the following:

- Identify the effect of different parameters on the fatigue life of the GFRP bars. By studying the literature comprehensively and comparing steel reinforcement and GFRP bars, the effect of main parameters can be shown, such as stress ratio, testing frequency, bar surface type, and concrete elements on the GFRP.

- Propose a simple probabilistic fatigue model to describe the fatigue data of the GFRP bars. The available fatigue models are accurate but complicated, which shows the need for easy and accurate models.

- Perform low-cycle fatigue tests on GFRP bars and correlate the results with high-cycle fatigue tests. Low-cycle fatigue tests subject the bars to higher stresses and can be conducted using a typical universal testing machine available in most laboratories. The objective is to offer a more accessible and cost-effective method for predicting the fatigue life of the bars, reducing the need for extensive high-cycle fatigue testing.

- Conduct high-cycle fatigue tests on GFRP bars. There is a lack of high-cycle fatigue tests, which are crucial for identifying the S-N curve and establishing code limits. These tests will also enhance understanding of the impact of different parameters, such as stress ratio and testing frequency.

- Test concrete beams reinforced with GFRP bars. These tests ensure that GFRP bars can sustain the fatigue life obtained from high-cycle fatigue tests on bare bars. Concerns arise regarding the interaction between GFRP bars and concrete, questioning whether GFRP bars can endure the expected fatigue life in concrete elements. Testing GFRP in reinforced concrete elements is essential to ensure its endurance under fatigue loads.

1.4 Thesis layout

This thesis comprises seven chapters analyzing and discussing the results of the experimental tests and analytical research work. The contents of the chapters and the appendices are as follows:

- Chapter 1 presents the introduction, motivation, research significance, research objectives and scope of work, and a brief description of the thesis layout.

- Chapter 2 provides the literature review of the available research work on the fatigue behaviour of concrete beams reinforced with GFRP bars and GFRP bars. The chapter reviews the fatigue of GFRP bars and the affecting parameters. It also reviews the available codes, guidelines, and testing protocols.

- Chapter 3 provides experimental results of the fatigue life of ribbed GFRP bars that are embedded in concrete beams. It does so by conducting a study program that considers aspects such as the strength of the concrete and the maximum applied fatigue stress. Furthermore, it presents a testing technique that employs a displacement-controlled system for conducting fatigue testing. This protocol effectively solves many problems related to force-controlled fatigue testing. In addition, the research examines the cracking behaviour, deflection, and slippage, offering valuable insights into the interaction between GFRP bars and concrete when subjected to fatigue loading.

- Chapter 4 presents the findings of prior research conducted at a frequency of 4 Hz while also exploring lower-frequency testing. Three adhesives were examined to determine the most effective gripping system capable of enduring fatigue loading.

- Chapter 5 investigates the effect of the stress ratio on the fatigue life of the ribbed GFRP bars. This chapter conducted tension-tension fatigue tests on ribbed GFRP bars at three different stress ratio values in order to assess their fatigue life.

- Chapter 6 introduces a more straightforward model by substituting the Weibull distribution with a normal distribution in the Sendeckyj model. The Sendeckyj model utilizes a normal distribution to analyze the fatigue data of GFRP, CFRP, and BFRP materials found in the existing literature. The obtained S-N-P curves are compared with the Sendeckyj model to validate the technique.

- Chapter 7 provides a summary of the conducted research work, the main conclusions drawn from this study, and the recommendations for future work.

- Appendix A provides additional figures on the experimental research work presented in Chapters 3,4 and 5 of the thesis. These additional figures cover some construction procedures and failure modes of the tested specimens.

It is important to note that there may be some overlap in the information. The information can be found in the introduction and background of each chapter, as well as the experimental test setup, design of specimens, testing instrumentations, and loading protocols. This is a result of the characteristics of the paper-based thesis format.

CHAPTER 2

Literature Survey

2.1 Types of test

Several types of tests have been performed to estimate the fatigue life of reinforcing bars. The following sections summarize three main types of tests, namely, axial tension in the air, axial tension in the concrete, and bending tests on beams, and discuss their effect on the test results.

2.1.1 Axial tension in the air

The axial tension-tension fatigue test is the primary test performed to obtain the properties of any material under fatigue loads. Compared to other fatigue tests, axial tension-tension fatigue tests are easier to perform and less expensive. Additionally, the test can be performed at a high frequency, reducing the time required for testing. The main challenge in performing such a test is gripping the GFRP bars. Many trials have been performed by researchers to find a gripping system to avoid premature failure of the bars in undesirable sections, close to the grip locations, due to high-stress concentration.

El Refai (2013) tested 4 GFRP bars under fatigue. The minimum stress was kept at 30% of the ultimate tensile strength (UTS), while the maximum stress of the test changed between 34 and 43%. All the failure modes were broom-shaped and occurred at the anchor zone, so the data collected from El Refai (2013) was not used for the comparison because this is considered a premature failure. Noël and Soudki (2014a) tested 15 sand-coated bare bars with a diameter of 16 mm under uniaxial fatigue tension. Three specimens were tested statically, and the remaining specimens were tested under fatigue loads until failure. In the fatigue tests, the maximum stress was between 255 and 355 MPa (32.5% and 45.3%), while the minimum stress was kept constant at 30 MPa (3.8%). To ensure a failure in the desired section, the cross-section of the bars was gradually reduced by approximately 43%. Janus et al. (2019) tested eighteen bare sand-coated GFRP bars. The testing frequency was 4 Hz. The maximum stress of the tests was 40, 50 and 60% of the ultimate stress of the bars. Based on the S–N diagram drawn by Janus et al. (2019), the bars tested in the air would not reach two million cycles. D'Antino et al. (2022) tested a bare sand-coated GFRP bar under a 10 Hz loading frequency. The tested maximum stress was 19.7% of the UTS, and the stress ratio was 0.1. The test was stopped after 5.1 million cycles with no apparent

failure to the bar. It is noteworthy that all tested bars are sand-coated. Only D'Antino et al. (2022) added a carbon fibre bundle helically wrapped around the cross-section of the sand-coated bar. The fatigue life of the axial fatigue tests is drawn on the S–N curve in Fig. 2.1.

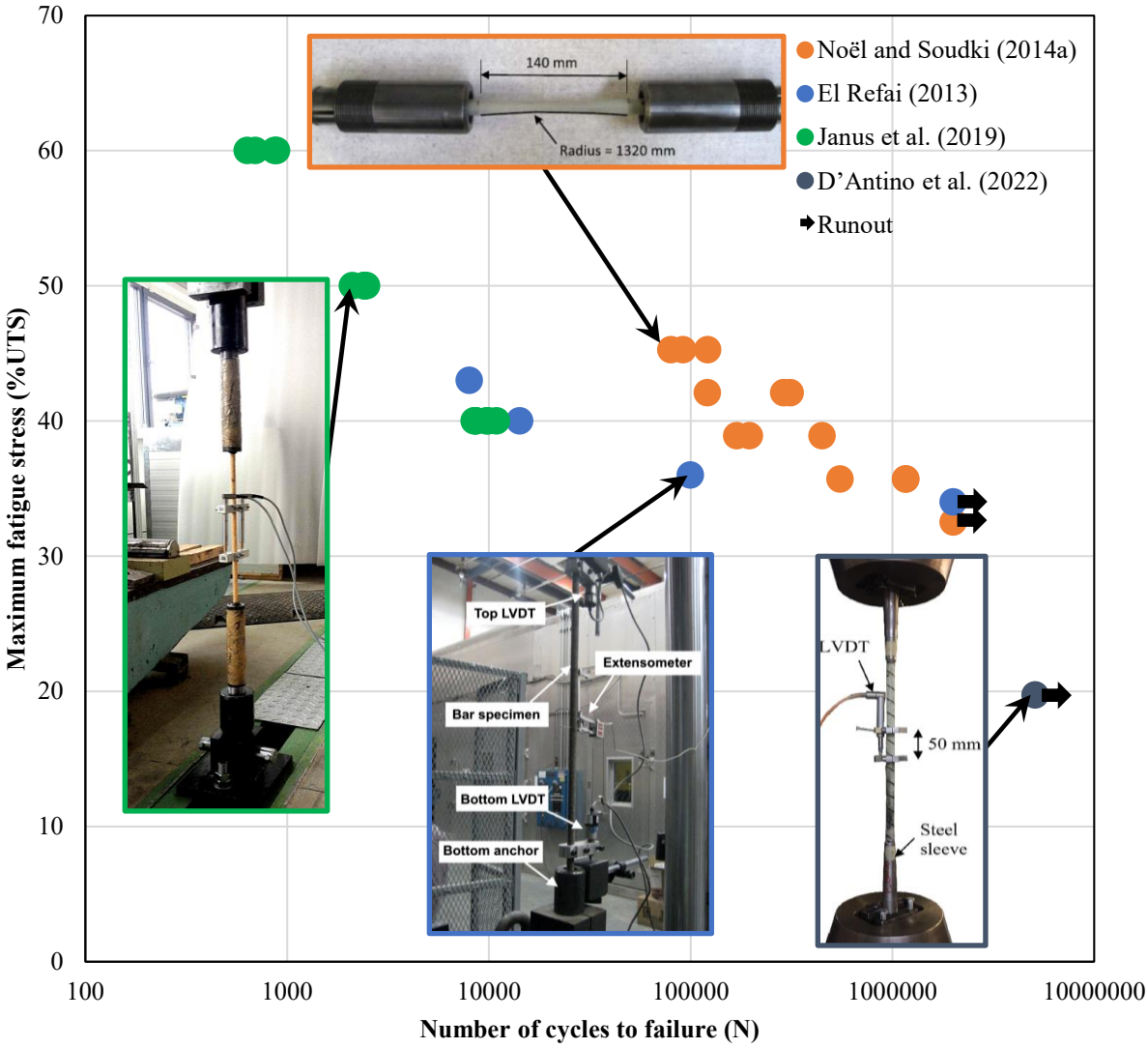

Fig. 2.1. S-N curve of GFRP bars tested in the air with photographs of the specimens

In Fig. 2.1, the maximum fatigue stress, as a percentage of the ultimate tensile strength (UTS), is drawn on the vertical axis, and the number of cycles to failure is drawn on the logarithmic scale on the horizontal axis. As shown in Fig. 2.1, the life data are scattered, and there is a large difference between the fatigue life tested at the same maximum stress level. For example, at the maximum fatigue stress of 0.4 of the UTS, the fatigue life of the tests done by Janus et al. (2019) is approximately ten thousand cycles, while at the same stress, the fatigue life based on the experimental results of Noël and Soudki (2014a) is approximately two-hundred thousand cycles. It is also evident that the tests conducted by Noël and Soudki (2014a) have longer fatigue life compared to the tests done by Janus et al. (2019). Given that all the GFRP bars tested had the same sand-coated surface profile, the higher fatigue life of specimens tested by Noël and Soudki (2014a) might be due to the grinding done in the middle section of their specimens to avoid premature failure section at the grip location. By grinding the surface of the GFRP bar, only the core is left, which normally consists of more fibre content (Noël and Soudki 2014a). Moreover, grinding the surface can remove the microcracks due to the sand-coating process.

2.1.2 Axial tension-tension in concrete

In the axial tension-tension fatigue tests in concrete, the GFRP bar is under tension-tension fatigue while embedded inside the concrete as a reinforcement. There are two types of such a test method performed in the literature: (a) testing a GFRP bar inside a concrete prism and (b) beam-hinge bending tests where GFRP bars are on the tension side.

The concrete prism test reinforced with GFRP bars was first performed by Adimi et al. (1997) to study the fatigue life of GFRP bars. They tested 13 sand-coated GFRP bars encased with concrete blocks. The tests had the same stress ratio of 0.1, and the stress range varied between 21.7% and 81.1% of the ultimate tensile strength. The loading frequency was set to 4 Hz. Using the results, two S–N curves were proposed. The first S–N curve was the relation between the maximum fatigue stress and the number of failure cycles. The second curve showed the ratio of the maximum fatigue stress to the ultimate tensile strength on the vertical axis and the number of cycles until fatigue failure on the other axis. Additionally, nine specimens were tested to study the effect of the concrete salinity level on fatigue life. It was concluded that the salinity level has a negligible effect on fatigue life.

Noël and Soudki (2014a) tested 15 sand-coated GFRP bars embedded in a beam-hinge bending test. Three beams were tested monotonically, and the remaining specimens were tested under fatigue loads until failure. The beam-hinge specimens were reinforced with one 16 mm sand-coated GFRP bar. The beam-hinge fatigue test stress ranged between 20 and 55% of the average ultimate strength of the GFRP bars, while the minimum stress was constant at 30 MPa. The results showed that the fatigue life of the rebars tested under uniaxial tension is longer than that of the beam-hinge test by an entire order of magnitude. A fatigue stress factor was introduced to account for the abrasion between the reinforcing rebar and the concrete. Janus et al. (2019) performed an experimental study by testing twelve sand-coated GFRP bars embedded in concrete under fatigue loading at a frequency of 4 Hz. They observed some degradation to the surface of the rebars due to friction with the concrete. The maximum stress was 40, 50 and 60% of the ultimate stress of the rebars. Janus et al. (2019) concluded that rebars encased in concrete have better fatigue than those tested in air. The rebars tested in concrete can reach two million cycles of fatigue life at approximately 17.5% maximum ultimate stress.

2.1.3 Bending tests on beams

Fatigue bending tests in concrete beams reinforced with steel reinforcement showed slightly longer life than those tested in air (Tilly 1979). Bending tests have a longer life with steel reinforcement because the maximum stressed areas of the rebars are usually limited to the crack locations, which reduces the probability of having a defect of the rebar at the location of the cracks.

Janus et al. (2021) studied the performance and behaviour of GFRP bars as the primary reinforcement in concrete beams. Five GFRP RC beams were tested under monotonic and fatigue loading. The beams were reinforced with one sand-coated GFRP bar with a 10 mm diameter. One beam was tested monotonically and failed due to concrete compression. The first fatigue-tested beam was tested under constant amplitude to reach maximum stress in the GFRP bar at 20% of its UTS; the stress ratio was 0.1. The fatigue test was performed under a frequency of 2 Hz and reached two million cycles. Consequently, the beam was tested monotonically to identify the residual strength. The other three specimens were tested under fatigue loading for 50,000 cycles with maximum stress in the rebar equal to 20% of the ultimate tensile strength. After that, the load was increased with steps of 5% of the ultimate strength; each load level was cycled 50,000 cycles until failure. Two specimens failed when the load reached 40% of the ultimate strength; one survived until 2800 and cycled under 45% of the ultimate tensile strength. Miner's rule (Miner

1945) was then used to estimate the accumulated failure of the beams. The tested samples showed that GFRP could survive more than two million cycles with a maximum stress of 20% of the UTS without a noticeable reduction in static strength.

Only one beam tested under a constant stress level by Janus et al. (2021) was considered in the analysis. The results of three beams tested under different loading levels were not considered here due to the different nature of the test and analysis. Similar to tested specimens in air, all rebars tested in concrete are sand-coated rebars. Fig. 2.2 presents the S–N curve of the experimental results along with a representative test setup. Comparing Fig. 2.1 and Fig. 2.2, it is evident that the variation of data in tests performed on the GFRP bars in concrete is less than the tests of bare bars.

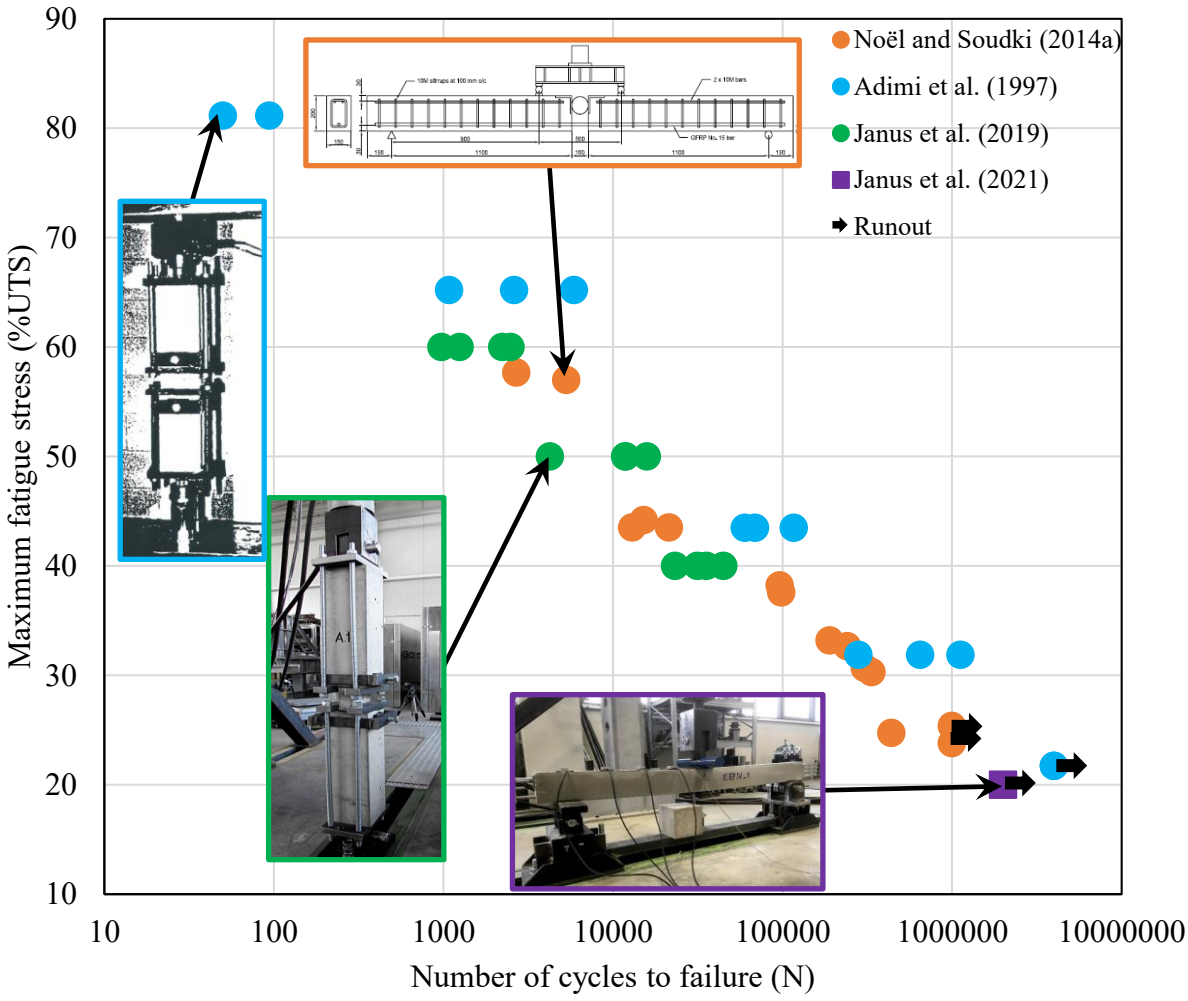

Fig. 2.2. S–N curve of GFRP bars tested inside concrete with depicted photos of the test setups.

Janus and Noël are the only studies where both GFRP tests were conducted for bare bars and rebars embedded in concrete. Their results are presented in Fig. 2.3. There is a contradiction between the results presented by Noël and Soudki (2014a) and Janus et al. (2019).

The small dimensions of the beams require very accurate instrumentation; any small changes in the load can cause considerable errors. Additionally, construction errors will cause a significant difference between the actual and designed specimens. The fatigue load of the first fatigue beam was consistent with 4 kN and deformations of approximately 2 mm, which represents small values of loads and deformations compared to the actual loads and deformation subjected to the structures. Last, the fixed support used to maintain the beam position causes negative moments at the support, which makes the estimation of the maximum stress on the rebar difficult. Janus et al. (2019) concluded that the fatigue life in concrete is longer than in the air.

Noël and Soudki (2014a) concluded that bare bars have a longer fatigue life than those tested in concrete. In the beam-hinge bending test, the rotation in the beam resulted in a stress gradient on the rebar that might increase the stress. On the other hand, the bare bars tested were ground to ensure the failure occurred in the desired section, which had a higher fibre ratio in the core. Noël and Soudki (2014a) explained that the longer fatigue life in bars tested in the air was due to the bond and friction caused by concrete. The friction shortened the fatigue life of the GFRP bars, as mentioned before.

Considering both Fig. 2.1 and Fig. 2.3, it is reasonable to conclude that the life of the bars tested by Noël and Soudki (2014a) might need modification due to grinding the bars. Noël and Soudki (2014a) calibrated a modification factor such that the results of the beam-hinge test could match the results of the bare bars. Studying all the results tested by other researchers, it appears that this modification factor might not be accurate, and another or no modification should have been used.

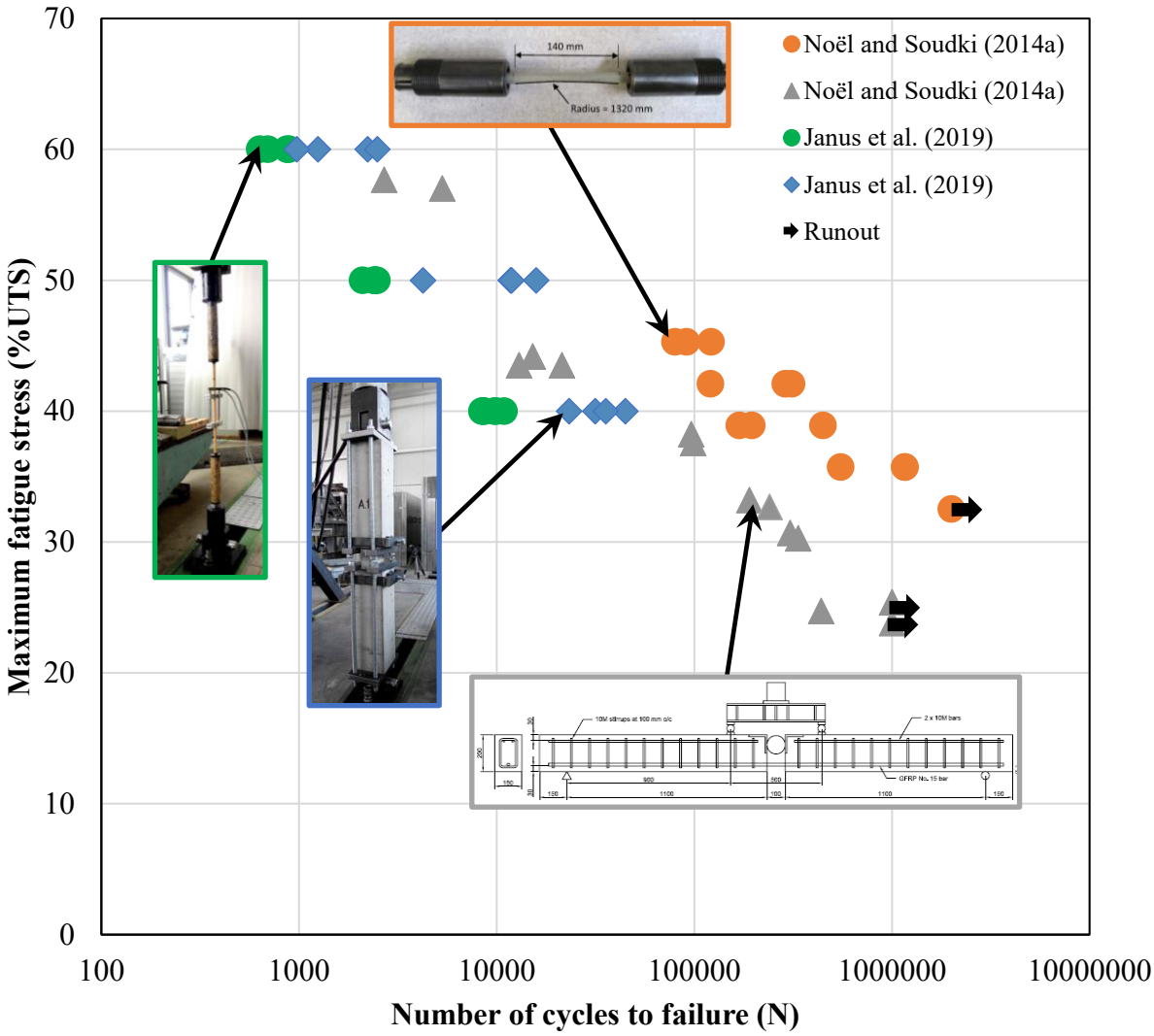

Fig. 2.3. Results of Noël and Soudki (2014a), and Janus et al. (2019).

2.2 Fatigue in the design codes, guidelines and standards for GFRP RC elements

2.2.1 Limits of GFRP bars subjected to considerable fatigue stresses

CSA S807-10 (CSA 2010), specification for fibre-reinforced polymers, limits the fatigue strength at 2 million cycles to a minimum of 35% of the ultimate tensile strength of the GFRP bar where fatigue application is considered. The recent version of CSA S807-19 (CSA 2019) imposes the same stress limit for 1 million cycles instead of 2 million.

Several design codes, guidelines and standards addressing FRP rebars as a primary reinforcement for structural concrete have been published (AASHTO LRFD for GFRP 2018; CSA S6 2019; CSA S806 2021; ACI 440.11 2022). The fatigue design provisions incorporated in these documents are still not based on enough experimental or field results.

CSA S6-19 (CSA 2019) stated that the maximum fatigue stress in the GFRP bars calculated from the fatigue limit state combinations shall not exceed 25% of the ultimate tensile strength. This is applied in any structural element reinforced with GFRP, such as slabs and beams. However, unlike beams, fatigue might not cause problems on deck slabs due to the arching effect (CSA S6 2019). However, the shear behaviour of slabs reinforced with GFRP is still under investigation (Noël and Soudki 2014b).

AASHTO LRFD Bridge Design Guide Specifications for GFRP-reinforced concrete (AASHTO 2018) specified that fatigue should not be investigated on GFRP-reinforced bridge decks. On the other hand, for any other structural element reinforced with GFRP bars, the code used a reduction factor of 0.25 to the design tensile strength of GFRP reinforcing rebars. The fatigue reduction factor can be increased if the manufacturer provides a report following (ASTM D3479/D3479M 2012).

ACI 440.1R-15 (ACI 2015b) mentioned that E-glass and S-glass fibres are not susceptible to fatigue failure; however, delayed rupture occurs due to stress concentration induced by crack propagation of the surface flaws. Based on the previous fatigue-tested GFRP results, a loss of 10% of the static tensile strength is observed with each decade of a logarithmic lifetime, compared to approximately 5 to 6% in CFRP. ACI 440.1R-15 (ACI 2015b) limited the fatigue stress to 20% of the design tensile strength, the same as the creep rupture stress limit. The fatigue stress limit was not mentioned in ACI 440.11-22 (ACI 2022), but the creep rupture stress limit was increased to 30% of the design tensile strength.

2.2.2 Discussion of the stress ratio and stress range

The stress ratio is defined as the ratio between the minimum and maximum fatigue stresses. The stress range is a widely used factor that is defined as the difference between the maximum and minimum stresses.

CSA S806-21 (CSA 2021) specified the testing method and calculations required to investigate the fatigue life of FRP bars and draw the S–N curve. Two loading protocols are described in CSA S806-21 (CSA 2021) for performing the fatigue test: fixing the average load and varying the load range or fixing the minimum load and varying the maximum load. Notably, by adopting either of the two testing protocols, there will be two variables during testing: maximum load and load ratio. The code allowed the stress ratio to be different from the 0.1 stress ratio typically adopted in FRP fatigue tests; dead and design loads can be used in the tests.

ACI 440.3R-12 (ACI 2012) specifies that the fatigue test should be load-controlled by applying a constant load amplitude or constant stress amplitude. Three loading protocols are defined to perform the fatigue test. The test can be conducted using the same load protocols used in CSA S806-21 (CSA 2021), or it can be conducted by changing the maximum and minimum loads with a fixed load ratio set to 0.1. In addition, AASHTO LRFD for GFRP (2018) referenced ASTM D3479/D3479M (2012) for the fatigue testing of tension-tension polymer matrix composite materials. ASTM D3479/D3479M (2012) specifies two procedures in which the fatigue test cycles between minimum and maximum stress or strain. However, no specific testing protocols are specified. Additionally, CSA S6-19 (CSA 2019) has no testing protocol mentioned.

In both CSA S6-17 (CSA 2017) and CSA S6-19 (CSA 2019), the fatigue stress limit on the steel rebars is a function of the stress range, not the maximum fatigue stress, while the stress limits for FRP are only a percentage of the ultimate tensile strength of the rebar. The 2014 edition of CSA S6-14 (CSA 2014) limits the stress range in the steel reinforcement rebars to 125 MPa, regardless of the maximum and minimum values of fatigue stress. In the 2019 edition of CSA S6-19 (CSA 2019), the stress range is a function of the minimum fatigue stress as a variable; the new stress range is as shown in Eq. (2.1).

$$Stress\ range = 165 - 138(\frac{f_{sf}}{f_y}) \quad (2.1)$$

where f_{sf} is the minimum fatigue stress calculated from the fatigue limit state combinations in MPa, and f_y is the yield stress of the reinforcement rebar in MPa. The relation between the stress ratio, range and maximum allowed fatigue stress is shown in Fig. 2.4 and Fig. 2.5.

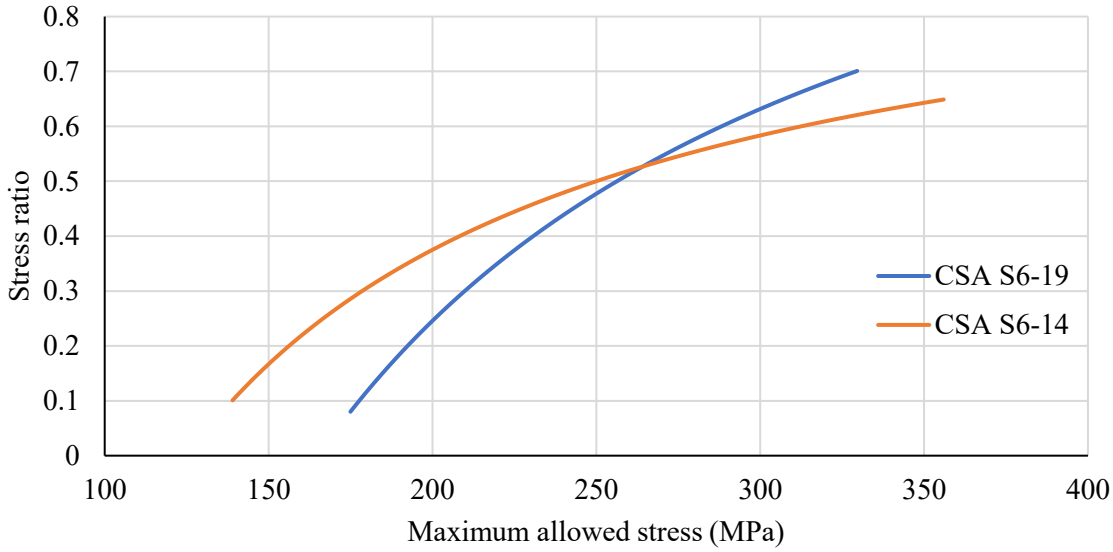

Fig. 2.4. Relationship between the stress ratio and maximum allowed fatigue stress.

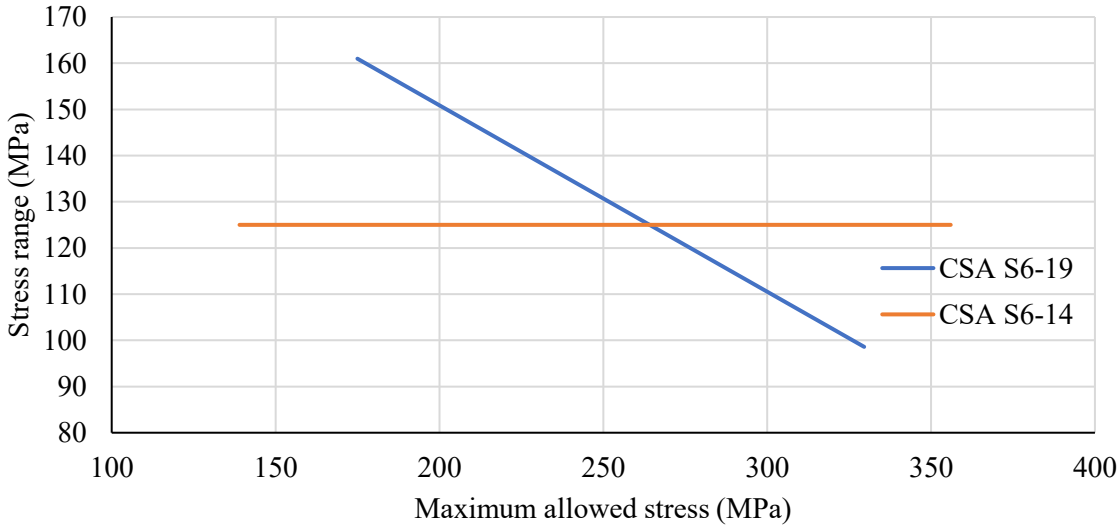

Fig. 2.5. Relationship between stress range and maximum allowed fatigue stress.

As shown in Fig. 2.4, and Fig. 2.5, the stress ratio and stress range affect the allowed maximum fatigue stress acting on the steel rebar. As shown in Fig. 2.4, if the stress ratio is considered, the

maximum allowed fatigue stress increases by increasing the stress ratio. Moreover, the maximum allowed fatigue stress increases by decreasing the stress range, as shown in Fig. 2.5.

AASHTO LRFD (2020) permitted a constant fatigue amplitude for straight reinforcement as per Eq. (2.2).

$$(\Delta F)_{TH} = 180 - 150(\frac{f_{min}}{f_y}) \quad (2.2)$$

where $(\Delta F)_{TH}$ is the constant-amplitude fatigue threshold in MPa, f_{min} is the minimum live load fatigue stress along with the unfactored permanent load stresses in MPa; and f_y is the yield stress of the reinforcement rebar in MPa. The f_y in Eq. 2.2. Is limited between 410 and 690 MPa.

The moment ratio of 56 bridges reported by Kim et al. (2022) is used to verify the calculated data in this study. The data on the 56 bridges were originally calculated and reported by Nowak (1999). Those data were then modified by Kim et al. (2022) to accommodate the effect of dynamic load allowance. Stress in the rebars is calculated directly from the moment, so the ratio can be assumed to be equal. The minimum and maximum stress ratios from Kim et al. (2022) are drawn in Fig. 2.6.

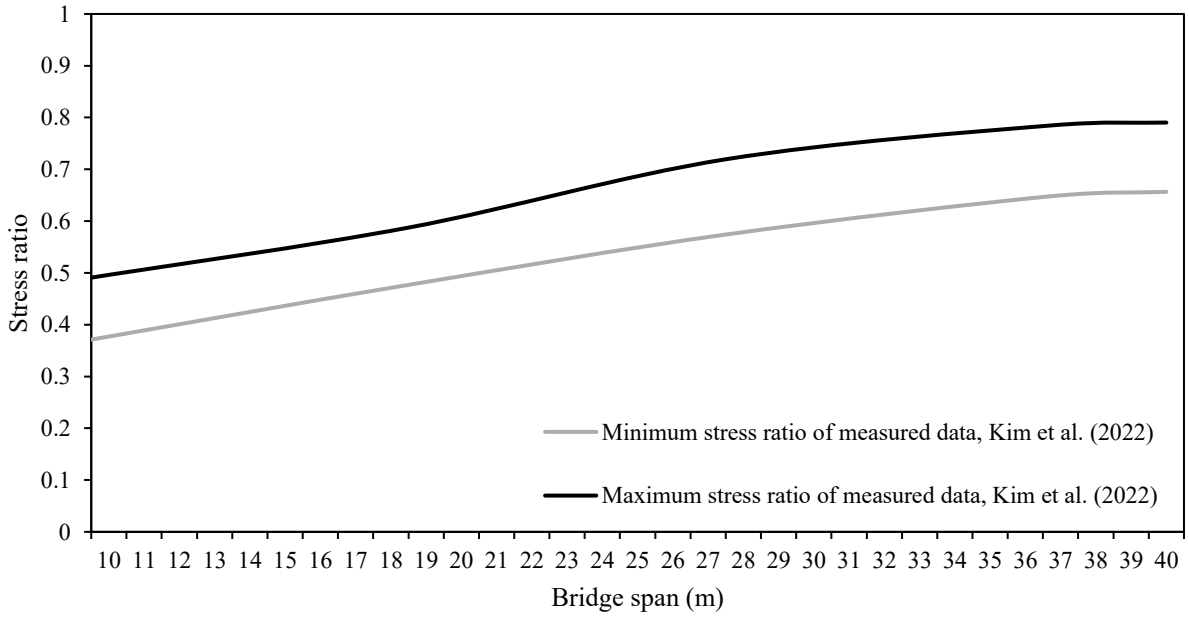

Fig. 2.6. Relation between the stress ratio and bridge span.

As shown in Fig. 2.6, there is excellent agreement between the results calculated in this study and the stress ratios reported by Kim et al. (2022). Additionally, the stress ratio in both calculations is always greater than 0.1 and, in most cases, more than 0.4. These values of the stress ratio can

pinpoint the need for performing fatigue tests with the stress ratio as a variable instead of assuming the worst-case scenario, which is 0.1. On the other hand, the allowable maximum fatigue stress can be an equation as a function of the stress ratio.

2.2.3 Discussion on testing frequency

Fatigue tests are commonly performed with high frequency due to the long duration of the tests. Adimi et al. (2000) tested CFRP rebars inside a concrete elements. The effect of frequency was thoroughly tested. Fourteen CFRP rebars were tested at room temperature with a stress range of 5% to 45% of the ultimate tensile strength. The minimum fatigue life tested at 8 Hz frequency is 3862 cycles, while the specimens survived 400 thousand cycles at a frequency of 0.5 Hz.

The testing frequency is an influential parameter. In the codes, the frequency ranges between 1 and 10 Hz for bars tested in the air. In CSA S806-21 (CSA 2021), the testing frequency can be between 1 and 10 Hz, and closer to 4 Hz is recommended. The test can be discontinued after 4 million cycles. In ACI 440.3R-12 (ACI 2012), the number of cycles until fatigue failure occurs should range between 1000 and 2 million cycles. ACI 440.3R-12 (ACI 2012) used the same values as CSA S806-21 (CSA 2021) for the loading frequency, but the test may stop after 2 million cycles. The effect of frequency in testing GFRP bars tested in the air or if used as reinforcement in concrete.

For plain concrete, ACI PRC-215-21 (ACI 2021) stated that the frequency of fatigue tests has a minimal effect when tested between 1 and 15 Hz. On the other hand, the tests performed with a frequency of 1/16 Hz have one order of magnitude lower fatigue life compared to tests performed under 4 Hz.

2.3 S–N curve

S–N curves are drawn to represent the fatigue life of any material. S represents the maximum stress, stress range, or stress amplitude (or strain), and N represents the number of fatigue cycles to failure. When considering the probabilistic models when drawing the S–N curves, the resulting curves can be referred to as S–N–P.

2.3.1 Fatigue models

The relationship between stress (S) or strain (ε) and the number of fatigue cycles to failure is referred to as the S–N curve. This can be a linear equation, as in ASTM E739 (2015). The equations mentioned in the ASTM standards are shown in Eq. 2.3 and Eq. 2.4.

$$\log N = A + B(S) \quad (2.3)$$

$$\log N = A + B \log(S) \quad (2.4)$$

In Eq. 2.3 and Eq. 2.4, the stress (S) can also be replaced by the strain (ε), and A and B are constants calibrated based on the tested data. Noël (2019) described the difference between the power law function (Eq. 2.5) and the logarithmic equation (Eq. 2.6) and stated that the power law function could be flattened to catch the low cyclic fatigue range.

$$S = A\, ln(N) + B \quad (2.5)$$

$$S = A\, N^{B} \quad (2.6)$$

CSA S806-21 (CSA 2021) specified that the S–N curve should be drawn between an arithmetic scale of maximum stress, stress range, or stress amplitude and a logarithmic scale of the number of cycles until failure. The fatigue strength shall be identified from the S–N curve at 2 million cycles. ACI 440.3R-12 (ACI 2012) referenced ASTM E739 (2015) for the S–N curve. ASTM E739 (2015) draws the S–N curve between the number of cycles until failure on a logarithmic scale. The maximum amplitude of stress or strain applied on the specimen under a specific stress range, or the S–N equation, can be developed between N and the stress or load range under a specific mean stress. The equation can be drawn with any appropriate controlled parameters. The 95% reliability bands are then used on the fatigue life data to better estimate the fatigue life. Finally, the fatigue strength is similar to that of CSA S806-21 (CSA 2021) and can be determined at 2 million cycles.

2.3.2 Probabilistic models for the GFRP fatigue life data

In composites, there is a large scatter in fatigue life data, which might be caused by factors such as fibre content variation and defects. This scatter was reported to be more than one order of magnitude (Noël 2019). Due to the large scatter in the fatigue life data, many equations have been developed to describe the fatigue life considering the statistical distribution. For example, the initial crack propagating to failure will vary between bars and batches.

This section presents and applies probabilistic models to the available literature data. First, Noël (2018 and 2019) applied the equations that Sendeckyj (1981) proposed to many fatigue life data. The S–N curve can be derived using Eq. (2.7) and Eq. (2.8) for any reliability level.

$$\sigma_a = \beta\{-\ln\big(P(N)\big)^{\frac{1}{\alpha}}\}[(N-A)C]^{-D} \quad (2.7)$$

$$A = -\frac{1-C}{\mathrm{C}} \quad (2.8)$$

where σ_a represents the applied stress, N is the number of cycles until failure, and P(N) is the probability of survival after N cycles. C and D are calibrated coefficients. α and β are Weibull distribution calibrated coefficients. The author calibrated this model using the experimental data available in a previous study by Noël and Soudki (2014a). The calibration coefficients C and D and Weibull distribution coefficients α and β were calculated through an iterative process. Then, the S–N curve is drawn.

The Sendeckyj method of fitting the Weibull distribution (Sendeckyj 1981) is used in this study to calibrate the fatigue data available in the literature. To represent all data in one graph, the maximum fatigue stress as a percentage of the ultimate tensile strength is used. Using the maximum likelihood technique, the model coefficients are calibrated. The coefficients α, β, C and D are 12.66, 96.92, 1 and 0.0725, respectively. The 95% reliability bands are then drawn in Fig. 2.7, for the GFRP bars tested in the air.

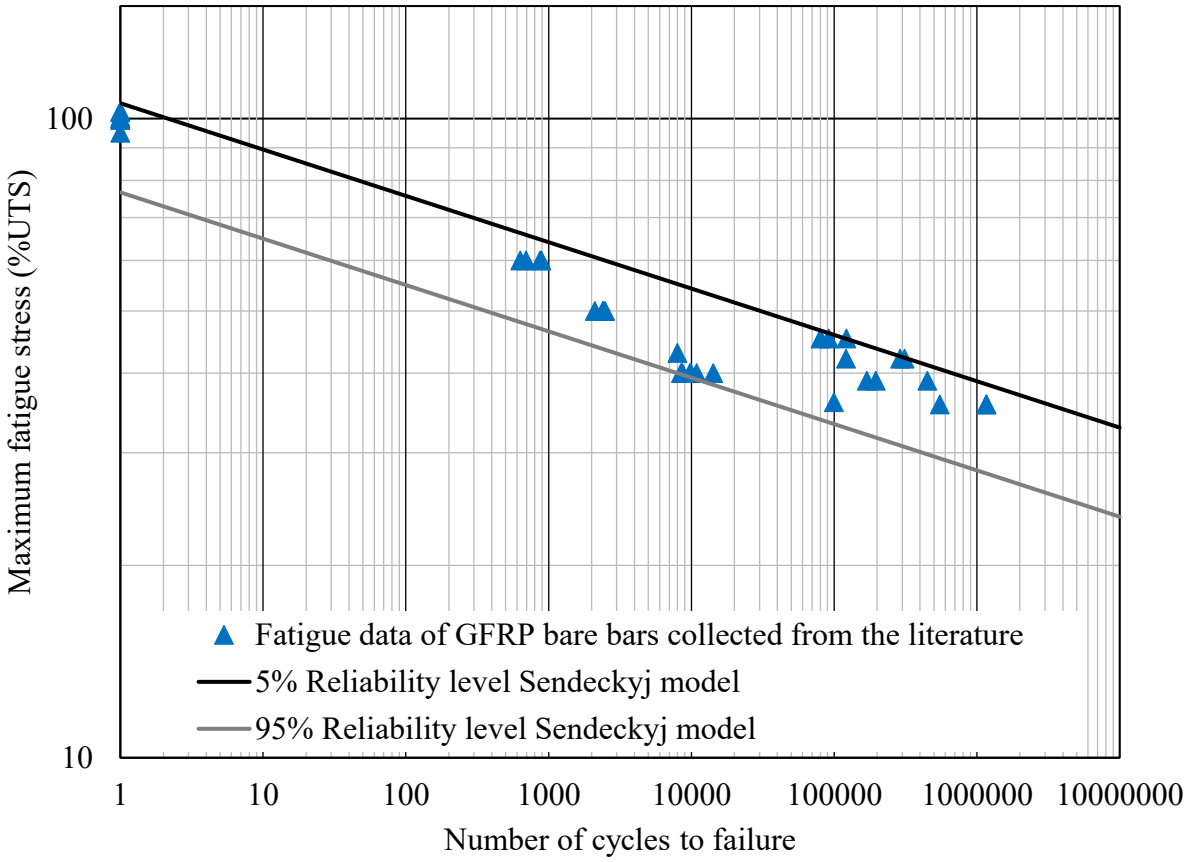

Fig. 2.7. Fitting GFRP bare bars with the Sendeckyj model.

As shown in Fig. 2.7, the Sendeckyj model captured the fatigue data well. However, there is a large scatter of data. This scatter is apparent when the expected maximum fatigue stress is calculated from the model. Table 2.1 shows the normalized maximum fatigue stress with 95% (P95) and 5% (P5) reliability for fatigue lives ranging from 1 to 10 million cycles.

Table 2.1. Maximum fatigue stress with 5% (P5) and 95% (P95) reliability for GFRP bare bars.

Number of cycles to failure	**P5 Maximum stress**	**P95 Maximum stress**
	%UTS	%UTS
1 M	38.8	28.2
2 M	36.9	26.8
10 M	32.9	23.8

As shown in Table 2.1, the GFRP bars tested under fatigue can survive 2 million cycles if tested with maximum fatigue stress ranging from 26.8% to 36.9% of the UTS. Fig. 2.8 shows the S–N

curve of GFRP bars tested in concrete. The Sendeckyj model is also used to fit the fatigue life data with coefficients of α, β, C and D equal to 11.86, 100.33, 0.033 and 0.115, respectively.

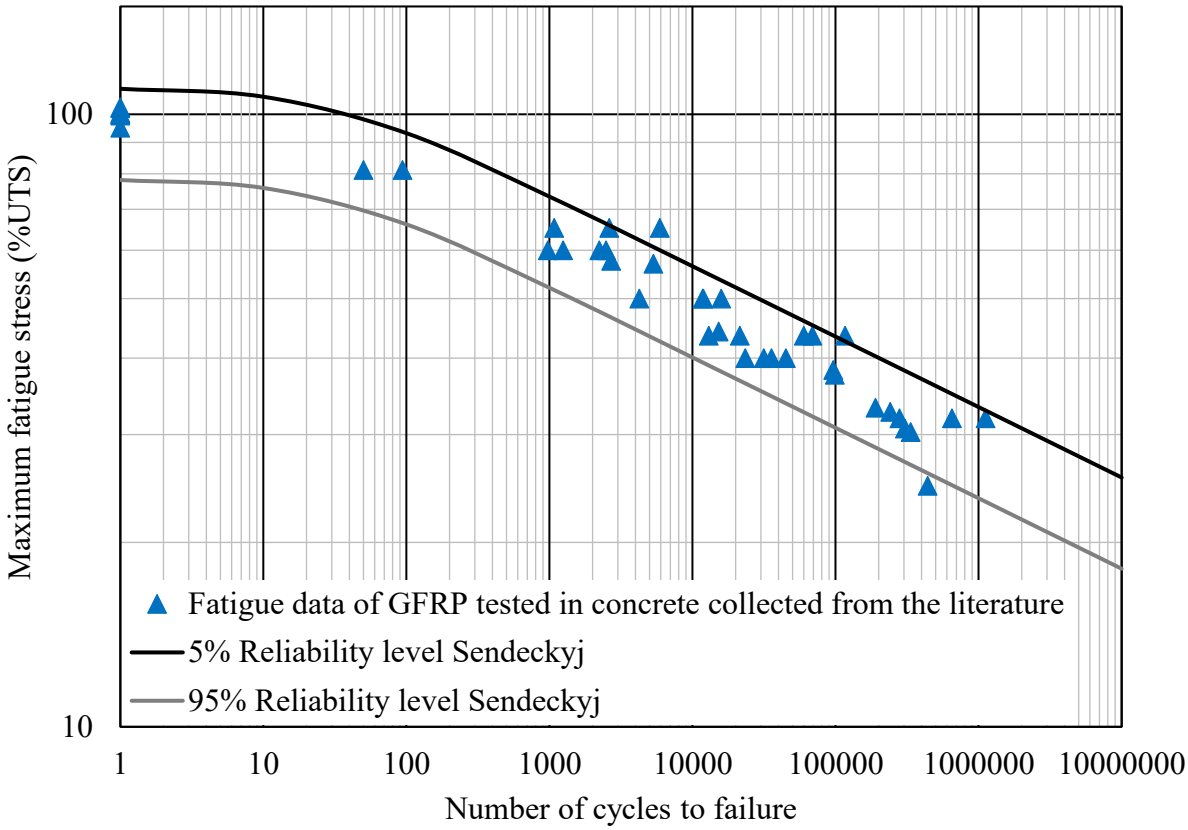

Fig. 2.8. Fitting GFRP bars tested in concrete with the Sendeckyj model.

The GFRP bars tested in concrete with maximum fatigue stress of 30.7% of UTS have a 95% chance of failure before 2 million cycles, while the rebars tested under 21.8% of UTS have a 5% chance of failure before 2 million cycles. Table 2.2 shows the normalized maximum fatigue stress with 95% and 5% reliability for fatigue lives of rebars tested in concrete ranging from 1 to 10 million cycles.

Table 2.2. Maximum fatigue stress with 5% (P5) and 95% (P95) reliability for GFRP bars tested in concrete.

Number of cycles to failure	**P5 Maximum stress**	**P95 Maximum stress**
	%UTS	%UTS
1 M	33.3	23.6
2 M	30.7	21.8
10 M	25.5	18.1

From the data shown in Table 2.1 and Table 2.2, bare bars tested under fatigue have a longer life than those tested in concrete, which might be attributed to the increase in fatigue life tested by Noël and Soudki (2014a) due to the grinding of rebars.

2.4 Other influential parameters

2.4.1 Fatigue of plain concrete under compression

Unlike metal materials, compressive fatigue causes damage to concrete under compression by the propagation of many microcracks, which diffuses damage. This diffusing damage affects various properties of concrete, such as the modulus of elasticity, compressive strength and increasing strain. The strain in concrete varies with the number of cycles due to crack growth, leading to permanent deformations (ACI PRC-215 2021). As per ACI PRC-215-21 (ACI 2021), the modulus of elasticity also decreases with an increasing number of fatigue cycles. The reduction in the modules of elasticity can be divided into three stages. In the first stage, the modulus of elasticity experiences a high reduction due to the initial growth of microcracks and the separation between the aggregate and cement paste. A linear decrease in the modulus of elasticity appears in the second stage. The reduction is linear in the second stage because the cracks progress in a stable and linear manner. The third stage is a rapid reduction in the elasticity modulus, where the crack length reaches a critical length, leading to failure. The loss in the modulus of elasticity means a loss in the structural stiffness of the elements subjected to cyclic loading. This loss in stiffness will cause an increase in vertical deformations, an increase in the structural period, and an increase in prestress losses.

It is essential to use probabilistic approaches to represent the fatigue life of the concrete. The fatigue life of concrete in compression shows a large scatter in the results. This can be two orders of magnitude when testing two identical specimens. When the reliability levels of the S–N curve are taken into consideration, the new curves are called (S-N-P curves). A sample of the S–N–P curve is drawn by Mindess et al. (2003).

2.4.2 Temperature effect of the GFRP

Mivehchi and Varvani-Farahani (2010) examined the influence of temperature on the cumulative fatigue damage (D) of laminated fibre-reinforced polymer (FRP) composites. The influence of temperature was incorporated into Varvani and Shirazi's previous formulation of the fatigue damage method. An analytical study was performed to evaluate the fatigue damage of FRP

composites at different temperatures. Included as inputs in the suggested study were temperature-dependent characteristics such as Young's modulus, ultimate tensile strength, and fatigue life. The suggested temperature-dependent factors and equations were assessed using the available experimental data. They showed that the temperature-dependent Young's modulus, ultimate tensile strength, and S–N ratio of unidirectional, cross-ply, and quasi-isotropic FRP laminates were influential. The suggested fatigue damage model was evaluated utilizing six sets of fatigue damage data and was shown to be promising for predicting the fatigue damage of unidirectional and orthogonal woven FRP composites at various temperatures. They also concluded that when the temperature rises, the cumulative fatigue damage increases.

Temperature can have a considerable impact on the mechanical characteristics of polymer-matrix composites, which are viscoelastic materials. Zhao et al. (2019) studied the fatigue performance of concrete beams reinforced with fibre-reinforced polymer (FRP) rebars after exposure to elevated temperatures. They performed static and fatigue tests on thirteen concrete beams reinforced with glass- and carbon-fibre-reinforced polymer (GFRP and CFRP) rebars after exposure to varying amounts of high temperatures. It was found that, below 400 °C, elevated temperature exposure affected the fatigue life of GFRP-reinforced concrete beams more than that of CFRP-reinforced concrete beams. However, when the exposure temperature reached 600 degrees Celsius, both the GFRP- and CFRP-reinforced concrete beams lost their bearing capabilities. Moreover, with the number of fatigue cycles, the elevated temperature accelerated the development of concrete strain, crack width, and deflection in FRP-reinforced concrete beams. Finally, they utilized several existing models to estimate the mid-span deflection. It was shown that the CEB-FIP model demonstrated the greatest accuracy with a coefficient of variation ranging from 2.8% to 7.0%. It was also found that the fatigue strength of GFRP- or CFRP-reinforced concrete beams is unaffected by temperatures up to 400 degrees Celsius for two hours.

2.4.3 Analytical study on the stiffness degradation of GFRP

The stiffness degradation of the GFRP reinforcement can be one of many factors of the overall stiffness degradation of the reinforced concrete elements. Reinforced concrete beams or slabs lose stiffness with fatigue cycles. The stiffness loss is due to crack propagation, the ineffective tension zone of concrete after fatigue cycles Dineshkumar and Ramkumar (2020), and the loss of stiffness of reinforcing bars. A sensitivity analysis is performed to study the effect of different parameters on the stiffness degradation of the fibre-reinforced composites.

Ramakrishnan and Jayaraman (1993) developed Eq. 2.9 to model the stiffness drop as a function of the number of fatigue cycles. This equation was originally developed based on experimental results in Ramakrishnan and Jayaraman (1993) and was further improved to include the effect of multilayer laminates (Shirazi and Varvani-Farahani 2010; Varvani-Farahani and Shirazi 2007).

$$\frac{E}{E_c} = 1 - A * [\{(1-f) * \ln(N+1)\} + f * N] - B * \ln(1 - \frac{N}{N_f}) \quad (2.9)$$

where A and B are constants related to the composite properties and factor f represents the fibre/matrix interface strength. E/E_c is the ratio between the modulus of elasticity of the FRP relative to the initial modulus of elasticity, and N/N_f is the due to FRP rupture N_f.

In this study, Eq. 2.9, was used to study the effect of different parameters on the stiffness degradation of the fibre-reinforced composites. Only the effect of unidirectional GFRP is presented here to compare it to the structural rebars. A sensitivity analysis is performed by changing the main influential factors by ±10%. Fig. 2.9 shows the stiffness degradation of the FRP laminates with respect to the fatigue life ratio. In this figure, *r* is the loaded stress to the ultimate strength of the laminate ($P_{applied}/P_{ultimate}$); E_f is the modulus of elasticity of the fibre in the FRP; the factor f represents the fibre/matrix interface strength; and E_m and V_m are the modulus of elasticity and volume of the matrix, respectively.

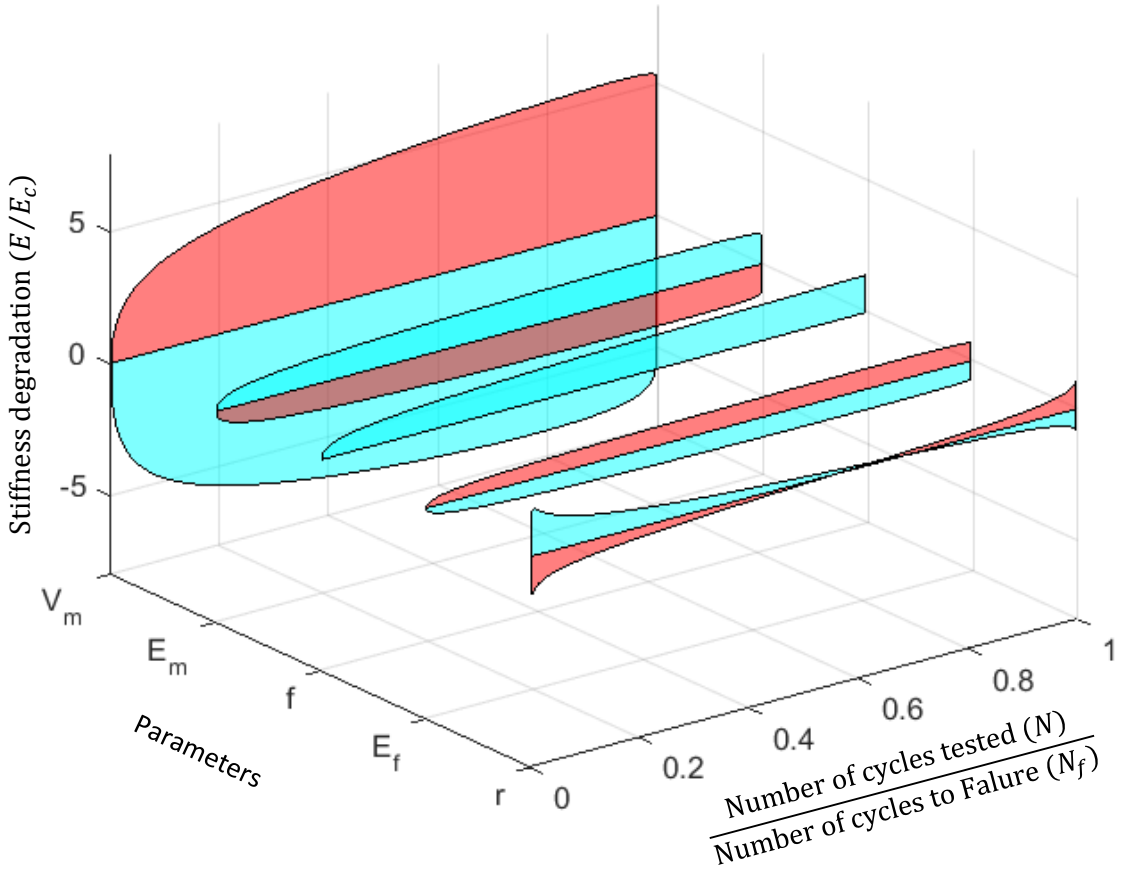

Fig. 2.9. Relationship between stiffness degradation of GFRP laminates and fatigue life ratio, Ramakrishnan and Jayaraman (1993).

As shown in Fig. 2.9, the most effective parameters on the stiffness degradation of the overall GFRP laminates are the volume and properties of the matrix used. The fibre/matrix interface strength (f) is a complicated parameter to evaluate and has a relatively small effect on the overall stiffness degradation (Ramakrishnan and Jayaraman 1993). Finally, the loading level and the fibre modulus of elasticity have a minimal effect on the stiffness degradation of the laminate. On the other hand, the loading ratio (r) significantly affected the fatigue life of the specimens. Fig. 2.10. shows the difference in fatigue life at different loading ratios.

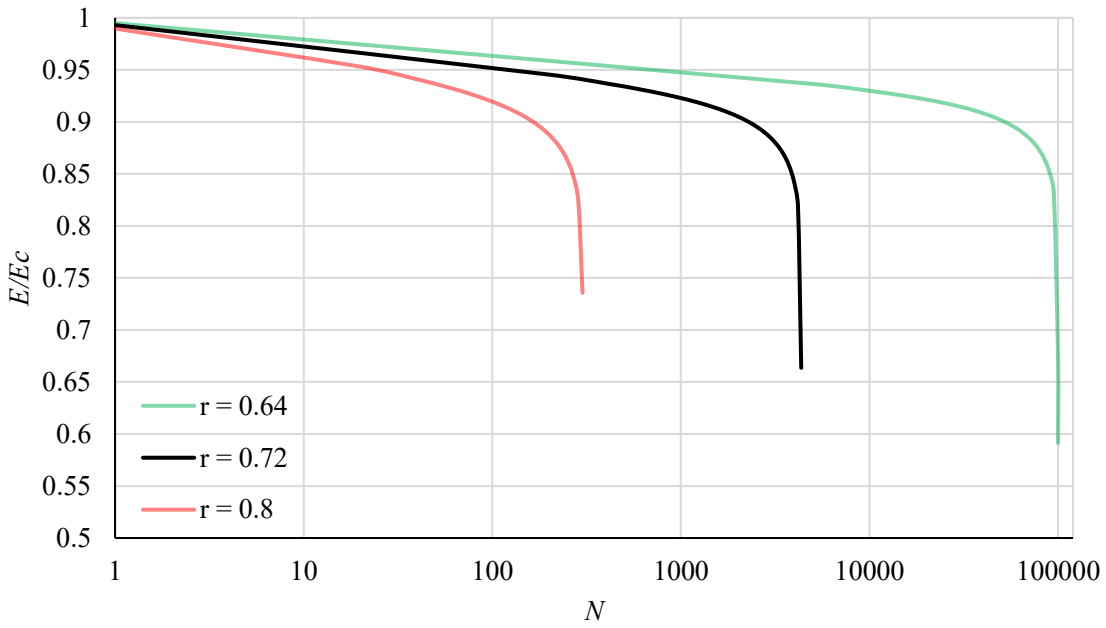

Fig. 2.10. Relationship between stiffness degradation of GFRP and fatigue life for various loading ratios (r), Ramakrishnan and Jayaraman (1993).

CHAPTER 3

Fatigue Life and Behaviour of GFRP Reinforced Concrete Beams

3.1 Abstract

Despite the growing adoption of glass-fibre reinforced polymer (GFRP) as an alternative to steel reinforcement, there is limited research addressing the fatigue performance of GFRP bars in reinforced concrete structures. Existing literature presents contradictory experimental data and conclusions regarding the fatigue behaviour of GFRP bars embedded in concrete. This study investigates the fatigue life of ribbed GFRP bars embedded in concrete beams through an experimental program, considering factors such as concrete strength and fatigue stress levels. Additionally, it introduces a testing protocol utilizing a displacement-controlled scheme to conduct fatigue testing, addressing many issues associated with force-controlled fatigue testing. Furthermore, the paper discusses cracking behaviour, deflection, and slippage, providing insights into the interaction between GFRP bars and concrete under fatigue loading. The results of this study demonstrated that ribbed GFRP bars can withstand 2 million cycles of fatigue loading at a 0.4 stress ratio. The obtained fatigue life exceeds findings in existing literature, emphasizing the impact of stress ratio and bar surface profile on fatigue performance.

3.2 Introduction

The corrosion-resistant characteristics of glass fibre-reinforced polymer (GFRP) reinforcing bars make them a viable alternative for steel reinforcements in structural applications exposed to harsh environmental conditions, such as bridges and parking garages (AASHTO LRFD for GFRP 2018; CSA S6 2019; CSA S806 2021; ACI 440.11 2022). Despite numerous research studies on the performance of GFRP-reinforced concrete (RC) elements under static loading, there is limited research on the fatigue behaviour of FRP composite materials in concrete structures. Additionally, conclusive experimental data regarding the fatigue performance of GFRP RC flexural elements are scarce.

Several design codes, guidelines and standards addressing fibre-reinforced polymer (FRP) bars as a primary reinforcement for structural concrete have been published (AASHTO LRFD for GFRP 2018; CSA S6 2019; CSA S806 2021; ACI 440.11 2022). (Elsayed Nagy et al. 2022, 2023a, 2023b, 2023c, 2024) However, the fatigue design provisions incorporated in these documents lack

sufficient experimental data. CSA S807-10 (CSA 2010), which specifies limits for the properties of different grades of FRP rebars, requires a minimum fatigue strength at 2 million cycles of 35% of the ultimate tensile strength (UTS) of the GFRP bar when fatigue applications are considered. The most recent edition of CSA S807-19 (CSA 2019) imposes the same stress limit but for 1 million cycles instead of 2 million cycles.

CSA S6-19 (CSA 2019) states that the maximum fatigue stress in the GFRP bars, calculated from the fatigue limit state combinations, shall not exceed 25% of the ultimate tensile strength. This applies to any structural element reinforced with GFRP, such as slabs and beams. However, CSA S6-19 (CSA 2019) notes that fatigue may not pose problems for deck slabs due to the arching effect (CSA S6 2019). AASHTO LRFD bridge design guide specifications for GFRP-reinforced concrete (AASHTO LRFD for GFRP 2018) specify that fatigue checks should not be conducted on GFRP-reinforced bridge decks. For any other structural element reinforced with GFRP bars, the guideline imposes a stress limit of 25% of the design tensile strength of GFRP reinforcing bars. The fatigue reduction factor can be increased if the manufacturer provides experimental evidence (ASTM D3479/D3479M 2012). ACI 440.1R-15 (ACI 2015b) mentions that E-glass and S-glass fibres are not susceptible to fatigue failure; however, delayed rupture can occur due to stress concentration induced by crack propagation of surface flaws. Based on previous fatigue-tested GFRP results, a loss of 10% of the static tensile strength is observed with each decade of a logarithmic lifetime, compared to approximately 5 to 6% in CFRP. ACI 440.1R-15 (ACI 2015b) limits the fatigue stress to 20% of the design tensile strength, the same as the creep rupture stress limit. The fatigue stress limit remains out of the scope of the ACI 440.11-22 (ACI 2022) code, but the creep rupture stress limit has been increased to 30% of the design tensile strength.

For steel reinforcement, both CSA S6-17 (CSA 2017) and CSA S6-19 (CSA 2019) limit the fatigue stress on the steel rebars as a function of the stress range, not the maximum fatigue stress, while the stress limits for FRP are only a percentage of the ultimate tensile strength of the rebar. The 2014 edition of CSA S6-17 (CSA 2017) limits the stress range in the steel reinforcement rebars to 125 MPa, regardless of the maximum and minimum values of fatigue stress. In the 2019 edition of CSA S6-19 (CSA 2019), the stress range is a function of the minimum fatigue stress as a variable.

The fatigue life performance of concrete beams reinforced with GFRP bar differs from the behaviour of bare bars tested under cyclic fatigue loading. Janus et al. (2021) concluded that the

GFRP bar tested in concrete had a higher fatigue life than that tested in air because the concrete prevented the premature failure of the rebar with no damaged core. On the other hand, Noël and Soudki (2014a) concluded that the presence of concrete reduces the fatigue life of rebar. The inconsistencies in the literature and the absence of unified code limits emphasize the need for more studies on the fatigue behaviour of GFRP bars.

GFRP bars are produced with different surface profiles, which can significantly influence fatigue behaviour in FRP-reinforced concrete elements. This study is organized into four main sections. The first section provides a review of the different types of fatigue tests performed in the literature using GFRP as reinforcement in concrete to quantify the fatigue life of GFRP bars. The second section illustrates the experimental program conducted in this study. Then, the high-cycle fatigue test used in this study to assess the GFRP-RC beams under fatigue loading is described and recommended. The final section presents the analysis and discussion of the results, with the primary aim of determining whether ribbed GFRP bars, when used as reinforcement, can sustain 2 million cycles of fatigue loading beyond code limits.

3.3 Background

3.3.1 Axial tension-tension of GFRP bars concrete prisms

In the axial tension-tension fatigue tests, GFRP bars are subjected to fatigue loading while embedded within the concrete as reinforcement.

Fatigue tests on concrete prisms reinforced with GFRP bars were performed by Adimi et al. (1997) to study the fatigue life of GFRP bars. In their study, they tested 13 sand-coated GFRP bars encased with concrete prisms. These tests maintained a consistent stress ratio of 0.1, with the stress range varying between 21.7% and 81.1% of the ultimate tensile strength. The stress ratio is the minimum stress divided by the maximum stress (ACI PRC-215 2021; CSA S806 2021). The loading frequency was set to 4 Hz. Adimi et al. (1997) concluded that the fatigue maximum stress should not surpass 22% of the Ultimate Tensile Strength (UTS) or 150 MPa in order to achieve a fatigue life of 4 million cycles. Moreover, the fatigue life can be improved by using a higher-quality vinyl ester or epoxy.

Janus et al. (2019) tested twelve sand-coated GFRP bars embedded in concrete under fatigue loading at a frequency of 4 Hz. In addition, Janus et al. (2019) tested eighteen sand-coated GFRP bars in the air using the same 4 Hz frequency. The stress ratio of the tests was a constant of 0.1.

The maximum stress of the tests was 40, 50 and 60% of the UTS of the bars for both bars tested in air and concrete. For the bars tested in concrete, they observed some degradation to the surface of the rebars due to friction with the concrete. They concluded that rebars encased in concrete have superior fatigue performance compared to those tested in air. The rebars tested in concrete can reach two million cycles of fatigue life at approximately 17.5% of the maximum ultimate stress.

3.3.2 Bending tests on beams

Fatigue bending tests in concrete beams reinforced with steel reinforcement showed a slightly longer life than those tested in air (Tilly 1979). Bending tests have a longer life with steel reinforcement because the maximum stressed areas of the rebars are usually limited to the vicinity of crack locations, which reduces the probability of having a defect of the rebar at the location of the cracks (Tilly 1979). The literature used two types of test methods for this purpose: (a) testing GFRP reinforced concrete beams and (b) beam-hinge bending tests where GFRP bars are positioned on the tension side.

Several studies were conducted on the fatigue performance of GFRP ribbed bars (Elsayed Nagy et al. 2022, 2023a, 2023b, 2023c, 2024). Noël and Soudki (2014a) conducted tests on 15 sand-coated GFRP bars embedded in a beam-hinge bending test configuration. Among these specimens, three beams underwent monotonic testing, while the remainder were subjected to fatigue loads until failure. Each of the specimens was reinforced with a single 16 mm sand-coated GFRP bar. The stress in GFRP bars ranged between 20% and 55% of the average ultimate strength of the GFRP bars, with a constant minimum stress of 30 MPa. The stress ratio was a variable for each test due to maintaining the minimum fatigue stress constant of 30 MPa. The frequency of the fatigue tests was 4 Hz. The results revealed that the fatigue life of the rebars tested under uniaxial tension is longer than that of the beam-hinge test by an entire order of magnitude. To address this difference, a fatigue stress factor was introduced to account for the abrasion between the reinforcing rebar and the concrete.

Janus et al. (2021) studied the performance and behaviour of GFRP bars as the primary reinforcement in concrete beams. Five GFRP RC beams were tested under monotonic and fatigue loading. These beams were reinforced with one sand-coated GFRP bar with a diameter of 10 mm. One beam was tested monotonically and failed due to concrete compression. The first fatigue-tested beam was tested under constant amplitude to reach maximum stress in the GFRP bar at 20% of its UTS. The stress ratio during the fatigue test was maintained at 0.1, and the testing frequency

was set at 2 Hz. This beam successfully endured two million cycles of fatigue loading. Consequently, the beam was tested monotonically to identify the residual strength. The statically loaded GFRP-RC beam had a flexural strength of 19.2 kN. After loading the beam with two million cycles, the residual flexural strength is 18.9 kN, which indicates minimal strength degradation. The remaining three specimens were tested under fatigue loading for 50,000 cycles with maximum stress in the rebar equal to 20% of the ultimate tensile strength. After that, the load was increased with steps of 5% of the ultimate strength, and each load level was cycled for 50,000 cycles until failure. Among these specimens, two failed when the maximum stress in GFRP bars reached 40% of the ultimate tensile strength, while one continued to survive up to 2800 and cycled under 45% of the ultimate tensile strength. Miner's rule (Miner 1945) was then employed to estimate the accumulated failure of the beams. The tested samples showed that GFRP could endure more than two million cycles with a maximum stress of 20% of the UTS without a noticeable reduction in static strength.

3.3.3 Fatigue testing guidelines and standards

The stress (or load) ratio and range are two terms commonly used to describe the fatigue behaviour of composite materials. The stress ratio is the ratio between the minimum and maximum fatigue stresses, while the stress range is defined as the difference between the maximum and minimum stresses.

CSA S806:12-R2021, Annex J (CSA S806 2021) specifies the testing methods and calculations required to investigate the fatigue life of FRP bars and draw the S–N curve. To conduct the fatigue test, CSA S806-21 (CSA 2021) describes two loading protocols: one involves fixing the average load and varying the load range, and the other entails fixing the minimum and maximum loads. Notably, by adopting either of these testing protocols, two variables come into play during testing: the maximum load and the load ratio. The code permits the stress ratio to be different from the 0.1 stress ratio typically adopted in FRP fatigue tests, allowing the use of dead and design loads in the tests.

ACI 440.3R-12 (ACI 2012) specifies that the fatigue test should be load-controlled by applying a constant load amplitude or stress amplitude. Three loading protocols are defined to perform the fatigue test. The test can be conducted using the same load protocols used in CSA S806-21 (CSA 2021), or it can be conducted by changing the maximum and minimum loads while keeping the load ratio fixed at 0.1.

Additionally, AASHTO LRFD for GFRP (2018) referenced ASTM D3479/D3479M (2012) for the fatigue testing of tension-tension polymer matrix composite materials. ASTM D3479/D3479M (2012) specifies two procedures in which the fatigue test cycles between minimum and maximum stress or strain. However, it does not provide specific testing protocols. Furthermore, CSA S6-19 (CSA 2019) does not mention any testing protocol. Fig. 3.1. illustrates the different loading protocols of CSA S806-21 (CSA 2021), ACI 440.3R-12 (ACI 2012), and AASHTO LRFD for GFRP (2018).

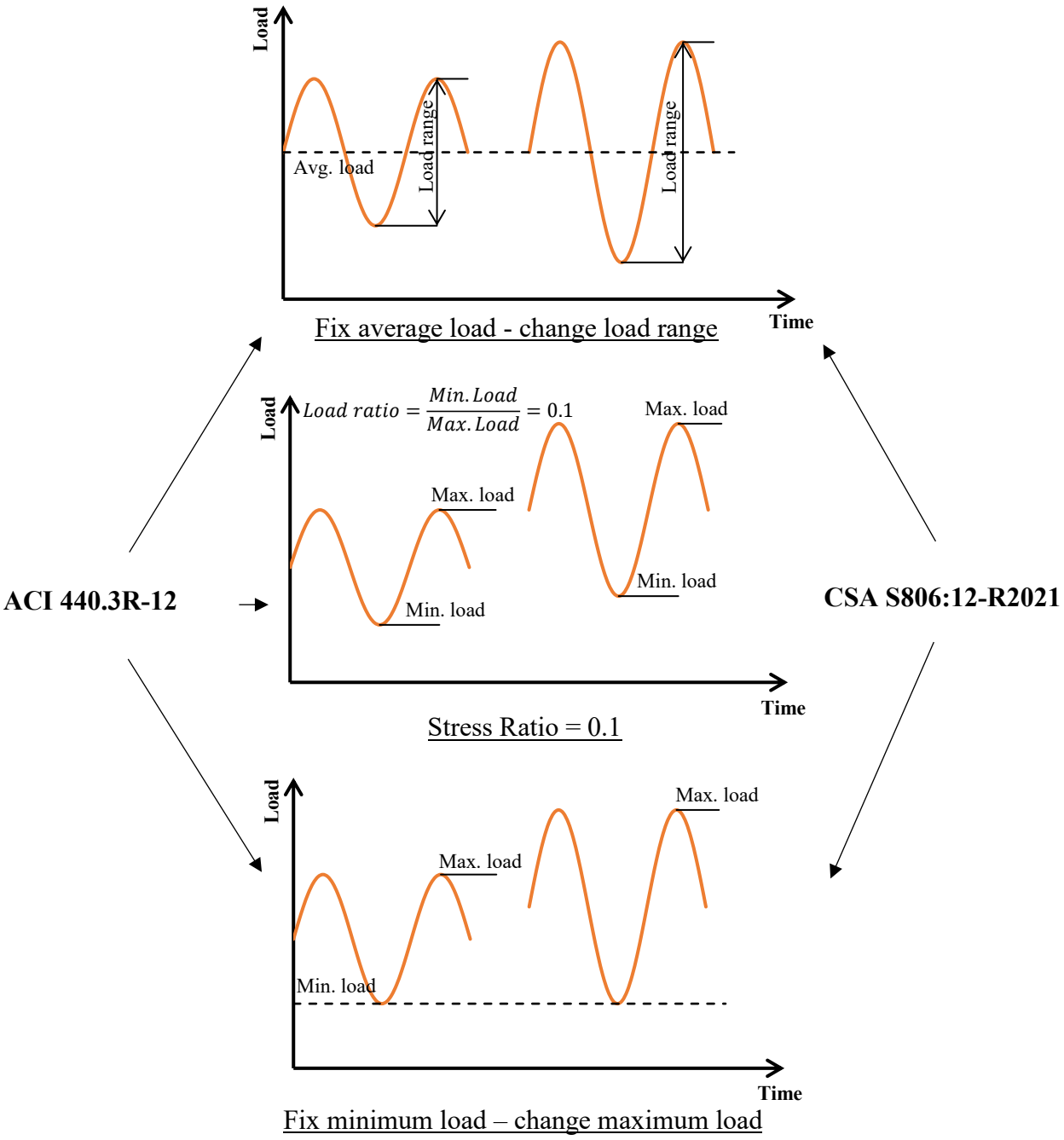

AASHTO LRFD → Referenced → **ASTM D3479/D3479M**
No specific testing protocol is specified.

CSA S6-19 → No test protocol

Fig. 3.1. Loading protocols

3.3.4 Fatigue of plain concrete under compression

Unlike metal materials, compressive fatigue causes damage to concrete under compression by the propagation of many microcracks, which diffuses damage. This diffusing damage affects various properties of concrete, such as the modulus of elasticity, compressive strength and increasing strain. The strain in concrete varies with the number of cycles due to crack growth, leading to permanent deformations (ACI PRC-215 2021). As per ACI PRC-215-21 (ACI 2021), the modulus of elasticity also decreases with an increasing number of fatigue cycles. The reduction in the modules of elasticity can be divided into three stages. As described in ACI PRC-215-21 (ACI 2021), in the first stage, the modulus of elasticity experiences a high reduction due to the initial growth of microcracks and the separation between the aggregate and cement paste. A linear decrease in the modulus of elasticity appears in the second stage. The reduction is linear in the second stage because the cracks progress in a stable and linear manner. The third stage is a rapid reduction in the elasticity modulus, where the crack length reaches a critical length, leading to failure. The loss in the modulus of elasticity means a loss in the structural stiffness of the elements subjected to cyclic loading. This loss in stiffness will cause an increase in vertical deformations, an increase in the structural period, and an increase in prestress losses.

It is essential to use probabilistic approaches to represent the fatigue life of concrete. The fatigue life of concrete in compression shows a large scatter in the results. This can be two orders of magnitude when testing two identical specimens (ACI PRC-215 2021). When the reliability levels of the S–N curve are taken into consideration, the new curves are called (S-N-P curves). A sample of the S–N–P curve was drawn by Mindess et al. (2003).

3.4 Experimental program

3.4.1 Test setup and instrumentation

3.4.1.1 Test setup

Five full-scale reinforced concrete beams were constructed and tested under a four-point bending test to investigate the fatigue life of GFRP-RC beams. The beams measured 200 × 300 × 3500 mm, with a loading span of 3000 mm, as shown in Fig. 3.3. A steel spreader beam transfers the load on two points with 1000 mm spacing.

All beams are designed to have flexural failure - crushing of concrete, and the shear span of the beam is reinforced with stirrups to prevent shear failure. They are reinforced with three #5 ribbed

GFRP bars with a nominal diameter of 15.9 mm, serving as longitudinal flexural reinforcement, while the top compression reinforcement consists of 2-10M steel rebars. Steel top compression reinforcement was used to sustain high compression stresses. Unlike steel reinforcement, GFRP bars cannot sustain high levels of compression stresses. The 10M steel stirrups at 100 mm spacing are provided in the shear span to prevent shear failure, while two 10M steel stirrups are provided within the moment span to facilitate cage construction and ensure uniform spacing between the rebars. The clear bottom cover for all beams is 30 mm. Fig. 3.2. shows a photo of the test setup, while Fig. 3.3. shows the test setup and beam dimensions.

Fig. 3.2. Test setup

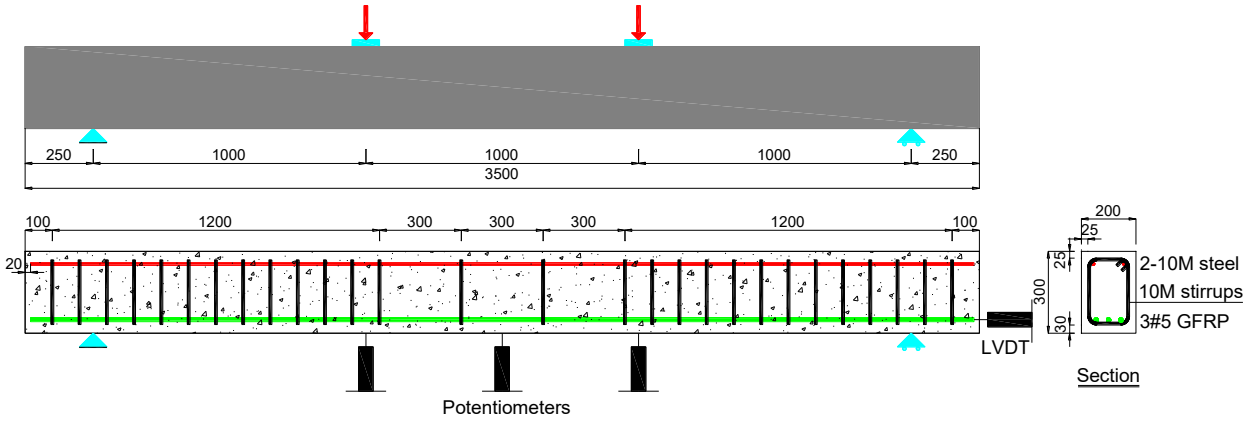

Fig. 3.3. Details of specimens.

To avoid any movements that can alter the desired purpose of the test, a set of supports was designed and manufactured, as shown in Fig. 3.4 (a). The hinged support was designed and manufactured to prevent the beam from moving in the horizontal, vertical and sideways directions, allowing only rotations, as shown in Fig. 3.4 (b). The roller support was designed to restrain the vertical and the sideways movements while allowing the beam to move in the horizontal direction and rotate freely, as shown in Fig. 3.4 (c).

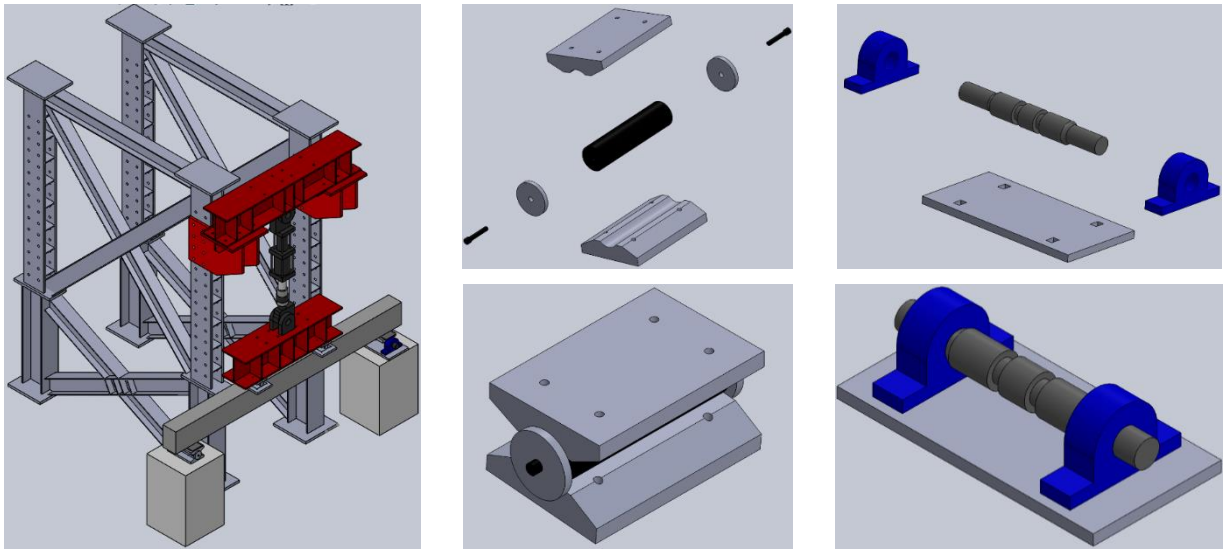

(a) Test setup (b) Hinged support (c) Roller support

Fig. 3.4. Fatigue test setup 3-D drawings.

3.4.1.2 Instrumentations

Each beam is instrumented with electrical resistance strain gauges. A compression electrical resistance gauge was installed on the middle section of the top fibre of the statically tested beam to measure the concrete strain. Due to fatigue loading, the strain gauges were damaged. A potentiometer is installed in the middle section of all the tested beams to measure the beam deflection. Additionally, a high-accuracy linear variable displacement transducer (LVDT) was placed on the edge of one of the GFRP reinforcing bars to measure slippage. A fatigue-rated load cell is used in line with the actuator to measure and control the fatigue loading during the test. A data acquisition system is utilized to collect and monitor the measured data for all the measuring devices during beam loading.

3.4.2 Test matrix

Five specimens were constructed and tested to achieve the objectives of this study. The specimens are designated as follows: the first letter (B1/B2) indicates the concrete batch number; the second letter (S/F) indicates the type of loading, S for static and F for fatigue; the third letter (DC/FC) indicates the method of controlling the loading of the test, DC for displacement control, FC for forced control. The last number (30 or 35) indicates the maximum fatigue stress as a percentage of the ultimate tensile strength (UTS) of the rebar. The test matrix of the tested beams is shown in Table 3.1.

Table 3.1. Test matrix of the tested beams.

Name	Loading protocol	f_c' MPa	Bar dia. mm	f_{fmax} MPa (% f_{frpu})	f_{fmin} MPa (% f_{frpu})	P_{max} kN	P_{min} kN	Fatigue life cycles
B1-S-DC	Monotonic	51.3	15.9	-				-
B1-F-FC-30	Force control fatigue			326 (30%)	130 (12%)	87.9	33.2	-
B1-F-DC-30	Displacement control fatigue			326 (30%)	130 (12%)	87.9	33.2	>2 million
B1-F-DC-35	Displacement control fatigue			380 (35%)	152 (14%)	103.1	39.3	94,875
B2-F-DC-35	Displacement control fatigue	84.2		380 (35%)	152 (14%)	103.8	39.6	>2 million

f_c': the compressive strength of concrete;
f_{frpu}: is the ultimate strength of the GFRP bars;
f_{fmax}, and f_{fmin}: maximum and minimum fatigue stress of GFRP bars, calculated using cracked section analysis
P_{max}, and P_{min} are the maximum and minimum fatigue forces of the GFRP-RC beams.

3.4.3 Material properties

3.4.3.1 Reinforcing bars

All beams are reinforced with #5 ribbed GFRP bars as longitudinal tensile reinforcement. Fig. 3.5 shows the ribbed GFRP bars used for reinforcement. Five samples were tested according to ASTM D7205/D7205M (2021) to measure the mechanical characteristics of the GFRP bars. Table 3.2. shows the tensile properties of the GFRP bars. The nominal cross-sectional area of the rebars (i.e., 199 mm^2 as per ASTM D7957/D7957M (2017) is used for the calculation of the tensile properties of the GFRP bars. The 10 M steel reinforced bars used for the top compression bars and the stirrups have a nominal yield strength of 400 MPa, nominal diameter of 11.3 mm, and nominal cross-sectional area of 100 mm^2.

Table 3.2. Mechanical properties of #5 GFRP bars.

No.	Ultimate tensile Strength (UTS), MPa	Modulus of Elasticity (E), GPa
1	1148	55.9
2	1047	56.1
3	1064	58.8
4	1016	56.9
5	1160	58.7
Average	1087	57.3
Standard deviation	64	1.4

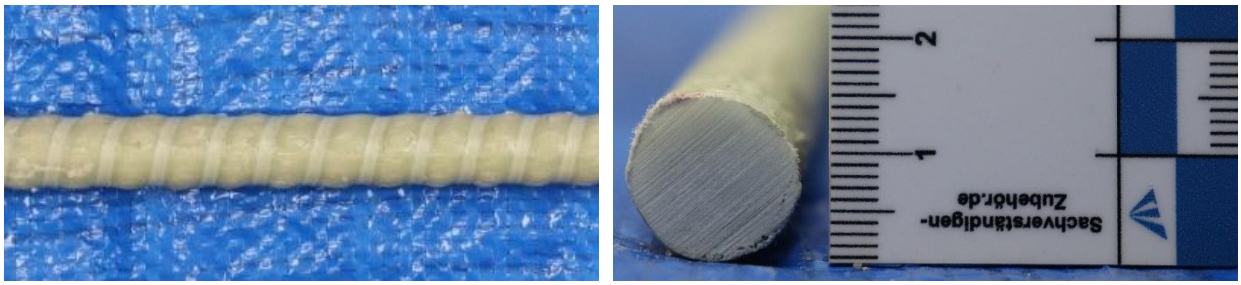

Fig. 3.5. Ribbed GFRP bar.

3.4.3.2 Concrete

In this study, two ready-mixed concrete batches are used to construct the beams (the design mix of the concrete batches was not stated by the supplier). The first batch of concrete is used for four beams, B1-S-DC, B1-F-FC-30, B1-F-DC-30, and B1-F-DC-35. The second batch of concrete is used for the construction of the fifth beam B2-F-DC-35. The compressive strength for each batch of concrete used is measured by testing concrete 100 × 200 mm cylinders according to ASTM-C39 / C39M (2021). The results of the concrete compression tests are shown in Table 3.3. At the same time as the first batch, three 150 × 150 × 500 mm concrete prisms were tested per ASTM C78 / C78M (2021) to quantify the modulus of rupture. The modulus of rupture (f_r) was 5.6 ± 0.1 MPa. Three 100 × 200 mm concrete cylinders were also tested per ASTM C496/C496M (ASTM C496 / C496M 2017) to measure the splitting tensile strength. The splitting strength (T) was 4.5 ± 0.4 MPa.

Table 3.3. Mechanical properties of concrete.

Batch No.	Test time	Compressive Strength (MPa)	Average (MPa)	Standard deviation (MPa)
B1	Same day as the B1-F-FC-30 beam test	47.4 54.5 50.4	50.7	3.6
	Same day as the B1-F-DC-30 beam test	49.7 54.5 58.8 49.1 44.3	51.3	5.5
B2	The same day as the B2-F-DC-35 beam is tested	84.7 85.3 82.7	84.2	1.4

3.4.4 Loading protocol

Generally, the fatigue stresses acting on the rebar can be tension-tension, tension-compression, or compression-compression. The test procedure used in this study focuses on tension-tension fatigue stresses in the reinforcing bars. The fatigue stresses acting on the rebars are calculated based on the cracked section analysis, assuming that the plain section remains plain after deformation. To calculate the fatigue stresses on the GFRP bars, elastic analysis is needed to calculate the cracked moment of inertia (I_{cr}), and the ratio of depth of the elastic neutral axis to the effective depth K_{cr} factor (ACI 440.11 2022). Eq. (R.24.6.1) in ACI 440.11 (2022) should be used to determine the stresses based on an assumed acting moment fatigue moment.

The first beam, B1-S-DC, was tested until failure under static loading at a displacement control rate of 1.2 mm/min. A hydraulic cylinder with a capacity of 5000 kN loaded the beam while the load was measured using a 500 kN load cell with an accuracy of ± 0.1 kN. The fatigue loading was applied using an MTS dynamic actuator with a capacity of 160 kN, while the loads were measured using a fatigue-rated 250 kN load cell.

The force-control scheme was used for beam B1-F-FC-30. First, to reach the maximum fatigue load from which the cycles will start, a static load was applied to induce cracking in the beam. The

initial attempt to load the beam using force control failed because an impact load occurred when the first crack was initiated. The initiation of the first crack led to a drop-in force, prompting the actuator to respond with a sudden increase in force and displacement, ultimately causing an impact load on the beam.

Second, to load beam B1-F-FC-30 under cyclic loads, the actuator was tuned. Based on the author's experience, the tuning process was affected by the specimen stiffness. As the number of cycles increases, the deflection of the beam increases, its stiffness decreases, and the initial tuning calibration becomes invalid, leading to various instabilities. These instabilities resulted in fluctuations in the loading force, where the actuator oscillated with forces exceeding the desired levels. As a solution, a displacement-control scheme was adopted. Notably, when controlling deflection instead of force, these instabilities were significantly reduced.

For beams B1-F-DC-30, B1-F-DC-35, and B2-F-DC-35, an algorithm is developed to apply load using displacement control instead of force control. In this algorithm, if the desired maximum and minimum applied fatigue loads deviate by more than 1% from the desired force, the displacements are automatically corrected to reach the target fatigue loads. The correction of displacements to achieve the desired forces is performed to account for stiffness degradation. This procedure effectively resolved the tuning issues associated with force control, eliminating instabilities. The loading protocol for beams B1-F-DC-30, B1-F-DC-35, and B2-F-DC-35, follows the steps outlined below:

1- The beams were aligned in the test setup, and all the required instrumentation was installed.
2- The beams were loaded statically with a displacement rate of 1.2 mm/min rate in accordance with CSA S806-12, Annex S (CSA S806 2012), until reaching the required maximum fatigue load.
3- After reaching the desired maximum fatigue load, fatigue cycles start. To perform fatigue loading without having instabilities in force due to tuning problems. Displacement control is used to apply the desired forces accurately by controlling the target displacements. The displacements are continuously and automatically updated to reach the fatigue loads with a 1% error. This process ensures accuracy while maintaining safety by avoiding the risks associated with force control.

3.4.5 Loading frequency

Noël and Soudki (2014a) tested rebar embedded in concrete with a frequency of less than 1 Hz. Additionally, Adimi et al. tested many specimens with a loading frequency of 2 Hz. Frequency was also studied as a parameter, as demonstrated by Adimi et al. (2000). In addition, Janus et al. (2021) recommended a testing frequency of 2 Hz. In this study, the chosen testing frequency is 2 Hz.

3.4.6 Stress ratio

The current codes only limit the maximum fatigue stress to a percentage of the ultimate tensile strength (UTS). These limits ignore the effect of other parameters, such as stress ratio and stress range. The code limits are based on a stress ratio of 0.1, which is a very conservative value. CSA S806-21 (CSA 2021) permits the stress ratio to be taken as the ratio between the dead and design loads, which gives the flexibility of using stress ratio values other than 0.1.

To better estimate the approximate values of the loading ratio acting on slab-on-girder bridges, simplified calculations are performed to estimate dead and live loads acting on the bridges. The girder is the main element of this study because the rebars are subjected to a high level of stress compared with the deck slab. The main variables considered in this study are the span (10 and 40 m), bridge width (between 6 and 28 m), number of lanes (up to 8 lanes), lane width (3.5 to 6m) and spacing between the girders (0.75 to 1.5 m).

For the dead loads, the deck slab thickness is estimated based on the acting loads, with a bituminous layer covering the deck slab. A rail of 500 mm in height is used on each side. Girder dimensions are designed and checked based on CSA A23.3 (2019 and CSA S6 (2019). A five-axle CL-W truck is used for the live load. The maximum moments are calculated from the moving load of the truck along with CL-W lane loads and multilane loadings. A dynamic load allowance is then applied to the moments. The ratio between the dead load moments and those calculated from the load combinations is then calculated. The calculated range of ratios shown in Fig. 3.6 is considered the stress ratio for the fatigue design of bridges.

The moment ratio of 56 bridges reported by Kim et al. (2022) is used to verify the calculated data in this study. The data on the 56 bridges were originally calculated and reported by Nowak (1999). Those data were then modified by Kim et al. (2022) to accommodate the effect of dynamic

load allowance. Stress in the rebars is calculated directly from the moment, so the ratio can be assumed to be equal. The minimum and maximum stress ratios are drawn in Fig. 3.6.

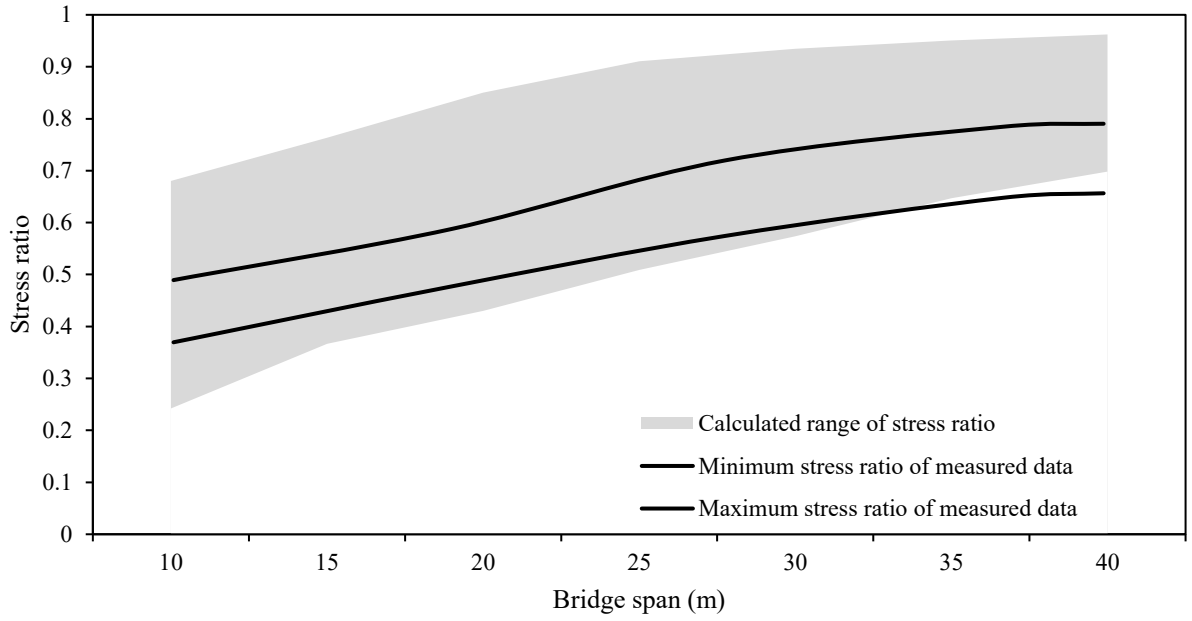

Fig. 3.6. Relation between the stress ratio and bridge span, Kim et al. (2022).

3.5 Experimental results

3.5.1 Cracking behaviour

Fig. 3.7 displays the condition of the beams after the test. In these figures, the initial cracks that occurred during the first loading cycle are marked in black, and their propagation during fatigue loading is marked in green. Additionally, Table 3.4 provides information on the cracking load, minimum and maximum crack spacing, and the crack height at the middle section.

All beams exhibited similar flexural cracking behaviour during the initial static loading phase, as shown in Fig. 3.7. As shown in Table 3.4, the cracking load for the beams constructed with batch 1 of concrete is approximately equal, while the beam constructed with batch 2 of concrete exhibited a higher cracking load. This difference is primarily attributed to the higher concrete strength of batch 2.

Furthermore, as listed in Table 3.4, the minimum crack spacing in all beams is nearly identical. However, the maximum crack spacing varies. Nonetheless, all beams developed seven cracks in

the middle flexural zone, with some of these seven cracks leading to the development of secondary cracks, as shown in Fig. 3.7.

The crack height at the middle section of the statically loaded beam, B1-S-DC, is 235 mm, as shown in Fig. 3.7 (a) and Table 3.4. In the case of beam B1-F-DC-35, the crack was initiated at 220 mm in height, then propagated to 235 mm after 20,000 cycles and maintained the same height until failure, as seen in Fig. 3.7 (c). For beams B1-F-DC-30 and B2-F-DC-35, the crack heights at the first cycle were 235 and 205 mm, respectively. After 10,000 cycles, the crack propagated in B2-F-DC-35 to 235 mm. Subsequently, in both beams, B1-F-DC-30 and B2-F-DC-35, the crack reached 245 mm and remained at this height until failure, as seen in Fig. 3.7 (c-d).

Table 3.4. Cracking load, minimum and maximum crack spacing, and middle section crack height.

Name	Cracking load (kN)	Minimum crack spacing (mm)	Maximum crack spacing (mm)	Crack height at the middle section (mm)				
				Cycle 1	Cycle 10,000	Cycle 40,000	Cycle 500,000	Cycle 2,000,000
B1-S-DC	14	100	165	235	-	-	-	-
B1-F-DC-30	14	100	210	235	235	245	245	245
B1-F-DC-35	15.5	90	190	220	220	235	-	-
B2-F-DC-35	21	100	160	205	235	235	245	245

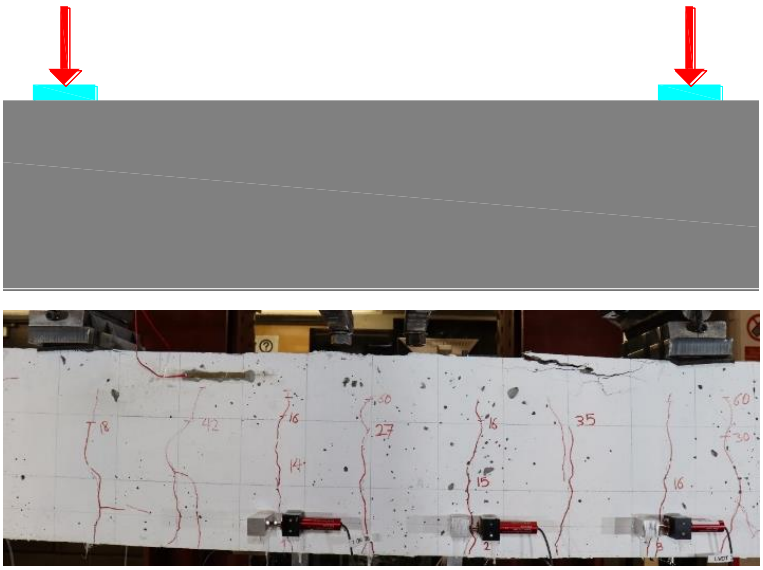

(a) B1-S-DC

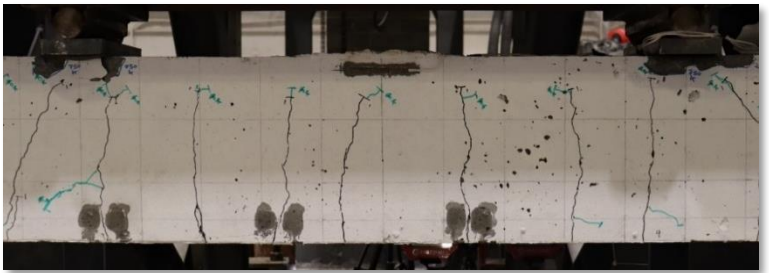

(b) B1-F-DC-30

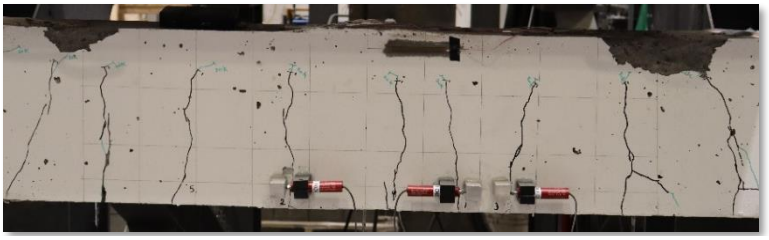

(c) B1-F-DC-35

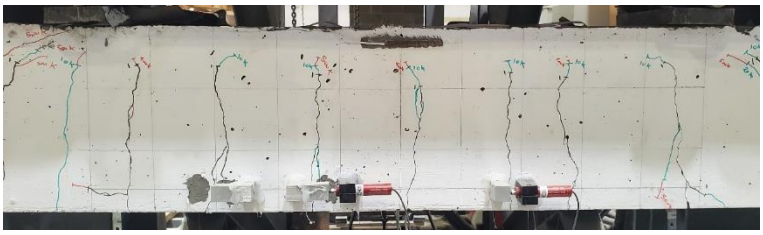

(d) B2-F-DC-35

Fig. 3.7. Tested GFRP-RC beams.

3.5.2 Deflection

The load-deflection curve for the statically tested beam B1-S-DC is shown in Fig. 3.8. The initial stiffness of the beam is high due to the high gross inertia of the uncracked section. Following the initiation of the first crack, the stiffness of the beam began to decrease. This reduction in stiffness continued at a lower rate as more cracks appeared and progressed. The beam then reached a stabilized stage where the stiffness remained constant, and the number and depth of cracks stopped progressing. Ultimately, this beam failed by concrete crushing at a maximum force of 171.2 kN. The corresponding deflection at the maximum load was 67.94 mm.

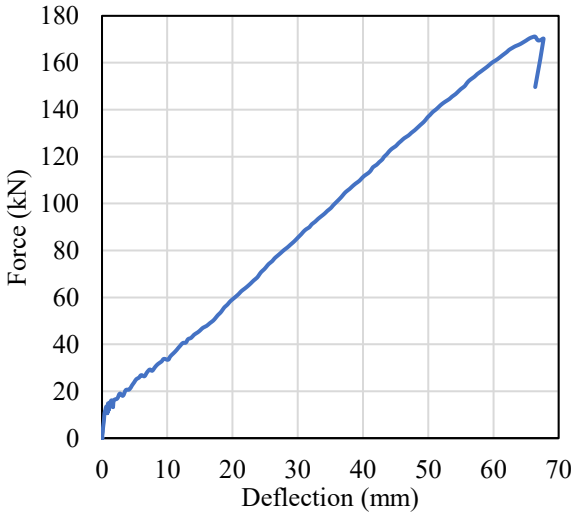

Fig. 3.8. GFRP-RC static load-deflection curve.

During fatigue testing of beams, the fatigue loading is periodically paused during each test to conduct a monotonic loading cycle. Those loading cycles are conducted at a slower rate of 12 mm/min. One of the reasons behind conducting these slower cycles is to facilitate data collection, which can be more challenging when dealing with high-frequency testing. Fig. 3.9 illustrates the changes in maximum deflection during fatigue loading, while Fig. 3.10 shows the load-deflection curves for the first loading cycle and various statically loaded cycles during the course of fatigue testing.

Fig. 3.9 illustrates an increase in deflection observed over the course of fatigue cycles. This observation aligns with the findings in Fig. 3.10, where the slope of the graphs for the intermediate fatigue cycles indicates a reduction in stiffness of the beam during early loading stages, while it remains almost constant throughout the rest of fatigue loading. The increase in deflection can be attributed to several factors, including crack propagation, stiffness degradation, and creep. The constant stiffness at higher fatigue cycles may suggest that the modulus of elasticity of the rebar is not significantly affected by the fatigue cycles. During the loading of beam B1-F-DC-30, the maximum deflection increased by approximately 30%, from an initial value of 27.3 mm to 35.5 mm, over the course of 2 million fatigue cycles. Notably, approximately 18.5% of the deflection increase occurred in the initial 125,000 cycles. The deflection increase was then slow and relatively constant until the test stopped after 2 million cycles. For beam B1-F-DC-35, cracks propagated within the beam, mainly during the initial 3 thousand cycles. The rate of damage was faster than that of beam B1-F-DC-30 since beam B1-F-DC-35 failed after fewer cycles. The initial maximum fatigue deflection was 34.1 mm, while the deflection near failure reached approximately 39.7 mm, resulting in a total deflection increase of approximately 16.5%. Beam B2-F-DC-35 exhibited a similar deflection behaviour to beam B1-F-DC-30, with the maximum deflection increasing during the initial cycles and maintaining a relatively constant rate of deflection increase. The maximum deflection increased from an initial value of 32 mm after static loading to 38.8 mm after 2 million cycles of fatigue, representing a 21% increase in deflection.

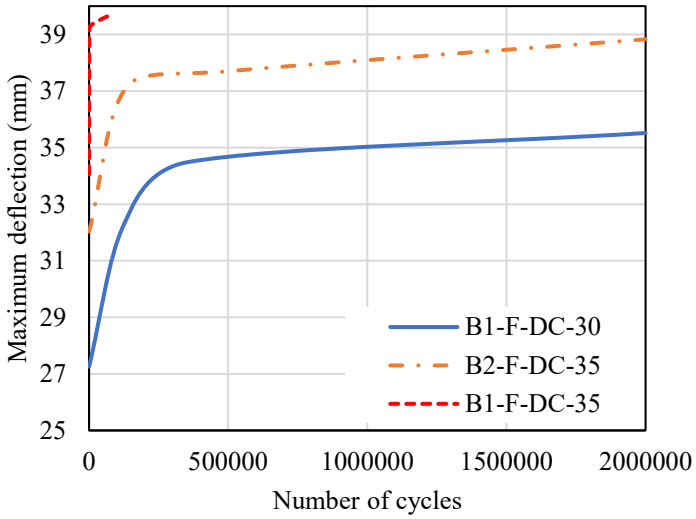

Fig. 3.9. Maximum deflection with number of cycles.

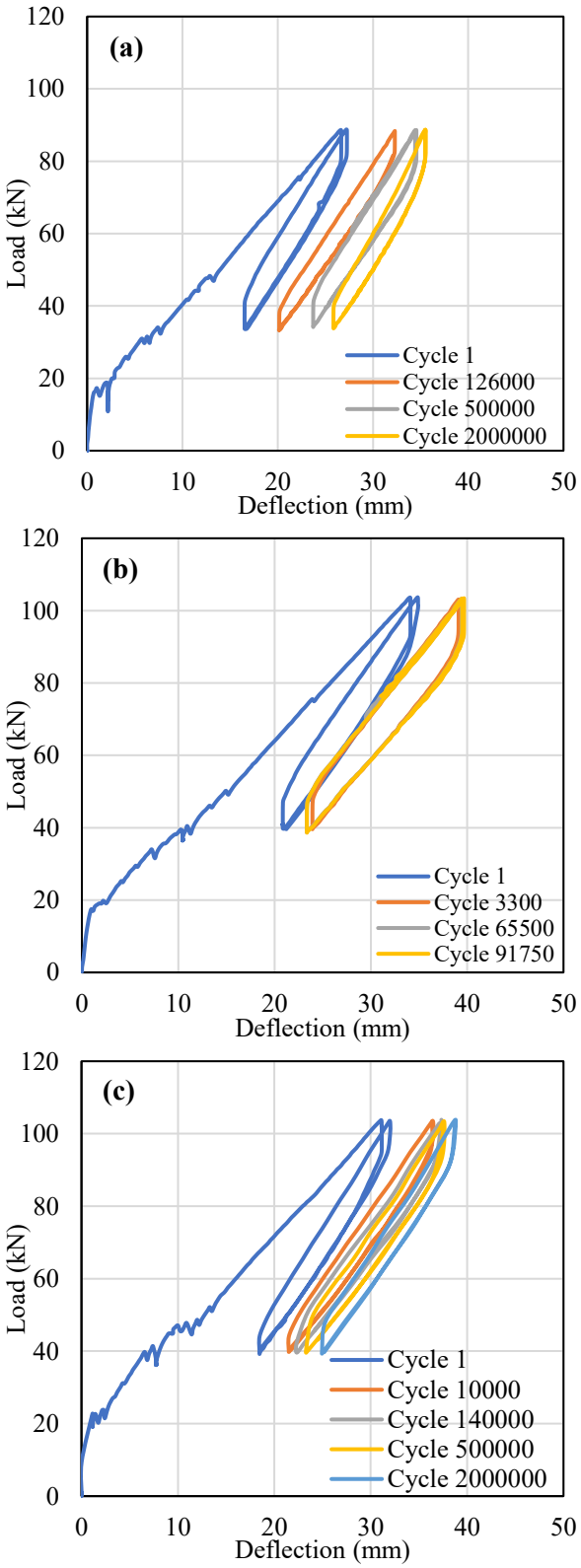

Fig. 3.10. Load-deflection curve for different cycles during fatigue loading: (a) B1-F-DC-30; (b) B1-F-DC-35; and (c) B2-F-DC-35

3.5.3 Strain and slippage

The recorded tension strains on the GFRP bars for the static beam B1-S-DC are presented in Fig. 3.11. The top concrete strains were not measured because the concrete strain gauge was damaged during testing. The concrete strains at the top fibre of the middle section are calculated and shown in Fig. 3.11. The calculated concrete strains are based on the model proposed by Michael P. Collins (1997). Before cracking, the strain in the GFRP bars remained very small, nearly zero. However, after the beam cracked, the stresses in the rebars increased linearly until failure. The maximum GFRP strain at the failure load reached approximately $12500\mu\varepsilon$, which is equivalent to approximately 716 MPa. Notably, the maximum stress in the GFRP bars at failure was less than the UTS because the beam failed in concrete compression crushing before the GFRP bars reached the UTS. As for the fatigue beams, B1-F-DC-30 and B1-F-DC-35, the strain gauges did not sustain the fatigue load, and there was no valid collected data.

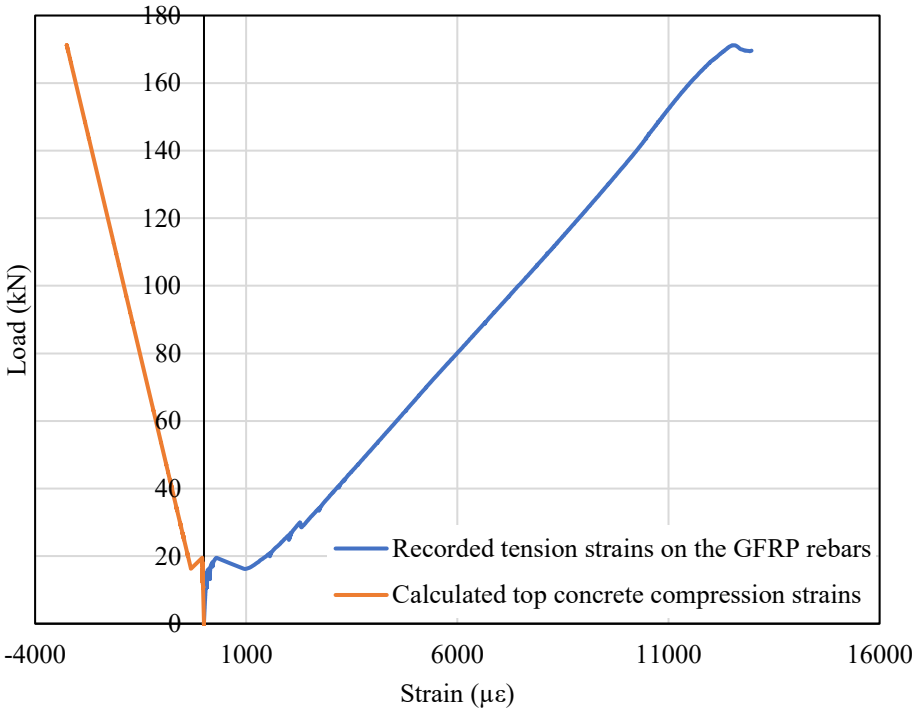

Fig. 3.11. B1-S-DC Strain with load.

As previously mentioned, a high-accuracy LVDT was placed on one of the GFRP bars at the beam end for all the beams to measure slippage. However, during both static and fatigue loading

of all beams, no significant slippage was measured. This negligible slippage indicates that sufficient embedment length was provided for the rebars within the shear span and beyond the supports, demonstrating a strong bond between ribbed GFRP bars and the concrete.

3.5.4 Discussion of the fatigue life

Beam B1-F-DC-30 was designed to endure fatigue loads, imposing maximum stress in the rebars of 30% of the UTS (326 MPa) with a stress ratio of 0.4. The calculated maximum fatigue compression stress acting on the top fibre of concrete was approximately $0.82f_c'$ (42 MPa). During testing, minor concrete spalling occurred on the top surface of the concrete under the loading points, primarily due to stress concentration resulting from slight surface irregularities. However, it is noteworthy that no rupture occurred to the GFRP bars, and the beam remained structurally sound until the test was stopped at 2 million cycles, as shown in Fig. 3.7 (b). This suggests that ribbed GFRP bars can sustain fatigue loading for 2 million cycles when stresses have a maximum fatigue stress of 30% of the UTS and a stress ratio of 0.4.

To investigate the behaviour of ribbed GFRP bars under higher fatigue loads, beam B1-F-DC-35 was designed to withstand fatigue loads corresponding to maximum stress in the rebars of 35% of the UTS (380 MPa) with a stress ratio of 0.4. The calculated maximum fatigue compression stress acting on the top fibre of concrete was approximately 95% of f_c' (49 MPa). The beam failed after 94,875 cycles in compression, as shown in Fig. 3.7 (c), without any indication of fatigue-induced rupture in the GFRP bars. The notable aspect of this test is the high level of compression stress that the concrete endured. This outcome highlights the need to establish concrete stress limits under fatigue conditions, particularly in the design of GFRP-reinforced concrete elements. Proposing such a compression stress limit requires in-depth studies and falls outside the scope of this study.

To mitigate the risk of concrete crushing due to fatigue loading corresponding to maximum stress in the rebars of 35% of the UTS (380 MPa), an additional beam, B2-F-DC-35, was constructed with higher concrete strength. The calculated maximum fatigue compression stress acting on the top fibre of concrete was approximately 65% of f_c' (55 MPa). The flexural zone of beam B2-F-DC-35 is shown in Fig. 3.7 (d). This beam did not fail after enduring 2 million cycles of fatigue loading. The results of fatigue tests conducted on beams B1-F-DC-30 and B2-F-DC-35

instill confidence in the ability of the ribbed GFRP RC beams to withstand fatigue when the GFRP bars are subjected to maximum fatigue stress of 35% of UTS with a stress ratio of 0.4.

3.5.5 Number of fatigue cycles

The fatigue life of the tested beams is drawn in Fig. 3.12 alongside data from the literature for comparison. The available literature data comprise fatigue life results of rebars tested by Adimi et al. (1997), Noël and Soudki (2014a), Janus et al. (2019), and Janus et al. (Janus et al. 2021). Only one beam tested under a constant stress level by Janus et al. (2021) was considered in the analysis. The results of three beams tested under different loading levels were not considered and were excluded from the data due to the different nature of their test and analysis compared to tests performed in this study. Notably, all the rebars in the literature data are sand-coated, whereas the rebars tested in this study are ribbed GFRP bars without sand-coating.

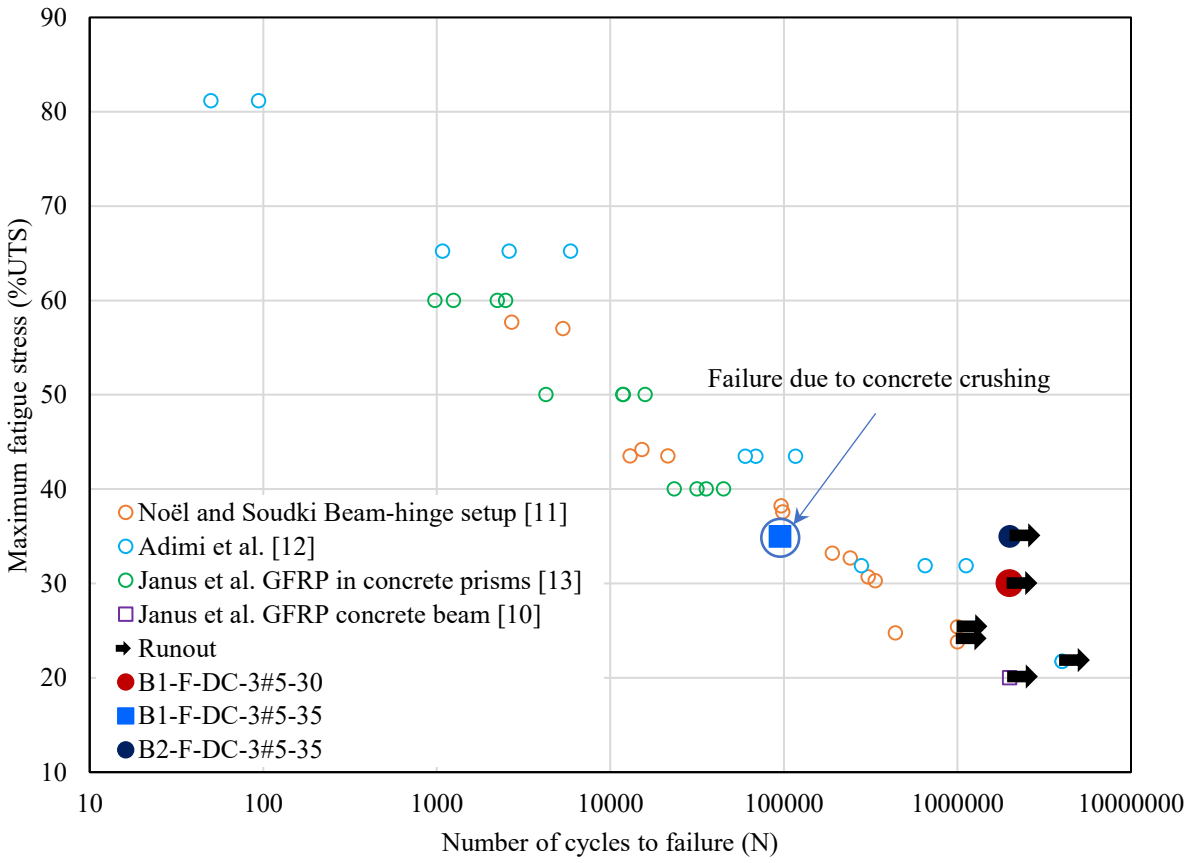

Fig. 3.12. S-N curve for the literature data and the beams tested in this study.

Fig. 3.12. presents the fatigue life of the experimental results. Some specimens displayed a runout mark, suggesting that they did not fail even after undergoing the fatigue loading cycles. Fig. 3.12. shows that the fatigue life of the tested beams is higher than the results of fatigue tests conducted on GFRP bars in the literature. Only the specimen tested by Adimi et al. (1997) survived more than 2 million cycles but was tested under lower maximum stress than the maximum fatigue stress used in this study. As shown, both beams B1-F-DC-30 and B2-F-DC-35, which survived 2 million cycles, have a higher fatigue life than the rebars tested under the same testing stresses in the literature. This high fatigue life might be justified by a few factors. The stress ratio tested in this study is 0.4, while the stress ratio of the test conducted in the literature is mostly 0.1. Last but not least, the rebar tested is ribbed GFRP, as opposed to sand-coated. The presence of sand-coating in other studies may lead to a reduction in fatigue life due to factors such as friction and initial damage caused by the sand-coating process. It is also important to note that the fatigue life of the beam B1-F-DC-35 is on the lower side of the S-N curve because of the premature failure of concrete.

3.5.6 Monotonic test after fatigue loading

Two beams survived 2 million cycles under fatigue loading. After applying 2 million cycles, the beams B1-F-DC-30 and B2-F-DC-35 underwent static loading testing until failure. The loading was applied using a displacement control rate of 1.2 mm/min. A hydraulic cylinder with a 3000 kN capacity applied a load to the beam, which was measured by a 500 kN load cell with an accuracy of ± 0.1 kN. The test setup is shown in Fig. 3.13.

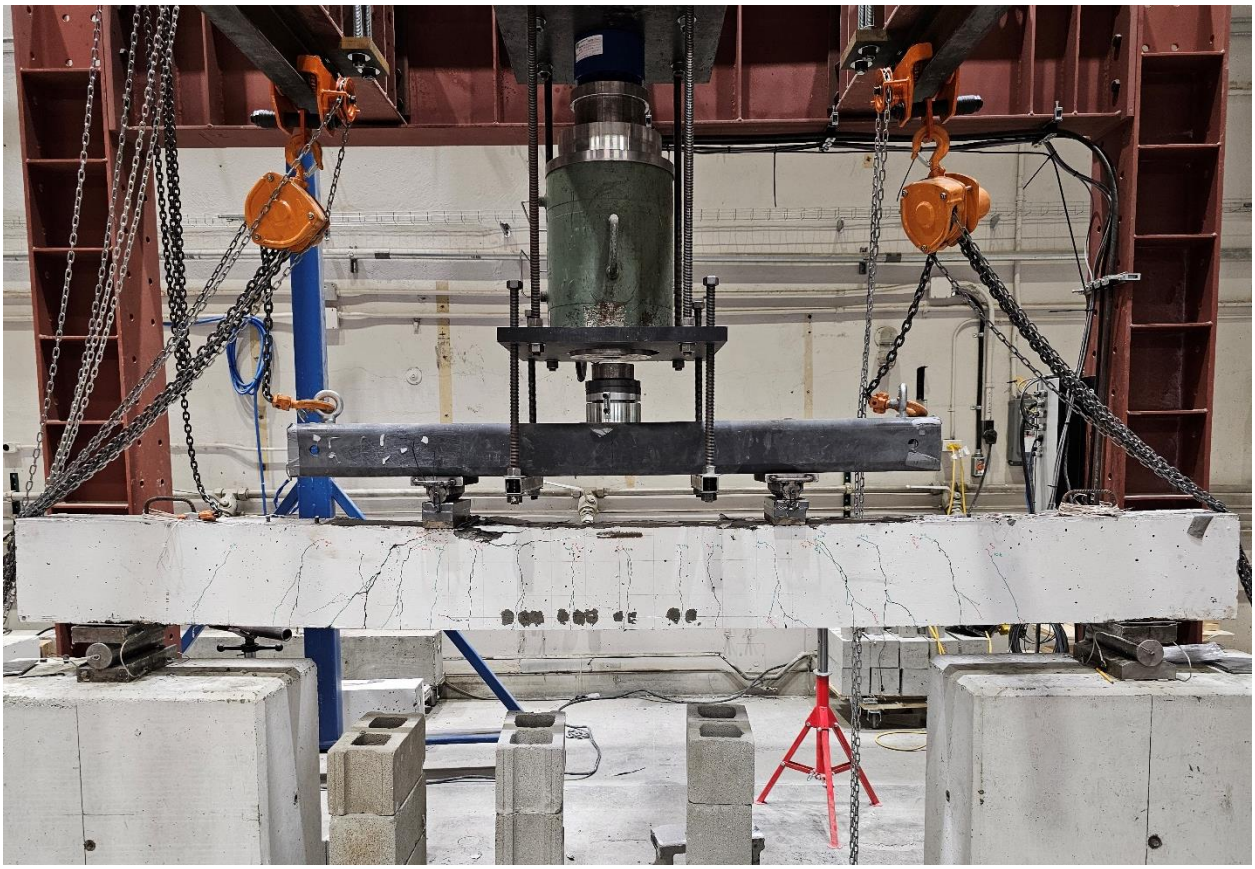

Fig. 3.13. Test setup for the beams tested after 2 million cycles of fatigue loading.

Both beams exhibited flexural failure - crushing of concrete, as shown in Fig. 3.14. The top concrete fibre is crushed at the mid-left section within the vicinity of the loading points. The failure load of beam B1-F-DC-30 was 150.7 kN (87% of the failure load of beam B1-S-DC). The load-bearing capacity of beam B1-F-DC-30 decreased by 13% after 2 million cycles compared to sample B1-S-DC. The beam B2-F-DC-35 failed with a load of 186.8 kN. No identical beam from the same concrete batch was tested for comparison.

(a) B1-F-DC-30

(b) B2-F-DC-35

Fig. 3.14. The failure mode of the beams was tested under static loads after 2 million cycles.

Fig. 3.15 displays the load-deflection curve for both beams B1-F-DC-30 and B2-F-DC-35. The beam's initial stiffness is a result of the cracked inertia. After applying the load, the beams entered a stable phase characterized by constant stiffness, with no further advancement in the number or depth of cracks. Near the end, the concrete started crushing with some drops in the loading. The deflection at the maximum load of the beam B1-F-DC-30 was 68.75 mm. There was a 1.2% variation in the maximum deflection between beams B1-F-DC-30 and B1-S-DC. For the beam B2-F-DC-35, the maximum deflection was 89.24 mm.

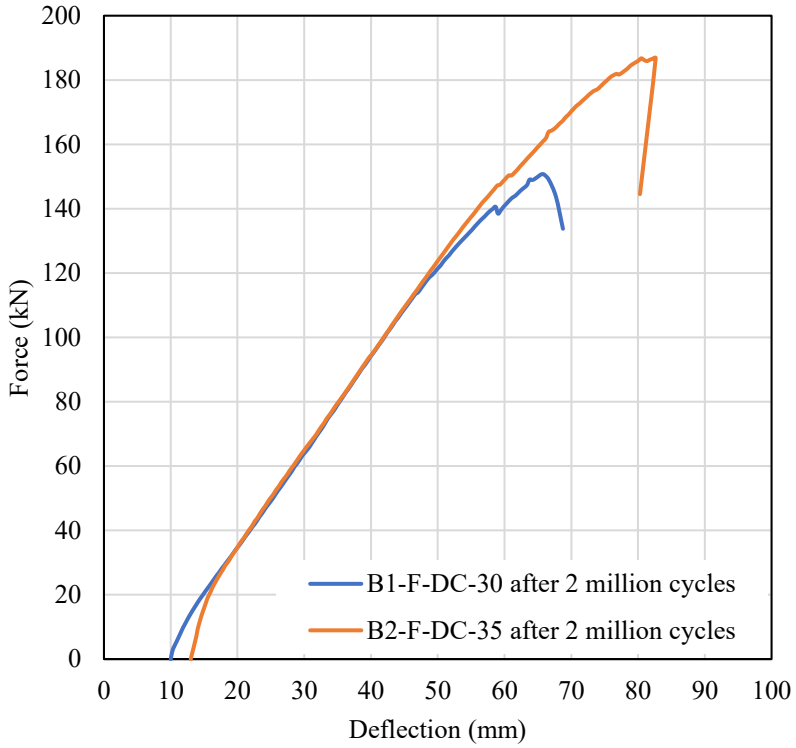

Fig. 3.15. GFRP-RC static load-deflection curves after 2 million cycles.

3.6 Summary and Conclusions

This study investigated the fatigue performance of concrete beams reinforced with ribbed GFRP bars. The experimental results reveal key insights into the cracking behaviour, deflection, and fatigue life of GFRP-RC beams. The following conclusions can be drawn from the results of this study:

1. In this study, the displacement-control scheme, wherein the target forces are kept within the desired range, proved to be the most suitable for conducting the fatigue testing of GFRP RC beams. In contrast, the force-control scheme exhibited instabilities attributed to sudden changes in beam stiffness due to cracking during fatigue testing.
2. Although performing fatigue tests at a stress ratio of 0.1 does offer conservative fatigue life for the GFRP bars, a more representative stress ratio that reflects the actual loading conditions of bridges and still can result in conservative fatigue life data is needed. This study recommends a stress ratio of 0.4 for the fatigue tests.

3. The available GFRP codes and standards do not impose limits on the concrete compression stress under fatigue loading. However, the failure of beam B1-F-DC-35 in compression emphasizes the need to consider concrete stress limits for RC elements under fatigue loading. Although no concrete compression fatigue stress limit is observed in this study, further investigation is recommended.
4. The ribbed GFRP bars used as reinforcement in the RC beams sustained 2 million cycles under maximum fatigue stresses of 30% and 35% at a stress ratio of 0.4. This suggests a potential for revising the fatigue stress limits recommended by AASHTO LRFD for GFRP and CSA S6-19. Further experimental data is required to confirm this conclusion for other types of GFRP bars available in the market.

CHAPTER 4

Tension-Tension Fatigue Behavior of Ribbed Glass Fiber-Reinforced Polymer Bars in Air

4.1 Abstract

Fatigue resistance is a crucial aspect in the design of structural components subjected to cyclic loading. Due to issues of corrosion of steel reinforcement, glass fibre-reinforced polymers are increasingly used in reinforced concrete members. However, very limited research has been conducted on the fatigue behaviour of glass fibre-reinforced polymer reinforcement. This study builds upon previous research performed at 4 Hz but also investigates low-frequency testing. Three adhesives were investigated to identify the optimal gripping system capable of withstanding fatigue loading. Non-shrink grout was determined to be the only suitable method to avoid unwanted failure modes. The study investigated stress levels ranging from 30% to 65% of the uniaxial tensile stress depending on the frequency used. Both tested frequencies gave results within the expected S-N curve as the prior studies. Moreover, the equations of Sendeckyj showed good reliability of the data. Although North American codes limit fatigue cycles between 1 and 15 Hz, this study found that the much lower investigated 0.03 to 0.04 Hz gave excellent results within the expected behaviour envelope. Low-frequency tests are attractive to testing facilities as standard universal testing machines can be used without the need for dynamic actuators.

4.2 Introduction

In use, many structural components are subjected to repetitive loading cycles. Fatigue loading is cyclic in nature and falls into two general categories, namely, low-cycle and high-cycle fatigue. When high-stress levels are applied to structures for a relatively low number of cycles, low-cycle fatigue is examined. Conversely, high-cycle fatigue occurs when low to moderate stress levels are applied to the structures. Bridges, parking garages, commercial buildings, stadiums, hospitals, wind power plants, and airport pavements are examples of structures subjected to high-cycle fatigue loading.

Due to the corrosion potential of traditional steel reinforcement, GFRP bars have emerged as a promising alternative for steel reinforcement due to their corrosion resistance, as per ACI 440.11-22 (ACI 2022). Ibrahim et al. (2023) developed design charts for replacing steel with GFRP, creating a hybrid section. Kuttagola et al. (2023) studied the behaviour of GFRP-reinforced

concrete beams as an alternative to steel bars. Given the extended service life provided by the use of GFRP, fatigue is a critical design limit state. Although the behaviour of GFRP bars under monotonic loading has been extensively studied in the past, only a limited number of studies have evaluated the fatigue life of GFRP bars (Janus et al. 2019; Noël and Soudki 2014; D'Antino et al. 2022). These studies used a relatively high frequency of 4 Hz and required specialized testing equipment.

The production technique and fibre content of GFRP materials used for reinforcement in concrete structures vary from those used in aerospace and space applications, which can impact the fatigue life of the materials (El-Ragaby 2007; Noël and Soudki 2014a). The interaction between the concrete and reinforcement can also affect the fatigue behaviour and life of GFRP bars, as per ACI PRC-215 (ACI 2021). Therefore, research studies focusing on GFRP composites used as reinforcement in concrete structures are essential.

Damage during cyclic loading of GFRP bars goes through three main stages (Ramakrishnan and Jayaraman 1993; Wu and Yao 2010), as shown in Fig. 4.1. In the first stage, the matrix starts cracking. In the second stage, one of two scenarios can occur: the initiated matrix cracks can propagate to form matrix interfacial debonding, or the matrix cracks can lead to fibre breakage. Finally, in the third stage, the GFRP bar fails. For GFRP bars, the occurrence of a single crack or rupture surface, as is typical for metals, is unlikely. Instead, failure occurs through breakage at multiple fibre cross-sections, which are then joined together by interfacial cracks within the matrix (Shirazi and Varvani-Farahani 2010).

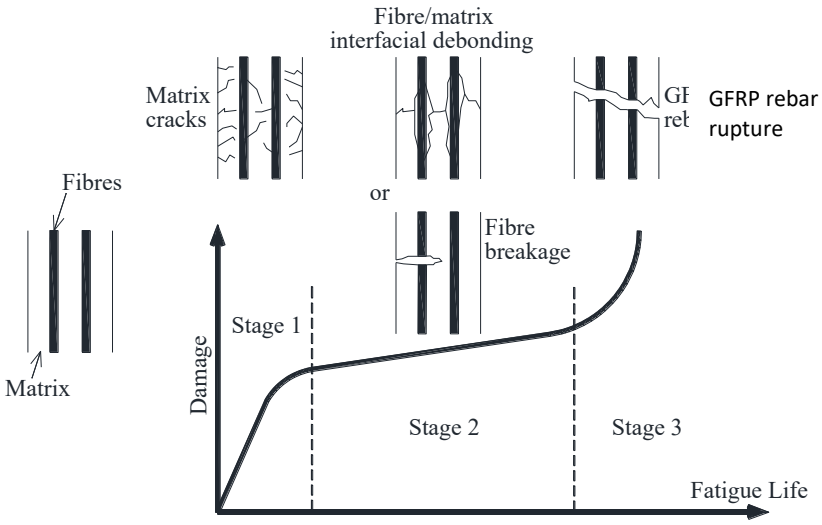

Fig. 4.1. Three stages of damage of the GFRP bars ((Ramakrishnan and Jayaraman 1993), redrawn)

Fatigue testing results in the generation of S–N curves to relate the number of cycles (N) until failure and the maximum stress (S) at failure. In those curves, S, representing the maximum stress, average stress, stress range or maximum stress as a ratio of static failure stress, is plotted on the vertical axis, and N, representing the number of cycles to failure, is plotted on the horizontal axis. Many factors affect the fatigue life of a reinforced concrete beam, namely, the maximum stress of the fatigue cycles, the stress ratio, and the load frequency (Tilly 1979). According to CSA S806:12-R21 (CSA 2021) and ACI PRC-215-21 (ACI 2021), the stress ratio is the minimum stress divided by the maximum stress.

The design codes and standards tend to unify the fatigue limit of GFRP bars regardless of variations in the bar surface profile and mechanical properties. Several important factors that directly affect the fatigue life of GFRP bars, such as the effect of the stress level, stress range, stress ratio, loading rate, surface type, and diameter, have not yet been investigated (Noël and Soudki 2014; Janus et al. 2019, 2021). Therefore, additional tests are needed to propose representative fatigue stress limits for the new generation of GFRP bars for implementation in the relevant design codes and guidelines.

Several types of tests have been performed to estimate the fatigue life of reinforcing bars, namely, axial tension in the air, axial tension in the concrete, and bending tests on beams. The axial tension-tension fatigue test is the primary test performed to evaluate the properties of any material under fatigue loads. Compared to other fatigue tests, axial tension-tension fatigue tests are easier to perform and less expensive (Tilly 1979). One of the main challenges in performing fatigue tests is gripping the GFRP bars. Many trials have been performed by researchers to find a gripping system to avoid premature failure of bars close to grip locations due to high-stress concentrations. An example of grip failure is the study by El Refai (2013), in which the failure modes were broom-shaped and occurred at the anchor zone, which is, therefore, considered a premature failure.

Noël and Soudki (2014) tested 12 sand-coated bare bars with a diameter of 16 mm under uniaxial tension-tension fatigue at 4 Hz in air (note – the study also included bars embedded in concrete cannot be directly compared). In the fatigue tests, the maximum stress was between 255 and 355 MPa (32.5% and 45.3% of the UTS), while the minimum stress was kept constant at 30 MPa (3.8% of the UTS). To ensure failure in the desired section, the cross-section of the bars was gradually tapered by approximately 43%. Fatigue failure was initiated at the minimum cross-

section, and then longitudinal cracks propagated through the matrix. Ultimately, breakage occurred in the desired middle section. Janus et al. (2019) tested eighteen bare sand-coated GFRP bars at a testing frequency of 4 Hz. The maximum stresses in the tests were 40, 50, and 60% of the UTS of the bars. Based on the S–N diagram drawn by Janus et al. (2019), the bars tested in air would not reach two million cycles. Longitudinal cracks and broomlike fragmentation were the two main failure modes that were observed during the testing of the bare bars (Janus et al. 2019). D'Antino et al. (2022) tested one sand-coated GFRP bar under a 10 Hz loading frequency in air. The tested maximum stress was 19.7% of the UTS, and the stress ratio was 10. The test was stopped after 5.1 million cycles with no apparent failure of the bar. It is noteworthy that for two studies, the tested bars were sand-coated, while only one sample tested by D'Antino et al. (2022) had a carbon fibre bundle helically wrapped around the diameter of the sand-coated bar.

Fatigue tests are commonly performed at high frequency to shorten the long duration of the tests. CSA S806:12-R21 (CSA 2021), the testing allows frequencies between 1 and 10 Hz, with 4 Hz recommended and testing terminated after 4 million cycles. According to ACI 440.3R-12 (ACI 2012), the number of cycles required for fatigue failure should range between 1000 and 2 million cycles. ACI 440.3R-12 (ACI 2012) has similar limits as CSA S806:12-R21 (CSA 2021) for the loading frequency, but the test may stop after 2 million cycles. For plain concrete, ACI PRC-215-21 (ACI 2021) stated that the frequency of fatigue tests has a minimal effect when tested between 1 and 15 Hz. On the other hand, tests performed at a frequency of 1/16 Hz have a one-order of magnitude lower fatigue life than tests performed at 4 Hz (ACI PRC-215 2021).

4.3 Research Significance

This study contributes to the state of the art by offering new information and experimental evidence on the tension-tension fatigue behaviour of ribbed glass fibre-reinforced polymer (GFRP) bars in the air. The fatigue characteristics of ribbed GFRP bars were evaluated, quantified, and compared with the results of the literature. The available literature utilizes high-cycle tests which require dynamic actuators. This study demonstrated that low-cycle tests that can be accomplished with standard universal testing machines give good results and eliminate the need for dynamic actuators.

4.4 Experimental Program

As seen from the available literature, very few fatigue tests on GFRP bars have been performed. As of yet, no fatigue tests have been performed on ribbed GFRP bars, with only sand-coated bars investigated previously. Also, others have not attempted testing at low frequency. The advantage of this low-frequency testing is that it does not require expensive specialized testing machines, and based on the author's experience, there is no need for highly skilled experts to operate them. To address the gaps in the literature, this study aims to present the results of fatigue tests performed on ribbed GFRP bars with two loading frequencies. One loading frequency of 4 Hz (equivalent to strain rates ranging from 0.04 to 0.06 ε/sec) was selected as it corresponds to previous studies. Also investigated was a low frequency of 0.03 to 0.04 Hz (equivalent to a strain rate of $0.00067\varepsilon/sec$). As mentioned, gripping GFRP bars is one of the challenges for testing. Three different gripping methods were investigated in this study to address this. In all gripping methods, each end of the GFRP bar was anchored inside a steel tube with an outside diameter of 42 mm, wall thickness of 4.85 mm, and length of 635 mm, which is a larger tube than the recommendations of ASTM D7205/D7205M (ASTM 2021). All the GFRP bars were 1780 mm long, with a free length of the bar between the anchors of 40 times the diameter of the bar (510 mm). The difference in gripping systems was the type of adhesive used to anchor the GFRP bars inside the tubes. A number of maximum applied stresses as a percentage of UTS was investigated depending on fatigue frequency, which is explained in subsequent sections. In all cases, the minimum applied stress was 10% of the maximum stress (a stress ratio of 10). In the results sections, specimens are designated as follows: the first letter (L/H) indicates the frequency, L for low and H for high-frequency; the second letter (Ex, Ep, or NS) indicates the grout type, Ex for expansive grout, Ep for two-compound epoxy (Dewalt 110+), and NS for non-shrink grout (Sika grout-212); and the third number (#4) indicates the bar size. The fourth number indicates the maximum fatigue stress as a percentage of the UTS, and the last number (S1, S2, or S3) indicates the numbering of similarly tested bars (duplicates or triplicates).

Each bar had a nominal diameter of 12.7 mm (No. 4), as shown in Fig. 4.2, and a similar size to that of prior studies. The nominal area of the GFRP bars (129 mm^2), as per ASTM D7957/D7957M (ASTM 2017), was considered when calculating the tensile properties. As per the manufacturer, the fibre content is 76% weight fraction. Five ribbed GFRP bars were tested under monotonic loading according to ASTM D7205/D7205M (ASTM 2021) to identify their

mechanical properties. The resulting average ultimate tensile strength (UTS) was found to be 1096 ± 43.4 MPa, and the Modulus of Elasticity was 57.6 ± 1.0 GPa.

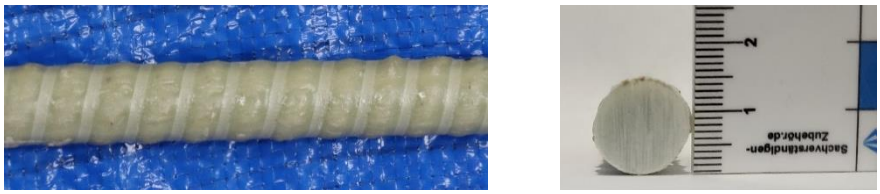

Fig. 4.2. Ribbed GFRP bar

4.5 Experimental details for GFRP bars tested at low-frequency fatigue loading

Fourteen ribbed GFRP bars were tested under maximum fatigue stresses of 50, 55, 60, and 65% of the UTS while maintaining a stress ratio of 10. Six bars were tested with expansive grout (expansive demolition grout) used as an adhesive to anchor the bars (samples labelled Ex). All the bars failed prematurely either inside the tubes or with longitudinal cracks near the grips, as shown in Fig. 4.3 (a and b). The underlying cause of these premature failures might be ascribed to the elevated temperatures generated during the curing process of the expansive grout or the transverse stresses caused by grout expansion, which can reduce the bar strength. This temperature increases potentially exceeded the glass transition temperature of the bars (T_g), thereby damaging the bars enclosed within the tubes and contributing to their premature failure. Despite the fact that FRP bars are non-combustible when placed inside concrete, the epoxy will nonetheless undergo softening. The temperature at which this softening occurs is known as the glass transition temperature (T_g). After passing the glass transition temperature (T_g), the elastic modulus experiences a substantial decrease. The glass transition temperature is determined by the type of resin used and often falls within the range of 65–120 °C (Alsayed et al. 2012). It is important to note that the expansive grout temperature was not measured; however, the grout mix was observed to reach its boiling point at some point during its curing process. Only one bar was tested, and the tubes were filled with a two-compound epoxy adhesive (samples labelled Ep). This use of a two-compound epoxy resulted in premature rupture of the bar within the tube, similar to Fig. 4.3 (b). After applying the fatigue cycles, the steel tubes filled with epoxy became very hot, making them difficult to touch. This gripping technique was not studied further in low-cycle testing. The third adhesive investigated was a non-shrink grout in hopes of overcoming the shortcomings of expansive grout and two-compound epoxy adhesive (samples labelled NS). Seven fatigue tests

were conducted for this adhesive, all of which took place three days after the pouring of the non-shrink grout to allow for the curing of the non-shrink grout. Out of seven samples, only one sample failed prematurely due to an unexpected power outage during the test, as shown in Fig. 4.3 (c and d).

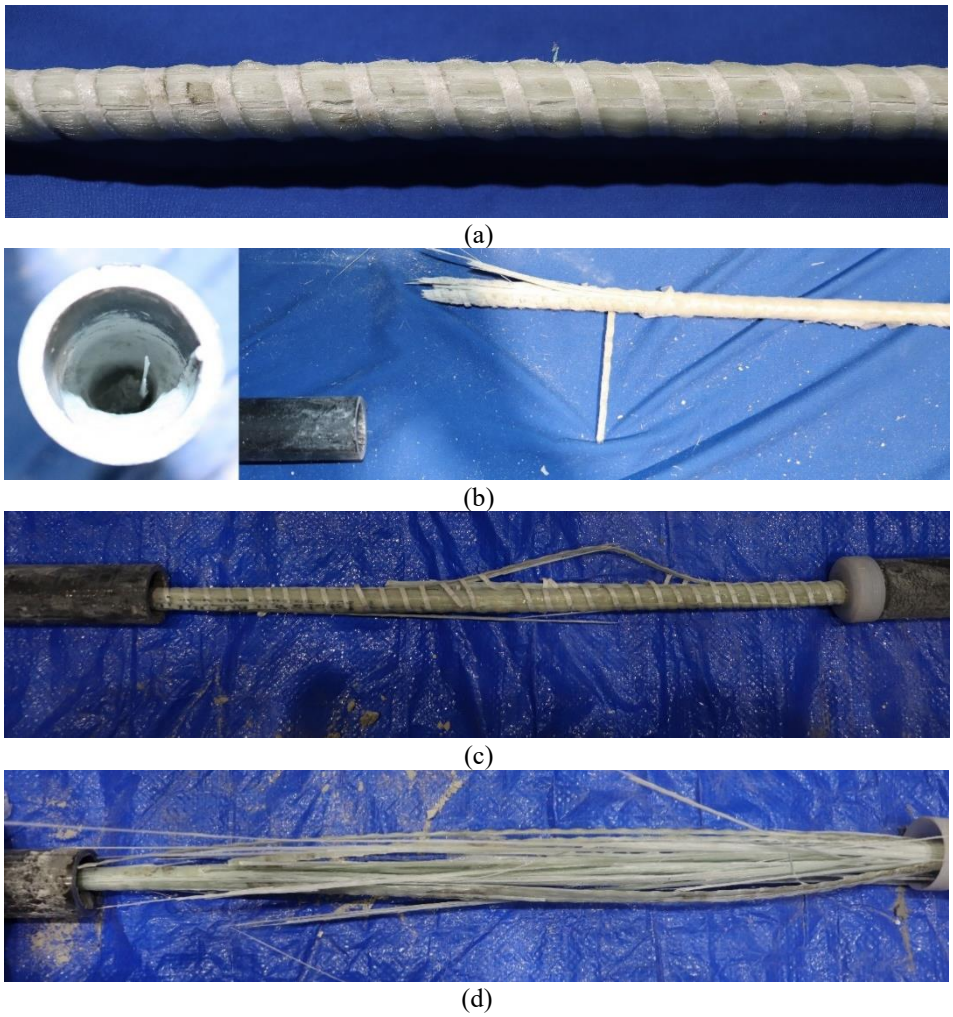

Fig. 4.3. Failure modes of GFRP bars (a) Longitudinal cracks near grips; (b) Rupture inside the tube; (c) Longitudinal cracks; and (d) Broomlike failure

The low-cycle fatigue tests were conducted using a universal testing machine, as shown in Fig. 4.4 (a). To ensure precise force control, a closed-loop control system was implemented and tuned, wherein the system was fed with both the maximum and minimum cycling forces. High-alloy steel vee-wedge grips were employed to hold the steel tubes securely at their midpoint, as shown in Fig. 4.4 (b). The fatigue cycles were performed at a constant loading rate of 5 kN/sec (38.8 MPa/sec),

translating to a strain rate of $0.00067\varepsilon/sec$. By maintaining a constant loading rate of 5 kN/sec while testing the specimens under varying maximum fatigue stress levels, the loading frequency for each specimen varied between 0.03 to 0.04 Hz. This loading frequency range is lower than the typical loading frequencies employed in fatigue tests. The maximum stress applied for this work was relatively high compared to the fatigue stresses allowed in the codes. A low loading rate necessitates high-stress values to ensure a reasonable testing duration. The stress ratio (maximum stress/minimum stress) is kept constant at 10.

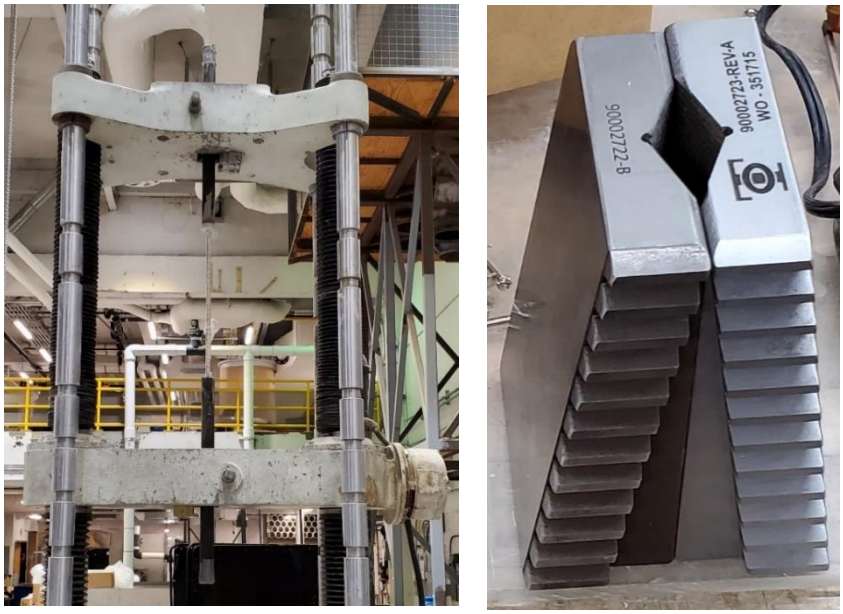

(a) (b)

Fig. 4.4. Test setup and grips (a) Test setup; (b) Vee-wedge grips.

The fatigue life of the GFRP bars tested under low-cycle fatigue is summarized in Table 4.1. As shown in Table 4.1, there was a significant variation in the fatigue life of the GFRP bars, as previously reported by other researchers (Noël 2019). Moreover, longitudinal cracks were the primary failure mode for the bar (see Fig. 4.3 (c)). All tests performed in this study were stopped after any sudden reduction (25% drop) in the testing force for safety reasons; this might have prevented the full breakage of the bars. The specimen (L-NS-#4-50-S1) exhibited a broom-shaped failure mode, as shown in Fig. 4.3 (d).

Table 4.1. The fatigue life of the tested GFRP bars (low-cycle).

Name	Max. fatigue stress (%UTS)	Max. fatigue stress (MPa)	Stress Ratio	Fatigue life (Cycles)	Failure mode	Grout type	No. of testing hours
L-Ex-#4-65-S1	65	713	0.1	409*	Longitudinal cracks near grips	Expansive grout	4
L-Ex-#4-65-S2	65	713		178*	Rupture inside the tube	Expansive grout	2
L-Ex-#4-60-S1	60	658		591*	Longitudinal cracks near grips	Expansive grout	5
L-Ex-#4-55-S1	55	603		1158*	Rupture inside the tube	Expansive grout	9
L-Ex-#4-55-S2	55	603		2865*	Longitudinal cracks near grips	Expansive grout	22
L-Ex-#4-50-S1	50	548		2042*	Rupture inside the tube	Expansive grout	14
L-Ep-#4-50-S1	50	548		3345*	Rupture inside the tube	Epoxy	24
L-NS-#4-60-S1	60	658		5682	Longitudinal cracks	Non-shrink grout	48
L-NS-#4-60-S2	60	658		8696	Longitudinal cracks	Non-shrink grout	74
L-NS-#4-55-S1	55	603		5350	Longitudinal cracks	Non-shrink grout	42
L-NS-#4-55-S2	55	603		14376	Longitudinal cracks	Non-shrink grout	112
L-NS-#4-50-S1	50	548		12048	Broomlike	Non-shrink grout	85
L-NS-#4-50-S2	50	548		24774	Longitudinal cracks	Non-shrink grout	175
L-NS-#4-50-S3	50	548		13107*	Failed early due to Power-outage	Non-shrink grout	93
* The fatigue life of samples with premature failure is not used in the analysis.							

4.6 Experimental details of GFRP bars tested at higher frequency fatigue loading

Ten ribbed GFRP bars were tested in a similar manner to the low-frequency loading tests. The main difference was that the outside diameter of the steel tubes was reduced from 42 mm to 35 mm over a length of 170 mm to mitigate stress concentration at the grip (see Fig. 4.5). A dynamic actuator with a capacity of 1500 kN was used to apply tension-tension fatigue loading on the bars (see Fig. 4.6 (a)). Steel vee-wedge grips are used to grip the steel tubes at the end of each bar by applying hydraulic pressure, as shown in Fig. 4.6 (b).

Fig. 4.5. Steel tubes used for fatigue testing

(a) (b)

Fig. 4.6. Test setup for high-cycle fatigue tests and Vee-wedge grips (a) Test setup and (b) Vee-wedge grips

Fatigue loading was applied on the bars at a frequency of 4 Hz. The maximum fatigue stress as a percentage of the ultimate tensile strength (UTS) ranges between 30% and 50%. The maximum fatigue stress of 30% of the UTS is chosen because it is 5% higher than the limits available in CSA S806:12-R21 (CSA 2021) and AASHTO LRFD for GFRP (2018). Like in the case of low-cycle fatigue tests, in the high-cycle fatigue tests, the stress ratio was 10. The fatigue life of the tested GFRP bars is listed in Table 4.2.

Table 4.2. The fatigue life of the tested GFRP bars (high-cycle)

Name	Max. fatigue stress (%UTS)	Max. fatigue stress (MPa)	Stress Ratio	Fatigue life (Cycles)	Failure mode	Test duration (Hrs.)	Grout type
H-Ex-#4-30-S1	30	329	0.1	450700*	Rupture inside the tube	31.3	Expansive grout
H-Ep-#4-30-S1	30	329		>2000000	Not failed	138.9	Epoxy
H-Ep-#4-30-S2	30	329		>2000000	Not failed	138.9	Epoxy
H-Ep-#4-35-S1	35	384		83075*	Rupture inside the tube	5.8	Epoxy
H-Ep-#4-35-S2	35	384		57865*	Rupture inside the tube	4.0	Epoxy
H-Ep-#4-50-S1	50	548		6073*	Rupture inside the tube	0.4	Epoxy
H-NS-#4-35-S1	35	384		610686	Longitudinal cracks	42.4	Non-shrink grout
H-NS-#4-35-S2	35	384		1589067	Longitudinal cracks beside grips	110.4	Non-shrink grout
H-NS-#4-50-S1	50	548		33107	Longitudinal cracks beside grips	2.3	Non-shrink grout
H-NS-#4-50-S2	50	548		17965	Longitudinal cracks	1.2	Non-shrink grout

* The fatigue life of samples with premature failure is not used in the analysis.

An algorithm was devised to employ fatigue loading through displacement control rather than force control. In this process, the displacements were automatically adjusted to reach the target forces (i.e., minimum and maximum) with a margin of error within 1% of the target force at each cycle. This protocol was developed to track the strain progression of a bar near failure, to prevent abrupt failure due to safety measures, and to eliminate any overshooting of the forces during loading near failure.

The tubes of one specimen (H-Ex-#4-30-S1) are filled with expansive grout. This specimen was tested with maximum fatigue stress of 30% of the UTS and failed prematurely inside the tube, as

shown in Fig. 4.7 (a). This type of adhesive is not used further in the high-frequency tests. A total of five tests were conducted using a two-compound epoxy. Two bars, H-Ep-#4-30-S1 and H-Ep-#4-30-S2, were tested under 30% of the UTS; they reached 2 million cycles without any sign of failure. The maximum stress was then increased to 35% and 50% of the UTS in specimens H-Ep-#4-35-S1, H-Ep-#4-35-S2, and H-Ep-#4-50-S1, respectively. The epoxy adhesive proved problematic in the low-frequency tests as well. The remaining 4 GFRP bars, H-NS-#4-35-S1, H-NS-#4-35-S2, H-NS-#4-50-S1, and H-NS-#4-50-S2, were tested with steel tubes filled with non-shrink grout. Similar to the bars tested at low frequency, longitudinal cracks were the primary failure mode, as shown in Fig. 4.7. (c and d). Table 4.2 shows the fatigue life of the GFRP bars tested at higher frequencies.

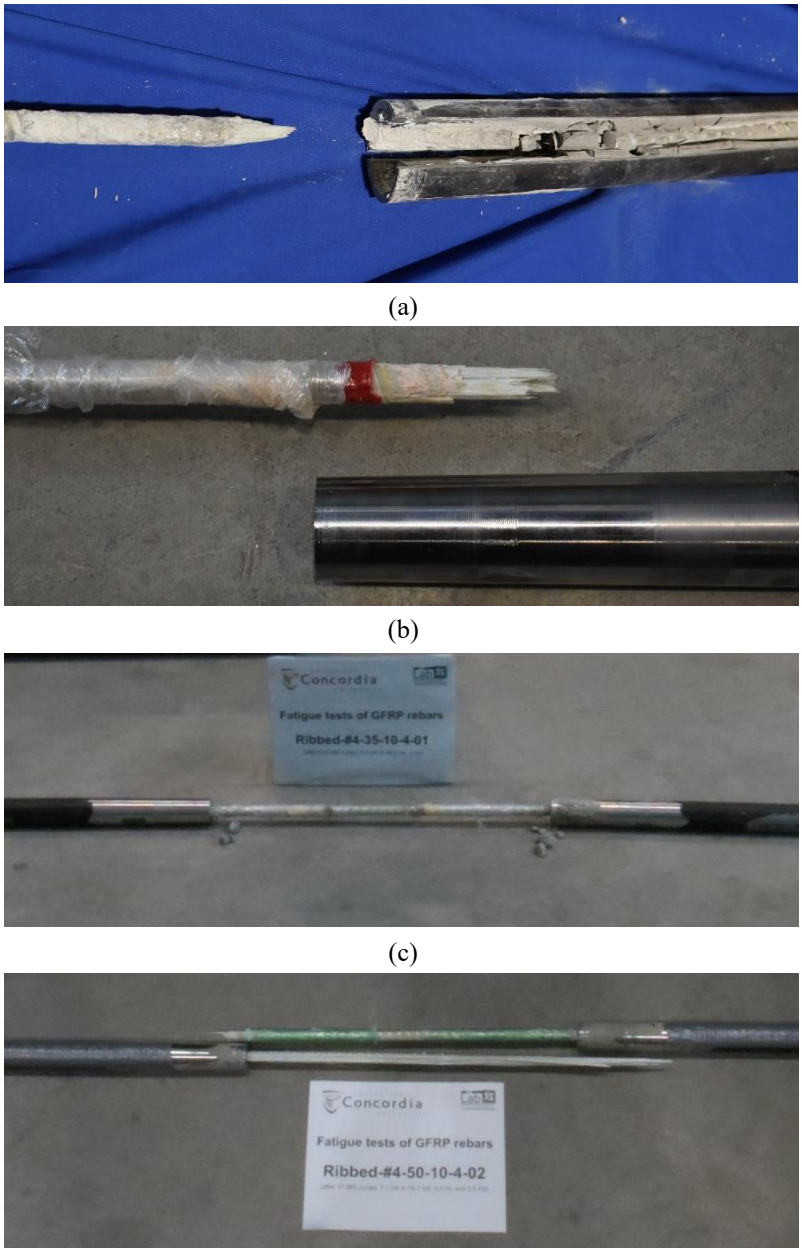

Fig. 4.7. Failure modes of high-cycle fatigue GFRP bars (a) H-Ex-#4-30-S1 (rupture inside the tube); (b) H-Ep-#4-35-S1 (Rupture inside the tube); (c) H-NS-#4-35-S1 (longitudinal cracks); and (d) H-NS-#4-50-S2 (longitudinal cracks beside grips

To investigate the damage to the GFRP bar during fatigue cycles, one of the bars tested under 30% of the UTS, H-Ep-#4-30-S1, was tested monotonically as per ASTM D7205/D7205M (ASTM 2021) after 2 million cycles of fatigue testing. The maximum strength of the bar is 1124 MPa, which is higher than the average tensile strength of the GFRP bars. This sample had a broom-

like failure mode (see Fig. 4.8). The modulus of elasticity was 56.3 GPa, representing a marginal 2.25% loss in the modulus of elasticity after 2 million cycles. The results indicate that the bar had no damage after 2 million cycles. The second bar, H-Ep-#4-30-S2, was damaged due to a power outage, so no duplicate monotonic tensile test data were available.

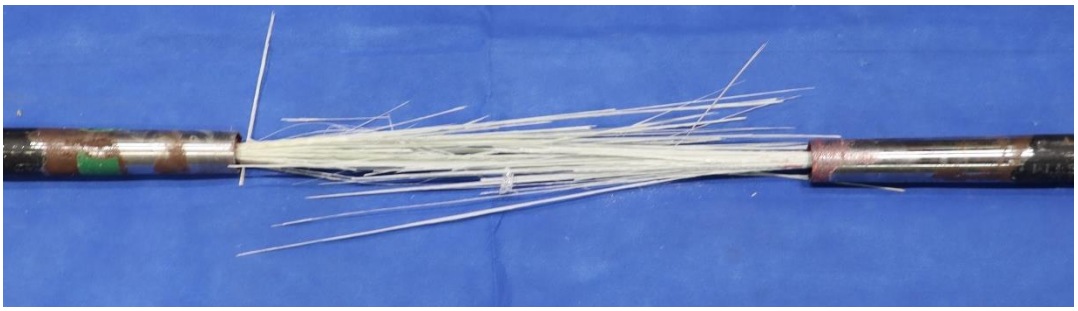

Fig. 4.8. Broom-like failure of specimen H-Ep-#4-30-S1 after 2 million cycles

4.6.1 Probabilistic models for the GFRP fatigue life

There is a large scatter in the fatigue life data in the literature for composite materials, which can be caused by factors such as fibre content variation and defects (Noël 2019). For example, the progression of initial crack propagation to failure will vary between bars and batches, and the data scatter has been reported to be more than one order of magnitude (Noël 2019). Due to the large scatter in fatigue life data, many models have been developed to describe fatigue life, considering a statistical distribution.

The S-N curve can be derived using Eq. (1) and Eq. (2) for any reliability level (Sendeckyj 1981).

$$\sigma_a = \beta\{-\ln\big(P(N)\big)^{\frac{1}{\alpha}}\}[(N-A)C]^{-D} \quad (1)$$

$$A = -\frac{1-C}{\mathrm{C}} \quad (2)$$

where σ_a represents the maximum applied fatigue stress (known), N is the number of cycles until failure (measured), and P(N) is the desired probability of survival after N cycles (for example, 95%). The constants C and D are calibrated coefficients. The constants α and β are determined by Weibull distribution. The calibration coefficients C and D and Weibull distribution coefficients α and β are calculated through an iterative process to draw the S–N curve. The Sendeckyj method of fitting the Weibull distribution (Sendeckyj 1981) was used to calibrate the data for the low- and higher-frequency fatigue tests performed in this study as it yields accurate and representative

reliability curves. This method was also used on sand-coated bars of similar size and testing frequency (4 Hz) Noël and Soudki (2014).

4.6.2 Fatigue life of GFRP tested at low frequency

The results reported in the literature and the data from this study are shown in Fig. 4.9. The fatigue testing frequency used by Noël and Soudki (2014) and Janus et al. (2019) was 4 Hz, whereas the low-frequency tests performed at two orders of magnitude less (0.03 to 0.04 Hz). The vertical axis of Fig. 4.9 shows the maximum applied fatigue stress as a percentage of the UTS determined by the monotonic tests. The number of fatigue cycles representing the fatigue life is shown on the horizontal axis.

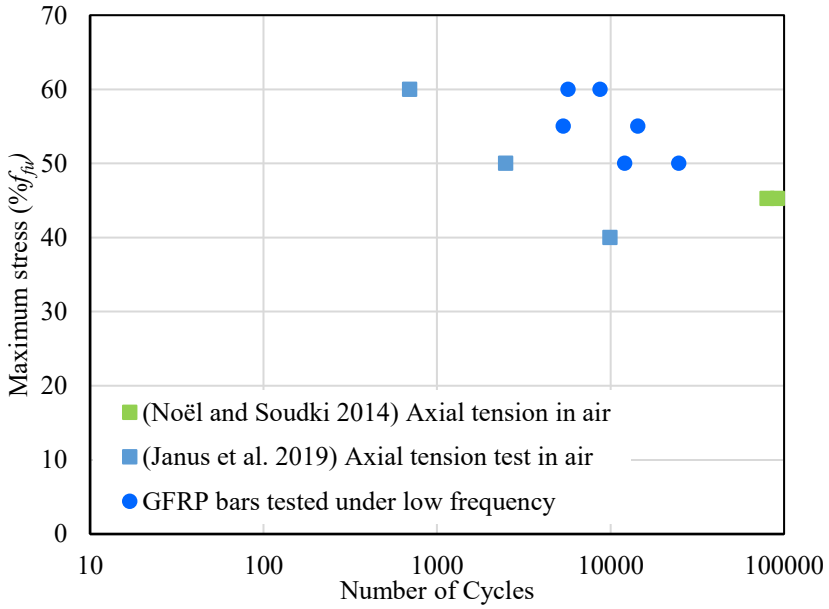

Fig. 4.9. S-N curve for the GFRP bars

As shown in Fig. 4.9, there was good agreement between the fatigue life of the GFRP bars tested in this study and those reported in the literature. Although the test frequency was almost 100 times lower, the fatigue life can be representative and within the expected range.

The coefficients α, β, C, and D were calibrated with the maximum likelihood method and found to be 26.07, 101.02, 0.0379, and 0.097, respectively. The maximum likelihood method was employed to estimate the coefficients of a probabilistic function by maximizing the likelihood function (Rossi 2018). The 95% confidence intervals are drawn in Fig. 4.10 for the GFRP bars tested in air at a low frequency.

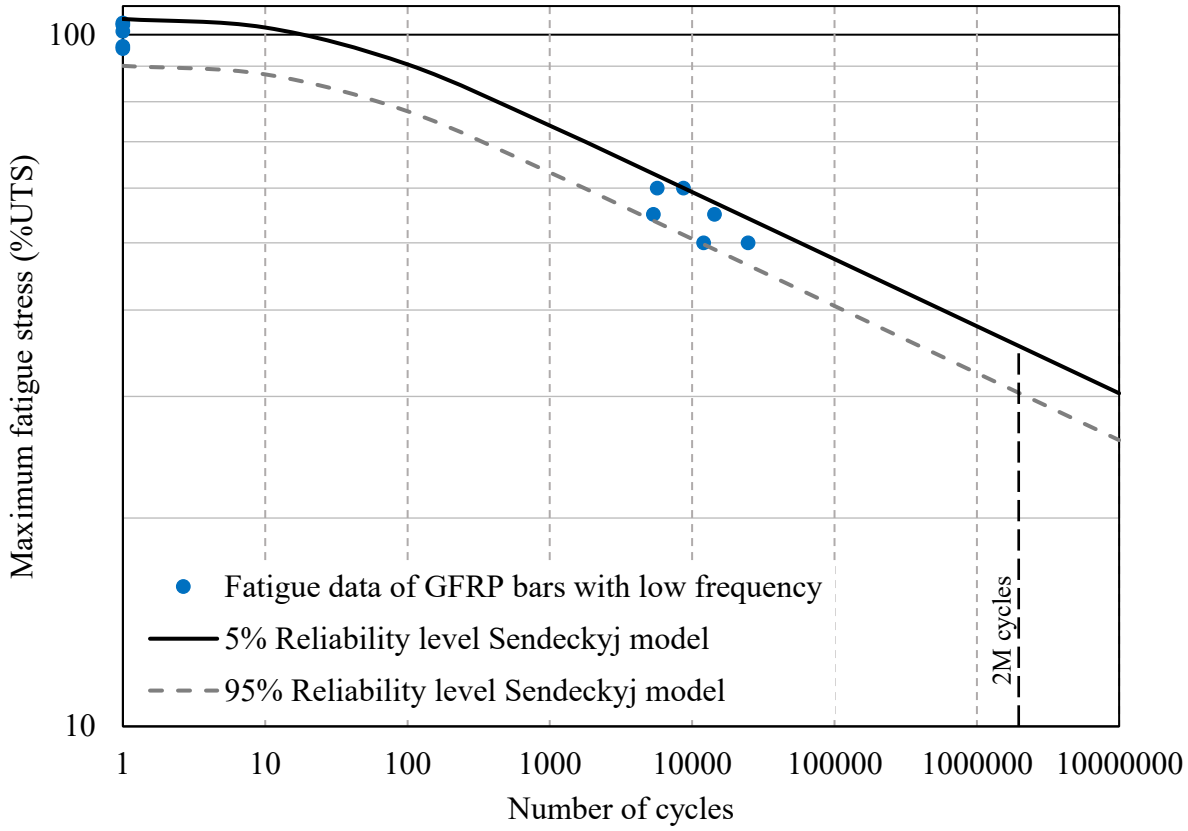

Fig. 4.10. Fitting GFRP bars tested at low frequency to Sendeckyj model

Table 4.3. Maximum fatigue stress with 5% (P5) and 95% (P95) reliability for GFRP bars tested under low frequency

Number of cycles to failure	P5 Maximum stress	P95 Maximum stress
	%UTS	%UTS
1 M	37.9	32.4
2 M	35.4	30.3
10 M	30.3	25.9

As shown in Fig. 4.9 and 4.10, the fatigue life for low-frequency tests is well described by the Sendeckyj model. The slope tends to decrease in the low-cycle fatigue range until 100 cycles. The expected fatigue life at low stresses is shown in Table 4.3.

As shown in Table 4.3, the estimated fatigue stress acting on the GFRP bars to survive 2 million cycles ranges from 30.3% to 35.4% of the UTS. This estimate is higher than the levels mentioned in the codes.

4.6.3 Fatigue life of GFRP bars tested at higher frequency

The fatigue lives of the tested bars in the literature, along with those of the GFRP bars tested in this study at both low and higher frequencies, are shown in Fig. 4.11. The maximum fatigue stress, as a percentage of the UTS, is drawn on the vertical axis, and the number of cycles to failure is drawn on the logarithmic scale on the horizontal axis.

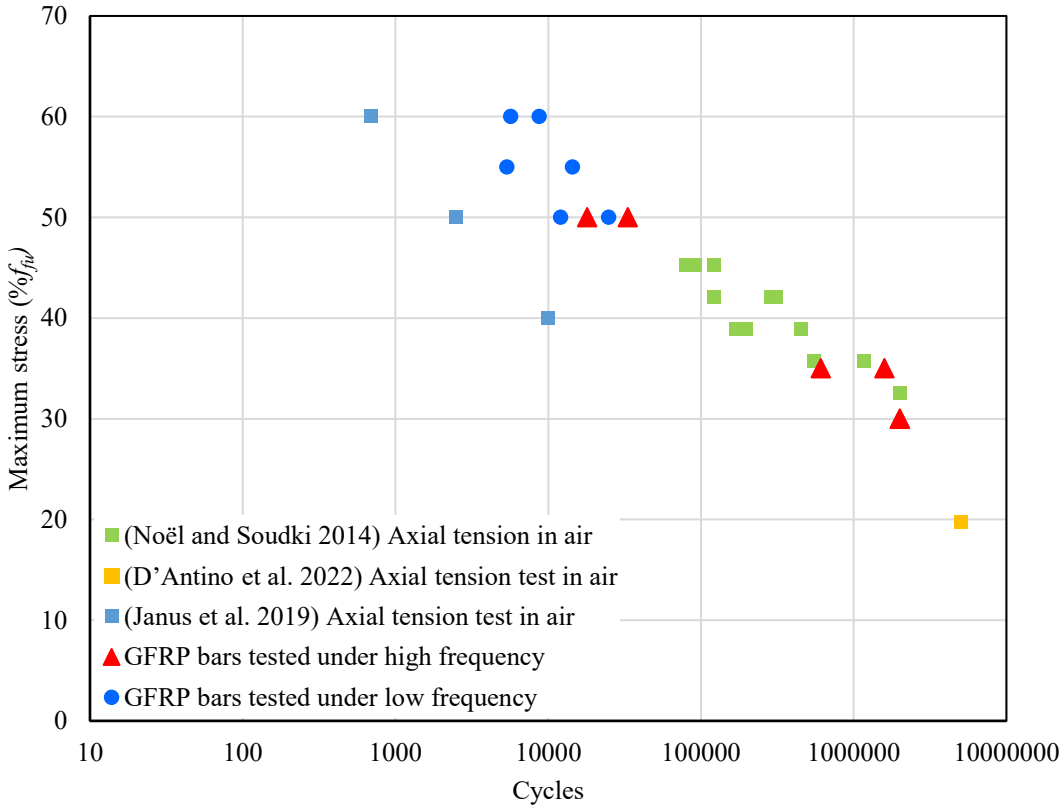

Fig. 4.11. S-N curve for the GFRP bars at both frequencies

As shown in Fig. 4.11, the fatigue life of the tested bars agrees well with those tested in the literature. The GFRP bars tested in this study have a higher fatigue life than the bars tested by Janus et al. (2019). However, the fatigue life matches the tests performed by Noël and Soudki (2014). The sand-coated bars tested by Noël and Soudki (2014) were ground to ensure that failure occurred in the desired middle section, while in this study, no grinding was needed.

The mechanical properties (E and UTS) affect the fatigue life, as does the grinding process. Grinding the surface can remove the surface microcracks initiated during the sand-coating process,

thereby increasing the fatigue life (Noël and Soudki 2014a). The comparison between this study, the results of Noël and Soudki (2014), and Janus et al. (2019) is performed because the available standards and guidelines limit the fatigue stresses as a percentage of the UTS (AASHTO LRFD for GFRP 2018; CSA S6 2019; CSA S806 2021; ACI 440.11 2022). The large difference between the fatigue life observed by Noël and Soudki (2014) and Janus et al. (2019) may suggest that code limits should be revisited to be dependent on variables including, but not limited to, mean stress level, stress ratio, modulus of elasticity of the GFRP bars, and UTS.

To directly compare the effect of frequency on fatigue life, four bars were tested at the same stress level (50% of the UTS): two at low frequency (L-NS-#4-50-S1 and L-NS-#4-50-S2) and two at higher frequency (H-NS-#4-50-S1 and H-NS-#4-50-S2). The average fatigue life obtained from the bars tested at 4 Hz is 25,536 cycles, whereas it is 18,411 cycles at a low frequency. The average number of cycles to failure is approximately 38% greater for the higher-frequency bars, but the individual data points overlap in a range of failure cycles. Although this high scatter in the fatigue life data might be expected (Janus et al. 2019; Noël and Soudki 2014a), it is difficult to draw statistically reliable conclusions.

The Sendeckyj model S-N-P is shown in Fig. 4.12 for the high-frequency tests. The α, β, C, and D coefficients are 37.1, 102.59, 0.149, and 0.087, respectively. As shown, the Sendeckyj model described the fatigue data well. Similar to the low-cycle fatigue results, the slope tends to decrease in the low-cycle failure range.

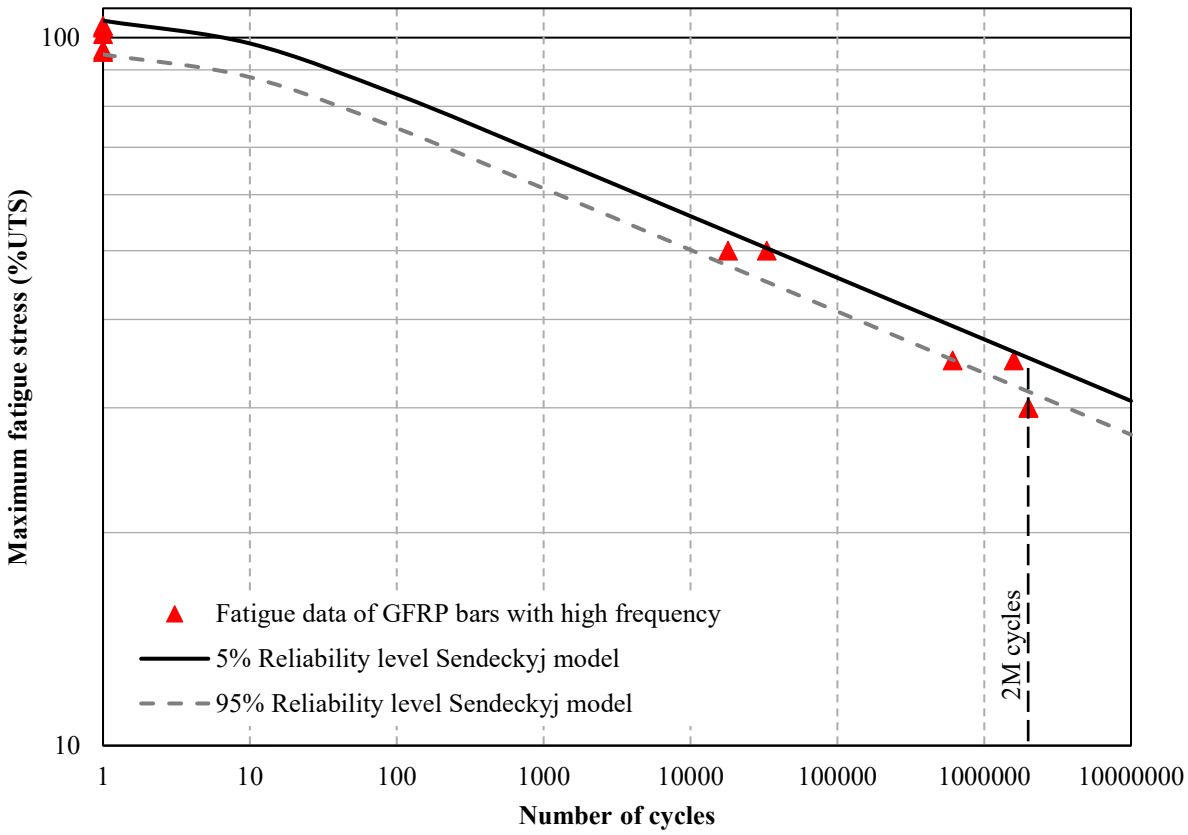

Fig. 4.12. Fitting GFRP bars tested at high frequency to Sendeckyj model

Table 4.4. Maximum fatigue stress with 5% (P5) and 95% (P95) reliability for GFRP bars tested under high frequency

Number of cycles to failure	P5 Maximum stress	P95 Maximum stress
	%UTS	%UTS
1 M	37.4	33.6
2 M	35.3	31.6
10 M	30.7	27.5

The estimated maximum fatigue stress required to survive different fatigue lives is listed in Table 4.4. As shown in Table 4.4, the estimated fatigue stress, which can be applied to the GFRP bars to survive 2 million cycles, ranged from 31.6% to 35.3% of the UTS. The fatigue life estimated from low-cycle fatigue is very slightly lower than that from high-cycle fatigue. The S-N-P curves of both the low- and high-cycle fatigue bars are shown in Fig. 4.13.

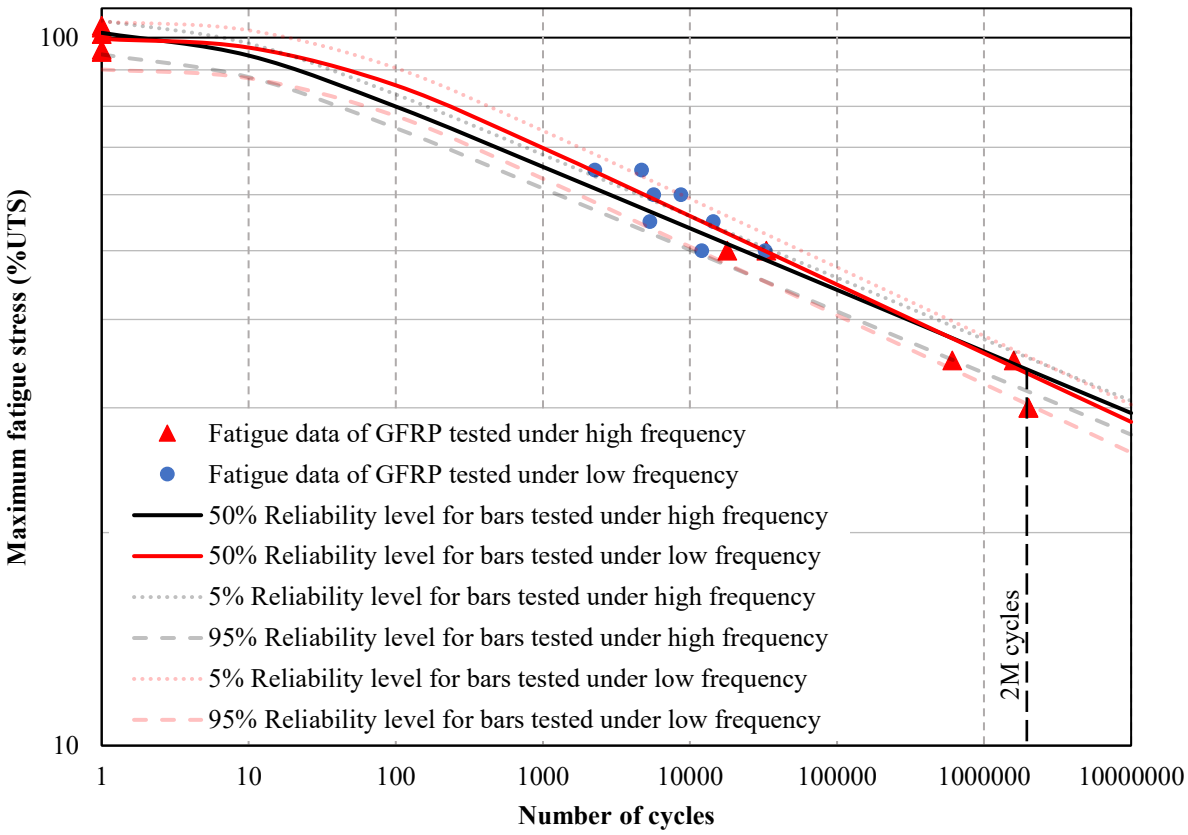

Fig. 4.13. S-N curve for GFRP bars tested at high and low frequencies (analyzed separately)

As shown in Fig. 4.13, both S-N curves fitted using the Sendeckyj model can describe the data well. It can be seen from the curves that the low-frequency fatigue tests overestimated the fatigue life in the low-cycle fatigue zone (i.e., maximum stress of approximately 40% of the UTS or greater). However, in the high-cycle fatigue range (i.e., maximum stress of approximately 40% of the UTS or lower), the low-frequency S-N curve slightly underestimates the fatigue life. This finding agrees with previous observations of the data provided in Table 4.3 and Table 4.4.

It can be concluded from the previous sections that the bars tested with low and higher frequencies follow the same trend and are within the same scatter band. Therefore, the results of both tests were analyzed together to improve the statistical model. The S-N-P curve for GFRP bars tested under low and higher frequencies is shown in Fig. 4.14. The α, β, C, and D coefficients are 25.4, 101.99, 0.038, and 0.097, respectively. The slope and trend of the S-N curve follow the same pattern as in Figs. 12 and 14. The estimated maximum fatigue stress required to survive different fatigue lives is listed in Table 4.5. For the combined results, the estimated fatigue stress, which

can be applied to GFRP bars to survive 2 million cycles, ranges from 30.5% to 35.8% of the UTS. This range was similar to the separate analyses shown in Tables 4.3 and 4.4.

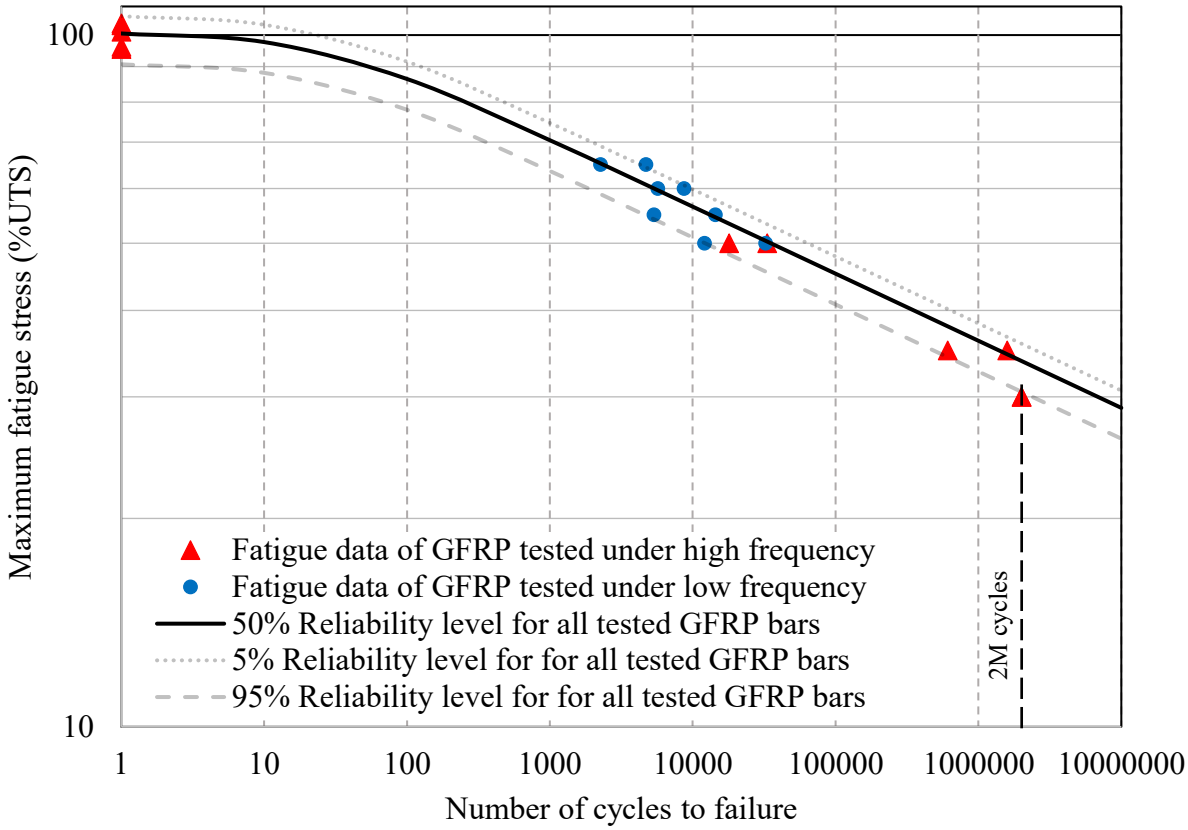

Fig. 4.14. S-N curve for GFRP bars tested at high and low frequencies (analyzed together)

Table 4.5. Maximum fatigue stress with 5% (P5) and 95% (P95) reliability for GFRP bars tested under high and low frequencies (analyzed together)

Number of cycles to failure	P5 Maximum stress	P95 Maximum stress
	%UTS	%UTS
1 M	38.3	32.6
2 M	35.8	30.5
10 M	30.6	26.1

Given S-N curves estimate the fatigue life of the GFRP bars well, it can be concluded from the curve that the low-frequency test results can be used as a conservative indication of fatigue life. This observation is quite significant from a testing perspective as low frequency tests can be

performed using more accessible universal testing machines without the need for expensive dynamic actuators.

4.6.4 Modulus of Elasticity and Maximum Strain

During the high-cycle fatigue tests, an extensometer with a 1-inch (25.4 mm) gauge length was used to measure the elongation of the bars. The strain was measured for 4 of the 6 bars that did not fail prematurely, i.e., H-NS-#4-35-S1, H-NS-#4-35-S2, H-NS-#4-50-S1, and H-NS-#4-50-S2. The modulus of elasticity of the GFRP bars was calculated as the second slope between the maximum and minimum applied stresses. The calculated values of E throughout the cycles and the mean value modulus of elasticity for the bars are shown in Fig. 4.15.

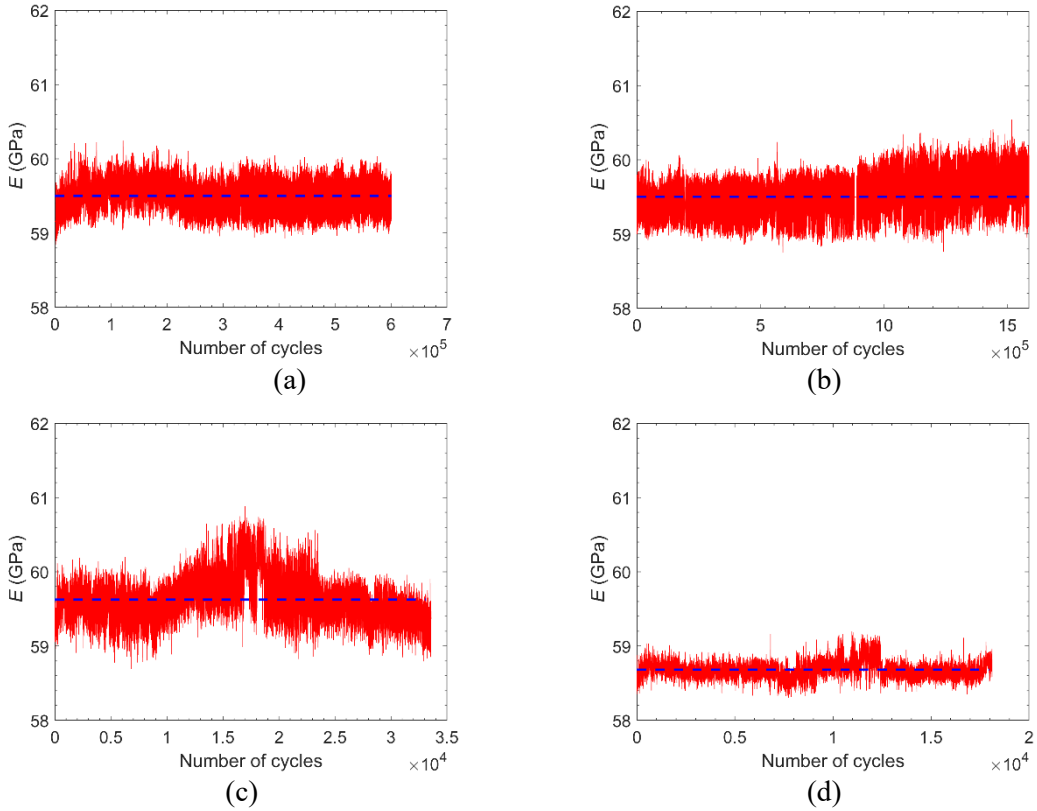

Fig. 4.15. Modulus of Elasticity with the number of cycles (note: the dashed lines show the average value of the Modulus of Elasticity) (a) H-NS-#4-35-S1; (b) H-NS-#4-35-S2; (c) H-NS-#4-50-S1; and (d) H-NS-#4-50-S2

As shown in Fig. 4.15, the Modulus of Elasticity was within a very narrow range throughout the fatigue cycles, and there is no apparent reduction in the modulus of elasticity with increasing test cycles. The values of the calculated E range from 58.7 to 59.6 GPa, which are 2 to 3.5% larger than the average statically determined modulus.

Fig. 4.16 shows the maximum strain in the tested bars, as measured by an extensometer. As shown in Fig. 4.16, the maximum strain increases through the fatigue life of the bar. This indicated that damage accumulated throughout testing. The maximum strain can be clearly divided into three stages. In the first stage, there is a jump in the initial few cycles where the initial maximum strain increases rapidly. This jump is clear in Fig. 4.16 (a and b) for specimens H-NS-#4-35-S1 and H-NS-#4-35-S2. The second stage of strain increase is the relatively slight increase that occurs during testing, and the rate of increase is almost constant. The third stage is the sudden increase in the maximum strain that occurred near failure. The percentages of the maximum strain increase for the H-NS-#4-35-S1 and H-NS-#4-35-S2 bars were 7.5% and 7.4%, respectively. H-NS-#4-35-S1 and H-NS-#4-35-S2 exhibited similar levels of accumulated strain damage throughout their fatigue life, although the damage occurred during different cycles. In the second stage, the maximum strain increased by 37% and 3% in specimens H-NS-#4-50-S1 and H-NS-#4-50-S2, respectively. There was a small change in the maximum strain in the H-NS-#4-50-S2 bar, while the damage in the H-NS-#4-50-S1 bar was the highest.

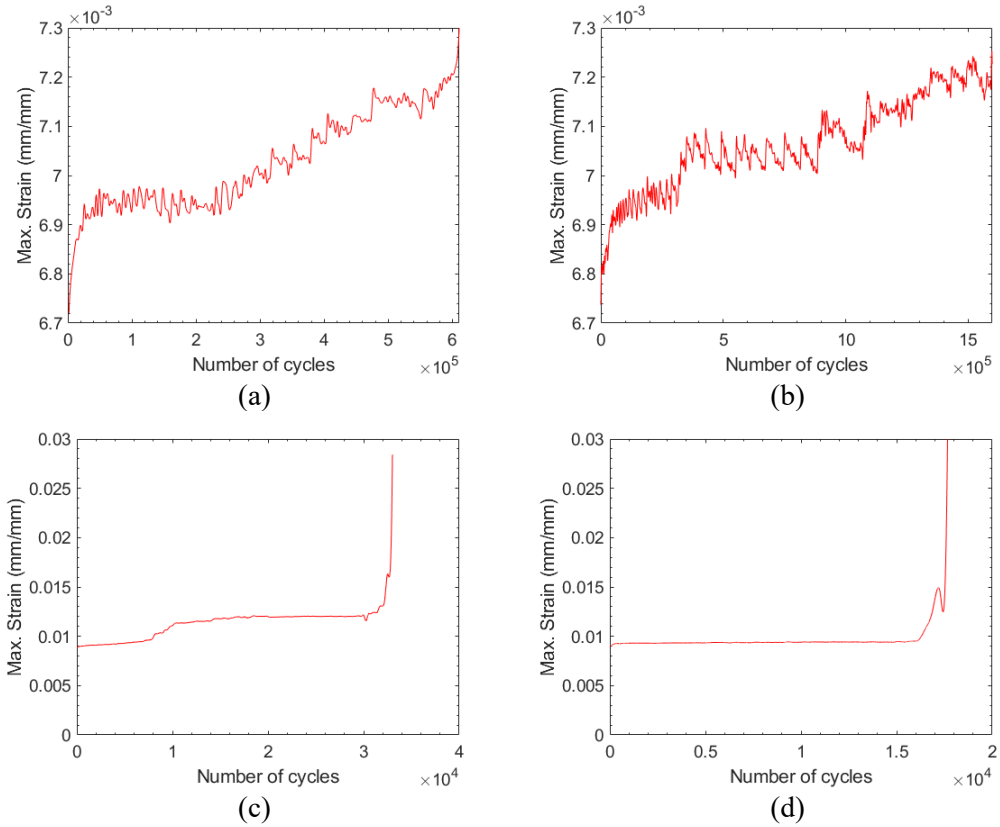

Fig. 4.16. Maximum strain with the number of cycles for (a) H-Ep-#4-35-S1, (b) H-Ep-#4-35-S2, (c) H-Ep-#4-50-S1, and (d) H-Ep-#4-50-S2

The high applied stress led to partial failure in bar H-NS-#4-50-S1; this partial failure might be the reason for the observed increase in maximum strain. Additionally, the bar H-NS-#4-50-S1 failed with longitudinal cracks near the grips, while the bar H-NS-#4-50-S2 failed with longitudinal cracks in the middle section. The strains during the fatigue cycles of the two specimens tested under 30% of the UTS were not measured in this study. However, as discussed earlier, the static test performed on one of the bars after 2 million cycles of fatigue loading indicated no damage to the bar during its fatigue life.

4.7 Summary and Conclusions

This research presents and discusses the results for 29 ribbed GFRP bars: 5 tested monotonically, 14 tested under low frequencies ranging from 0.03 to 0.04 Hz, and ten tested under a higher frequency of 4 Hz. This is the first known study to investigate low-frequency testing. The results were used to establish the S-N curves for bars tested under low and higher frequencies. The following conclusions can be drawn from this research:

- The results of high-cycle fatigue testing on the ribbed GFRP bars match the results reported by Noël and Soudki (2014) and are greater than those reported by Janus et al. (2019). This difference may be attributed to several factors, including but not limited to the gripping system utilized in this study, the slight differences in bar diameter, the mechanical properties, and the surface profile of the GFRP bars. Through a combined analysis of the low- and higher-frequency tests, it was determined that to reach 2 million cycles with a reliability of 95%, the maximum fatigue stress is 30.5% of the UTS.
- The modulus of elasticity remained relatively constant throughout the fatigue life, ranging between 2% and 3.5% higher than the statically measured modulus of elasticity. However, both the maximum and minimum strains increased progressively until failure. Specifically, bars H-NS-#4-35-S1, H-NS-#4-35-S2, H-NS-#4-50-S1, and H-NS-#4-50-S2 exhibited increases in maximum strain of 7.5%, 7.4%, 37%, and 3%, respectively.
- Multiple trials have been undertaken to determine the most effective gripping system for enduring fatigue loading. From the results, it was shown that non-shrink grout outperformed other methods in sustaining fatigue loading and effectively transferring loads to the GFRP bars; out of 11 specimens tested with non-shrink grout, only one had premature failure, which was due to a power outage. In contrast, out of the 13 GFRP bars gripped with expansive grout or epoxy, 11 experienced premature failure, occurring either within or in close proximity to the grip.
- The Sendeckyj model accurately represents the data, allowing for the calculation and presentation of reliability levels of stress required to survive one, two, and ten million cycles.
- The most significant finding was that low-frequency testing provided accurate and conservative values for fatigue design purposes. Most testing to date has been performed at significantly higher frequencies, but the good results achieved at low frequencies are attractive as they can be performed on standard universal testing machines and do not require specialized and expensive equipment.

Despite the contribution made by this study, further research is recommended to investigate the effects of several other influential parameters, such as the stress ratio, stress range, surface type, bar diameter, fibre content, testing frequency, temperature, and presence of concrete on the fatigue life of GFRP bars.

CHAPTER 5

Stress Ratio Effect on the Fatigue Behaviour of Ribbed Glass Fibre-Reinforced Polymer

5.1 Abstract

The ability to withstand fatigue is a critical consideration in designing structural components that experience repeated loads. Glass fibre-reinforced polymers (GFRP) are increasingly utilized in reinforced concrete structures due to concerns regarding the corrosion of steel reinforcement. Nevertheless, research on the fatigue behaviour of GFRP bars has been limited. Principally, literature in the field of stress was assembled and presented. An experimental program was designed and executed, where 3 levels of stress ratio were inspected to assess their impact on ribbed GFRP bars to designate their fatigue life. Measurements were undertaken, and results were obtained, analyzed, and compared to previous research results, where consistency was observed within both results. Additionally, the analyzed results highlighted that fatigue life could be described via a coefficient of stress ratio. Moreover, the analyzed results flagged that the fatigue limits vary in accordance with the acting stress ratio on the ribbed GFRP bars.

5.2 Introduction

GFRP bars have become a promising alternative to traditional steel reinforcement due to their corrosion resistance characteristics (ACI 2022). While there has been much research on the behaviour of GFRP bars under monotonic loading, only a few studies have specifically examined the fatigue life of GFRP bars (Janus et al. 2019; Noël and Soudki 2014; D'Antino et al. 2022). These experiments utilized a frequency of 4 Hz, and they will be used to compare the results of this study.

The fatigue life is influenced by the mechanical parameters, such as the elastic modulus (E) and ultimate tensile strength (UTS) (Tilly 1979). Additionally, the surface type affects the fatigue life of the GFRP bars (ACI PRC-215 2021). The fatigue life of a reinforced concrete beam is influenced by the maximum stress applied during fatigue cycles, the stress ratio, the stress range and the frequency of the applied load (Tilly 1979). As per CSA S806:12-R21 (CSA 2021) and ACI PRC-215-21 (ACI 2021), the stress ratio is the minimum stress divided by the maximum stress.

The design rules and standards aim to unify the fatigue limit of GFRP bars, regardless of any differences in the bar's surface profile and mechanical properties. The fatigue life of GFRP bars is influenced by various significant aspects that have not yet been well studied. These factors include the maximum fatigue stress, stress range, stress ratio, loading rate, surface type, and diameter of the bars (Janus et al. 2019; Noël and Soudki 2014; D'Antino et al. 2022). Hence, it is necessary to conduct more testing in order to establish accurate fatigue stress limits for GFRP bars, which can then be incorporated into the appropriate design rules and recommendations.

Fatigue stress limits for the GFRP bars are defined as a percentage of the UTS (AASHTO LRFD for GFRP 2018; CSA S6 2019; CSA S806 2021; ACI 440.11 2022). Unlike GFRP, steel reinforcement limits the fatigue stress on the steel rebars as a function of the stress range, not the maximum fatigue stress, CSA S6-14 (CSA 2017) and CSA S6-19 (CSA 2019). The 2014 version of CSA S6-14 (CSA 2014) imposes a maximum stress range of 125 MPa on steel reinforcing rebars, irrespective of the specific values of fatigue stress. The 2019 version of CSA S6-19 (CSA 2019) defines the stress range as dependent on the lowest fatigue stress.

S–N curves can be established from fatigue testing, which is the correlation between the number of cycles (N) leading to failure and the maximum stress (S) at the point of failure. The curves show the relationship between S, which represents various stress parameters such as maximum stress, average stress, stress range, or maximum stress relative to the static failure stress, shown on the vertical axis, and N, which represents the number of cycles before failure, represented on the horizontal axis.

Various tests have been conducted to assess the fatigue durability of reinforcing bars, including axial tension testing in both air and concrete, as well as bending tests on beams. The axial tension-tension fatigue test is the main test used to assess the characteristics of a material when subjected to fatigue loads. According to Tilly (1979), axial tension-tension fatigue tests are comparatively simpler and more cost-effective than other fatigue testing. A primary obstacle encountered during fatigue testing is the gripping of GFRP bars. Researchers have conducted numerous studies to discover a gripping method that can prevent bars from experiencing early failure caused by high-stress concentrations. An instance of grip failure can be observed in the

research conducted by El Refai (2013), where the failure modes were characterized by a broom-like form and happened near the anchor zone. Consequently, this failure is deemed premature.

Accordingly, this study was set to investigate GFRP bars under tension-tension fatigue, where the main tested parameters were maximum-fatigue stress and stress ratio to designate the fatigue life and relate it to the tested parameters. Consequently, the obtained results could be implemented to modify the code limits. This is attributed to the fact that the stress ratio is a major factor that affects GFRP fatigue life and fatigue stress limits.

5.3 Experimental Program

As seen from the available literature, very few fatigue tests on GFRP bars have been performed. As of yet, the effect of the stress ratio has not been tested. To address the gaps in the literature, this study aims to present the results of fatigue tests performed on ribbed GFRP bars with three stress ratios. The stress ratios used in this research are 0.1, 0.4, and 0.6. As mentioned, gripping GFRP bars is one of the challenges for testing. For all the GFRP bars tested, each end was anchored inside a steel tube with an outside diameter of 42 mm, wall thickness of 4.85 mm, and length of 635 mm, which is a larger tube than the recommendations of ASTM D7205/D7205M (ASTM 2021). The length of all the GFRP bars was 1780 mm, and the distance between the anchors, known as the free length, was 40 times the diameter of the bar, which is 510 mm. Non-shrink grout and epoxy were used to anchor the GFRP bars inside the tubes. A number of maximum applied stresses as a percentage of UTS was investigated depending on fatigue frequency, which is explained in subsequent sections. In the results sections, specimens are designated as follows: the first number (#4) indicates the bar size. The second letter (Ep, or NS) indicates the grout type, Ep for two-compound epoxy, and NS for non-shrink grout, and the third number indicates the maximum fatigue stress as a percentage of the UTS. The fourth number indicates the stress ratio used (0.1, 0.4, or 0.6), and the last number (S1, S2, or S3) indicates the numbering of similarly tested bars (duplicates or triplicates).

Each bar had a nominal diameter of 12.7 mm (No. 4). The tensile characteristics were calculated taking into account the nominal area of the GFRP bars (129 mm2), as specified in ASTM D7957/D7957M (ASTM 2017). According to the manufacturer, the fibre content constitutes 76% of the total weight. Five ribbed Glass Fiber fibre-reinforced polymer (GFRP) bars

were subjected to monotonic loading in accordance with the ASTM D7205/D7205M (ASTM 2021) in order to determine their mechanical properties. The average ultimate tensile strength (UTS) was determined to be 1096 ± 43.4 MPa, while the Modulus of Elasticity was measured to be 57.6 ± 1.0 GPa.

A total of fourteen ribbed glass fibre-reinforced polymer (GFRP) bars were tested. The outer diameter of the steel tubes was reduced from 42 mm to 35 mm throughout a length of 170 mm (See Fig. 5.1). This modification was made to reduce stress concentration at the grip. A 1500 kN capacity dynamic actuator was utilized to apply tension-tension fatigue loading on the bars, as shown in Fig. 5.1. Steel vee-wedge grips are utilized for securely holding steel tubes at the end of each bar through the application of hydraulic pressure.

The bars were subjected to fatigue loading at a frequency of 4 Hz. The maximum fatigue stress varied between 30%, 35%, 40%, and 50% of the ultimate tensile strength (UTS). The maximum fatigue stress is selected at 30% of the Ultimate Tensile Strength (UTS) because it exceeds the restrictions specified in CSA S806:12-R21 (CSA 2021) and AASHTO LRFD for GFRP (2018) by 5% in high-cycle fatigue tests. The stress ratio varied between 0.1, 0.4 and 0.6. The fatigue life of the tested Glass Fiber Reinforced Polymer (GFRP) bars is provided in Table 5.1.

A fatigue loading method was developed that utilize displacement control instead of force control. During this procedure, the displacements were automatically modified to achieve the desired forces, both minimum and maximum, with a tolerance of no more than 1% deviation from the goal force at each iteration. The purpose of this protocol is to monitor the gradual deterioration of a bar leading up to failure in order to prevent sudden failure by implementing safety measures and to avoid exceeding the maximum force during loading when the bar is close to failure.

Fig. 5.1. Test setup.

Table 5.1. Fatigue life of the tested GFRP bars.

Name	Max. fatigue stress (%UTS)	Stress Ratio	Fatigue life (Cycles)	Failure mode	Grout type
#4-Ep-30-10-S1	30	0.1	>2000000	Not failed	Epoxy
#4-Ep-30-10-S2	30		>2000000	Not failed	Epoxy
#4-NS-35-10-S1	35		610686	Longitudinal cracks	Non-shrink grout
#4-NS-35-10-S2	35		1589067	Longitudinal cracks beside grips	Non-shrink grout
#4-NS-50-10-S1	50		33107	Longitudinal cracks beside grips	Non-shrink grout
#4-NS-50-10-S2	50		17965	Longitudinal cracks	Non-shrink grout
#4-NS-35-40-S1	35	0.4	>2000000	Not failed	Non-shrink grout
#4-NS-35-40-S2	35		>2000000	Not failed	Non-shrink grout
#4-NS-50-40-S1	50		69380	Longitudinal cracks beside grips	Non-shrink grout
#4-NS-50-40-S2	50		145349	Longitudinal cracks beside grips	Non-shrink grout
#4-NS-40-60-S1	40	0.6	>2000000	Not failed	Non-shrink grout
#4-NS-40-60-S2	40		>2000000	Not failed	Non-shrink grout
#4-NS-50-60-S1	50		1657911	Longitudinal cracks beside grips	Non-shrink grout
#4-NS-50-60-S2	50		386828	Pre-mature failure due to power failure	Non-shrink grout

Two bars, namely #4-Ep-30-10-S1 and #4-Ep-30-10-S2, survived 2 million cycles without showing any signs of failure while using epoxy as a filler between the steel tube and the GFRP bar. The specimen was subjected to testing at a maximum fatigue stress level equal to 30% of its ultimate tensile strength (UTS) and did not experience failure. The remaining glass fiber-reinforced polymer (GFRP) bars were subjected to fatigue by using steel tubes filled with non-shrink grout.

Six bars sustained fatigue loading for 2 million cycles. One bar failed early due to a power loss, namely bar #4-NS-50-60-S2. The primary mode of failure for the remaining bars was longitudinal cracks, longitudinal cracks beside the grips, as illustrated in Table 5.1.

A sample of the GFRP bars that survived 2 million cycles and a sample of the failure modes are shown in Fig. 5.2. For the stress ratio of 0.1. Two bars survived 2 million cycles, namely, #4-Ep-30-10-S1 and #4-Ep-30-10-S2. Four bars are then tested under maximum fatigue stress of 35%

and 50% of the UTS. Subsequently, four bars undergo testing under a stress ratio of 0.4. Two bars survived 2 million cycles while being subjected to a greater maximum fatigue stress level equivalent to 35% of the Ultimate Tensile Strength (UTS). The fatigue stress endurance limit after 2 million cycles, with a stress ratio of 0.6, was 0.4 of the ultimate tensile strength (UTS).

Two bars failed with longitudinal cracks, namely, #4-NS-35-10-S1 and #4-NS-50-10-S2. Bar #4-NS-50-60-S2 experienced an early failure as a result of a power outage. The remaining five tested bars failed with longitudinal cracks beside the grips. Although, failure near the grips is considered a premature failure in some cases. The results were used because the failure occurred after a considerable amount of fatigue loading cycles, and no other way is known in the literature to solve this problem. Noël and Soudki (2014) grinded the bars to control the failure mode, but in this study, the surface was maintained because it is an influential parameter that can affect fatigue life.

(a) Not failed GFRP bar after fatigue loading (b) Longitudinal cracks (c) Longitudinal cracks beside the grip

Fig. 5.2. Failure modes of the tested GFRP bars.

In order to examine the deterioration of the GFRP bar during repetitive stress cycles, all bars that survived 2 million cycles of fatigue testing were then tested under static load. The static loading was continuous and unidirectional, according to the specifications outlined in ASTM D7205/D7205M (2021). The maximum strength of the tested bars is shown in Table 5.2.

Table 5.2. Tensile properties of the GFRP bar after 2 million cycles

Name	Ultimate tensile Strength after 2 million cycles	Modulus of Elasticity (E) After 2 million cycles
	MPa	GPa
#4-Ep-30-10-S1	1124	56.3
#4-Ep-30-10-S2	--	--
#4- NS-35-40-S1	1195	59.1
#4- NS-35-40-S2	1212	59.3
#4- NS-40-60-S1	1132	58.6
#4-NS-40-60-S2	1160	58.3

As seen in Table 5.2, the tensile strength of the GFRP bars is all within the tested static ultimate tensile strength. In fact, all the static strengths tested exceed the average tensile strength. These values of the tensile strength indicate that the bars did not sustain significant damage even after 2 million cycles of fatigue loading.

5.4 Analysis of Results

This section discusses the analysis of the fatigue life, modulus of elasticity and maximum strain of the tested GFRP bars. First, a probabilistic fatigue model is described to draw the S-N curve of the tested bars with different reliability ranges. Second, the GFRP bars tested with low frequency are compared with the available data in the literature. After that, the high-frequency bars are compared with the data available in the literature and the low frequency to check the relation between the fatigue life results. Finally, the changes in the modulus of elasticity and maximum strain during the high-frequency GFRP bar tests are presented and discussed.

5.4.1 Probabilistic models for the GFRP fatigue life data

The fatigue life data of composite materials exhibits significant scatter, potentially attributed to factors such as variations in fibre content and the presence of flaws (Noël 2019). For instance, the crack that initially spreads and leads to failure would differ among bars and batches. The reported data scatter was greater than ten times (Janus et al. 2019, 2021; Noël 2018, 2019; Noël

and Soudki 2014a; b; El Refai 2013). Various models have been created to describe the statistical distribution of fatigue life data due to the significant variation in the data.

The S-N curve can be derived using Eq. 1 and Eq. 2 for any reliability level (Sendeckyj 1981).

$$\sigma_a = \beta\{-\ln\big(P(N)\big)^{\frac{1}{\alpha}}\}[(N-A)C]^{-D} \quad (1)$$

$$A = -\frac{1-C}{\mathrm{C}} \quad (2)$$

The symbol N represents the number of cycles till failure, P(N) represents the chance of survival after N cycles, and σa represents the maximum applied stress. C and D are coefficients that have been adjusted to a standard or reference value. α and β are parameters used to calibrate the Weibull distribution. Noël (2018, 2019) utilized the equations developed by Sendeckyj (1981) to analyze fatigue life data and construct the S–N curve. The author validated this model by utilizing the empirical data provided in a prior investigation conducted by Noël and Soudki (2014). An iterative approach was used to obtain the calibration coefficients C and D, as well as the Weibull distribution coefficients α and β, in order to plot the S–N curve.

The Sendeckyj approach, originally described by Sendeckyj (1981), is employed in this work to adjust the data for low and high-frequency fatigue testing. Further details can be found in the subsequent sections. Sendeckyj is selected for its precise and representative reliability curves.

5.4.2 Fatigue life of GFRP tested

Fig. 5.3 shows the fatigue life of the bars examined in this study, as well as those reported in the literature (D'Antino et al. 2022; Janus et al. 2019; Noël and Soudki 2014a). The vertical axis represents the maximum applied fatigue stress, represented as a percentage of the ultimate tensile strength (UTS). The horizontal axis represents the number of cycles until failure, displayed on a logarithmic scale.

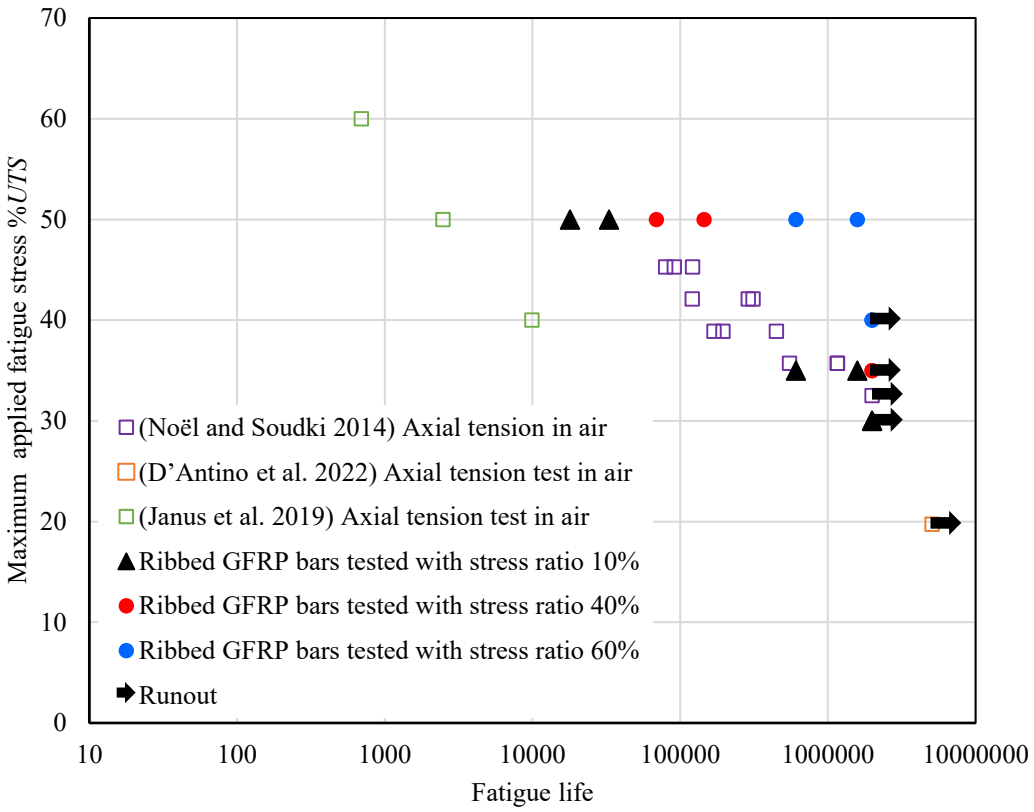

Fig. 5.3. S-N curve for the GFRP bars.

As shown in Fig. 5.3, the fatigue life of the tested bars agrees well with those tested in the literature. The GFRP bars tested in this study exhibit a superior fatigue life compared to the bars examined by Janus et al. (2019). Nevertheless, the fatigue life of the bars tested with a stress ratio of 0.1 corresponds to the tests conducted by Noël and Soudki (2014). In contrast to the sand-coated bars examined by Noël and Soudki (2014), which required grinding to induce failure in the appropriate middle section, our investigation did not require any grinding. There is no clear relation between the fatigue life of the bar tested by D'Antino et al. (2022) because only one bar was tested and did not reach failure.

As clearly shown in Fig. 5.3, the fatigue life of the bars tested with stress ratios of 0.4 and 0.6 have a longer fatigue life than those tested with a stress ratio of 0.1. For all the bars reported in the literature, the stress ratio tested was 0.1, which indicates that the stress ratio has not been studied (D'Antino et al. 2022; Janus et al. 2019; Noël and Soudki 2014a). However, the fatigue life of the bars tested in the literature has a lower fatigue life than those tested with a stress ratio of 0.4 and

0.6. The bars #4-NS-50-60-S1 and #4-NS-50-60-S2 show longer fatigue life with more than one order of magnitude than the bars tested with a 0.1 stress ratio (in the level of maximum applied fatigue stress of 50% of the UTS). Additionally, bars #4-NS-50-40-S1 and #4-NS-50-40-S2 have more than double the fatigue life of the bars tested with a stress ratio of 0.1.

The Sendeckyj model was used to draw the S-N-P for the bars tested in this study. A different S-N curve was drawn for each set of data with stress ratios of 0.1, 0.4, and 0.6. A straight S-N curve was assumed, which means that the c coefficient used was assumed to be 1. The remaining coefficients α, β, and D for each stress ratio are shown in Table 5.3. The S-N curves are shown in Fig. 5.4.

Table 5.3. Sendeckyj model coefficients

Coefficient values	Stress ratio 0.1	Stress ratio 0.4	Stress ratio 0.6
α	31.36	23.97	46.21
β	102.11	105.83	102.19
D	0.072	0.065	0.051

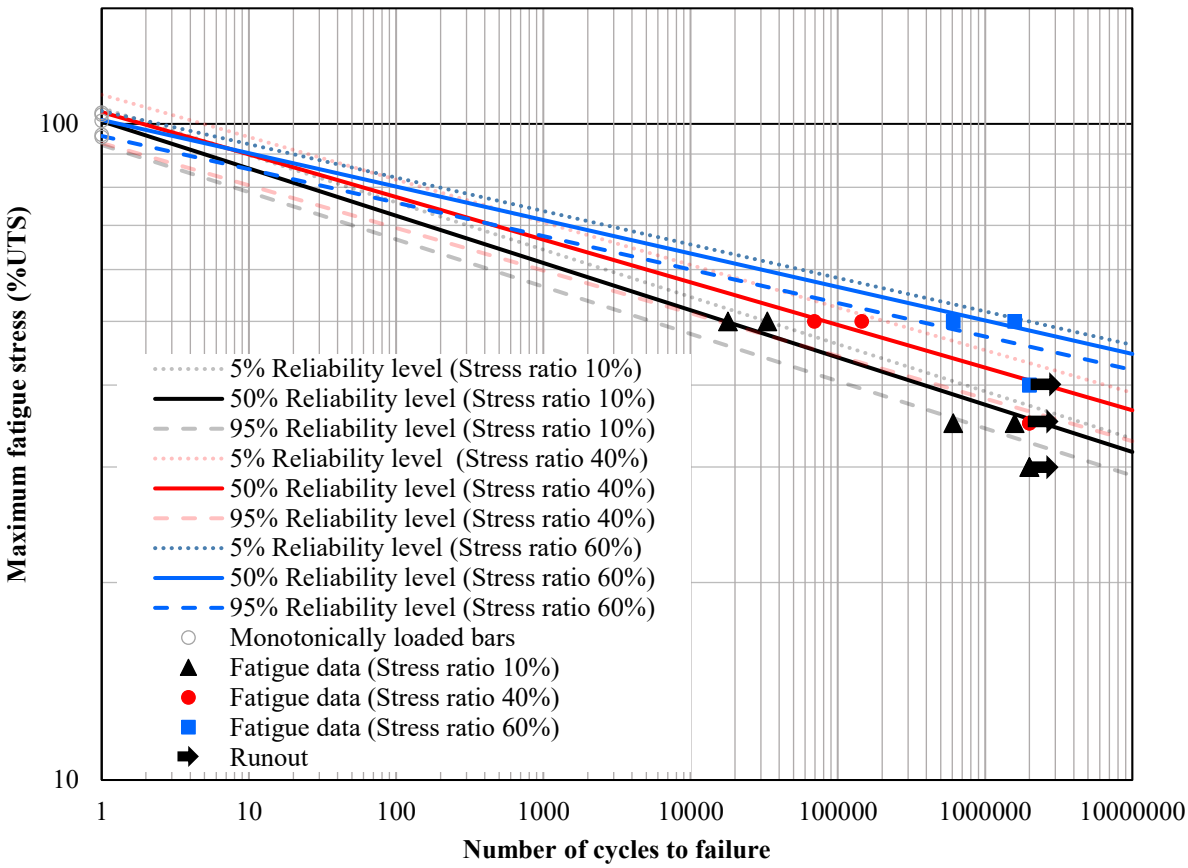

Fig. 5.4. Fitting GFRP bars tested with high frequency.

As shown in Fig. 5.4, the S-N curves for different stress ratio levels were fitted using the Sendeckyj model. The Sendeckyj model accurately represents the data. By assuming that the S-N curves are linear, it can be seen that all curves intersect with the vertical axis in the same region as the statically tested UTS. The slope then differs from one curve to the other, but the S-N curve has the highest slope, which gives the most conservative fatigue lives than the other tests. The slope then tends to flatten with each stress ratio, which indicates a higher fatigue life at the same maximum applied fatigue stress. The S-N curve for the specimens tested with a stress ratio of 0.6 estimated the highest fatigue life.

To directly compare the effect of the stress ratio on fatigue life, six bars were tested at the same stress level (50% of the UTS): two at stress ratio 0.1 (#4-Ep-50-10-S1 and #4-Ep-50-10-S2), two at stress ratio 0.4 (#4-NS-50-40-S1 and #4-NS-50-40-S2), and two at stress ratio 0.6 (#4-NS-

50-60-S1 and #4-NS-50-60-S2). The specimens #4-Ep-50-10-S1 and #4-Ep-50-10-S2 had a fatigue life of 33107 and 17965, respectively. The specimens #4-NS-50-40-S1 and #4-NS-50-40-S2 had a fatigue life of 69380 and 145349, respectively. Specimens #4-NS-50-60-S1 and #4-NS-50-60-S2 had a fatigue life of 1657911 and 386828, respectively (knowing that specimen #4-NS-50-60-S2 failed early due to a power outage). This indicates that the average fatigue life of the bars tested with a stress ratio of 0.6 is approximately 4000% higher than the bars tested with a stress ratio of 0.1. In addition, the bars tested with a stress ratio of 0.4 have longer fatigue life than those tested with a stress ratio of 0.1 by approximately 420%. This comparison to the effect of the stress ratio on the fatigue life means that the stress ratio has a huge effect on the number of cycles to failure. Additionally, this shows the need to identify more realistic values for the stress ratios, which can lower the fatigue stress limits in the codes. The estimated values of the maximum fatigue stress with different reliabilities for the tested ribbed GFRP bars are shown in Table 5.4.

Table 5.4. Maximum fatigue stress with 5% (P5) and 95% (P95) reliability for ribbed GFRP bars tested

Expected number of cycles to failure	**P5 Maximum stress (%UTS)**			**P95 Maximum stress (%UTS)**		
	Stress ratio 0.1	Stress ratio 0.4	Stress ratio 0.6	Stress ratio 0.1	Stress ratio 0.4	Stress ratio 0.6
1M	39.1	45.2	51.8	34.4	38.1	47.4
2 M	37.2	43.2	50.0	32.7	36.5	45.8
10 M	33.1	38.9	46.0	29.1	32.8	42.2

The fatigue stress necessary to endure various fatigue lifespans is provided in Table 5.4. According to the data presented in Table 5.4, the estimated fatigue stress required for the GFRP bars (tested with a stress ratio of 0.1) to endure 2 million cycles falls within the range of 37.2% to 32.7% of the ultimate tensile strength (UTS). The estimated fatigue life obtained from stress ratios 0.4 and 0.6 are higher than 0.1 (43.2% to 36.5%) and (50.0% to 45.8%), respectively. The rise in the estimated maximum fatigue stress in order to survive 2 million cycles indicates the need for designing using accurate and representative stress ratio values. The relation between the stress ratio and maximum applied fatigue stress with 95% reliability is shown in Fig. 5.5.

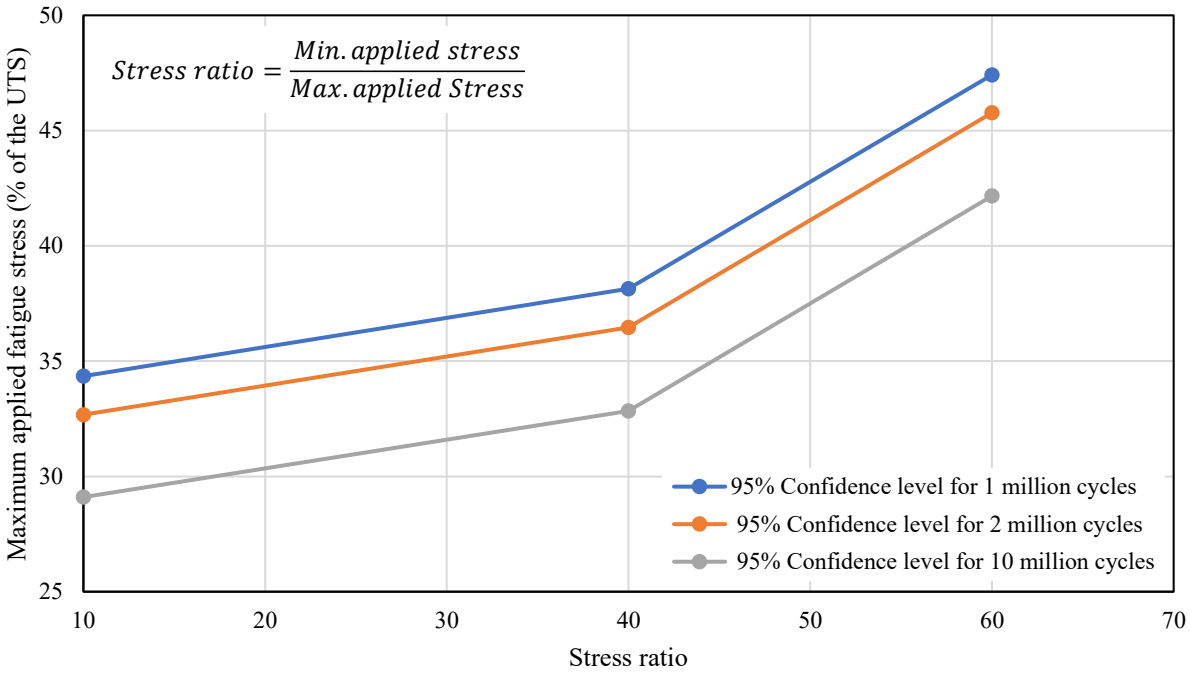

Fig. 5.5. S-N curve for GFRP bars tested with high and low frequencies.

It can be clearly seen from Fig. 5.5. which agrees with the previously analysed and discussed data that the stress ratio have an influential effect on the fatigue life of the ribbed GFRP bars. As seen that just by increasing the stress ratio from 0.1 to 0.6 the estimated maximum applied fatigue stress to survive the same fatigue life do increase more than 0.1.

Table 5.5. Tensile properties of the GFRP bar after 2 million cycles

No.	Ultimate tensile Strength (UTS)	Modulus of Elasticity (E)
	MPa	GPa
#4-Ep-30-10-S1	1124	56.3
#4-Ep-30-10-S2	--	--
#4- NS-35-40-S1	1195	59.1
#4- NS-35-40-S2	1212	59.3
#4- NS-40-60-S1	1132	58.6
#4-NS-40-60-S2	1160	58.3

As seen from Table 5.5. there is a slight variation between monotonic average tensile strength and UTS measured from the specimens tested after applying 2 million fatigue cycles. The modulus of elasticity also shows low variation in the monotonic testing results. Additionally, all tested bars with stress ratios of 0.4 and 0.6 have slightly higher values than those of the monotonic tests. These

slight variations indicate that the ribbed GFRP bars tested in this study survived 2 million cycles and did not sustain a lot of damage.

5.5 Modulus of Elasticity

An extensometer with a gauge length of 1 inch (25.4 mm) was utilized to measure the elongation of the bars throughout the high-cycle fatigue tests. The modulus of elasticity of the GFRP bars was determined by calculating the secant slope between the greatest and minimum applied stresses. Fig. 5.6 displays the computed values of the Modulus of Elasticity at various points in the cycles, as well as the average modulus of elasticity for the bars.

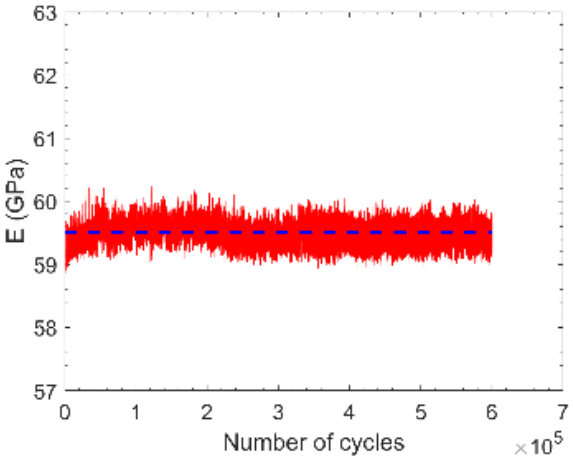

(a) #4-NS-35-10-S1

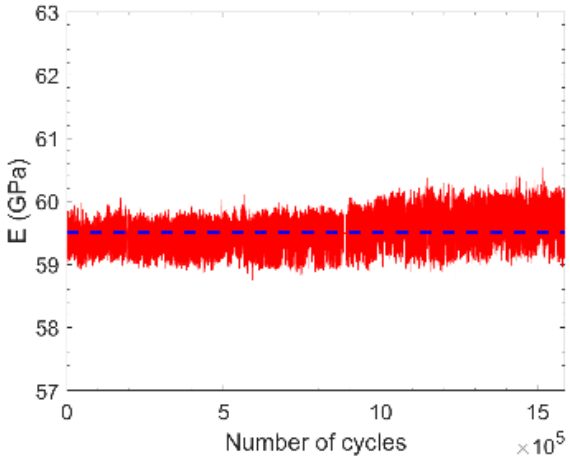

(b) #4-NS-35-10-S2

8.5

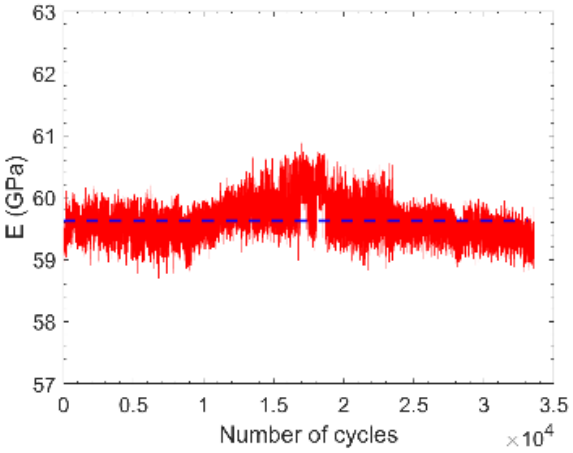

(c) #4-NS-50-10-S1

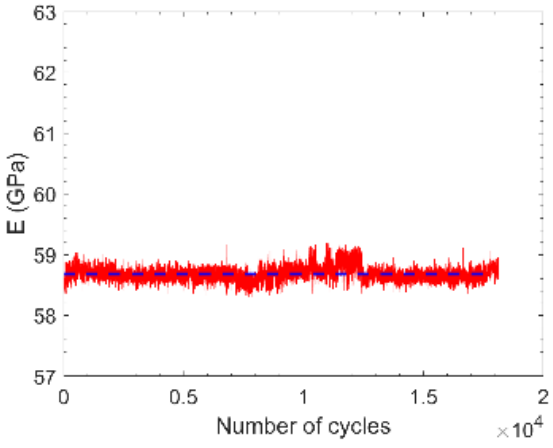

(d) #4-NS-50-10-S1

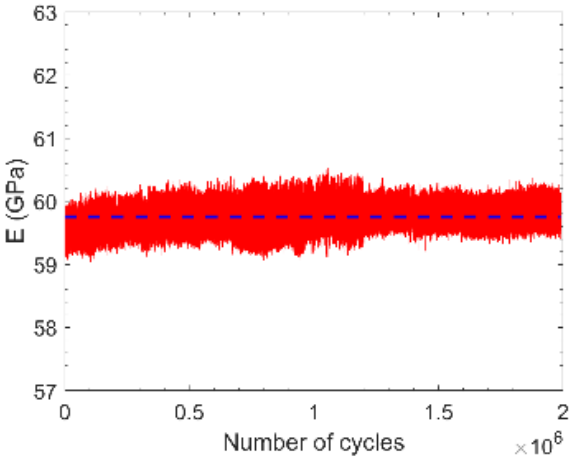

(e) #4-NS-35-40-S1

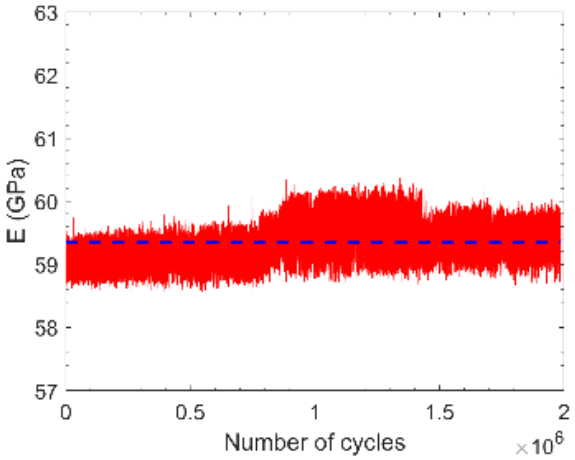

(f) #4-NS-35-40-S2

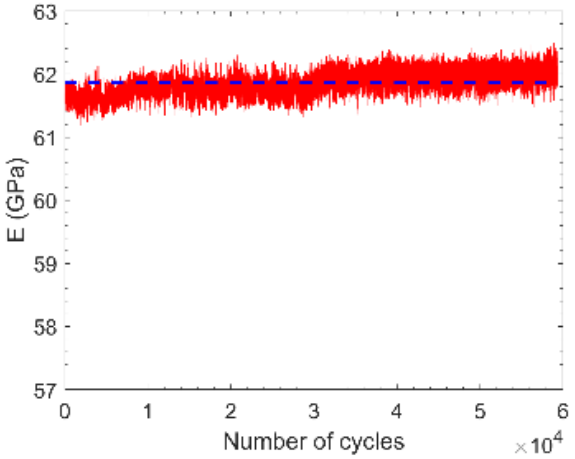

(g) #4-NS-50-40-S1

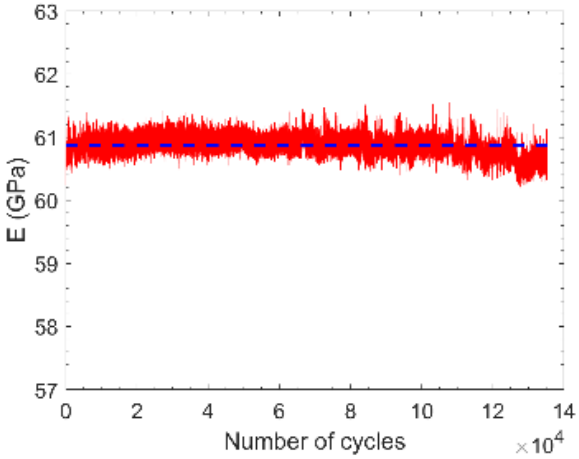

(h) #4-NS-50-40-S2

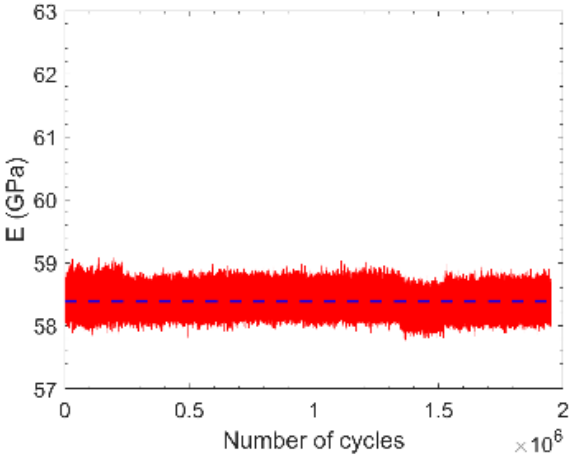

(i) #4-NS-40-60-S1

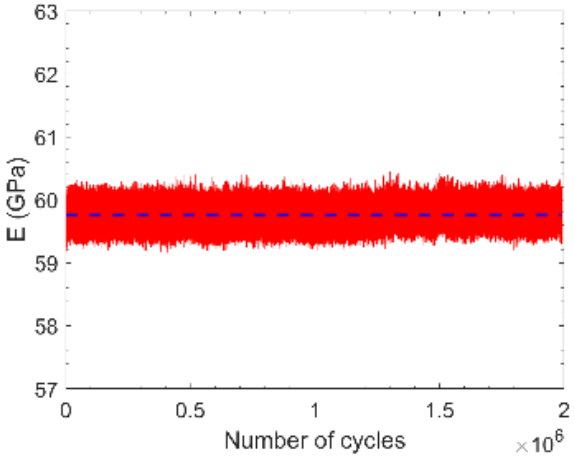

(j) #4-NS-40-60-S2

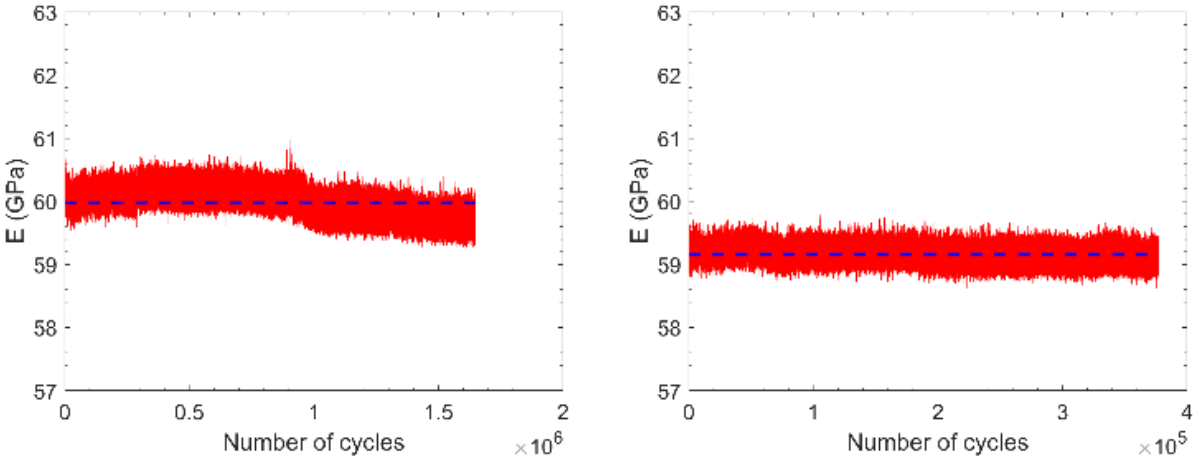

(k) #4-NS-50-60-S1 (l) #4-NS-50-60-S2

Fig. 5.6. Modulus of Elasticity with the number of cycles (note: the dashed lines show the average value of the Modulus of Elasticity)

As shown in Fig. 5.6, the modulus of elasticity remained consistent within a small range throughout the fatigue cycles. The computed average values of the modulus of elasticity are listed in Table 5.6.

Table 5.6. Average Modulus of Elasticity measured during fatigue tests

No.	Modulus of Elasticity (E)
	GPa
#4- NS-35-10-S1	59.5
#4- NS-35-10-S2	59.5
#4- NS-50-10-S1	59.6
#4-NS-50-10-S2	58.7
#4-NS-35-40-S1	59.8
#4-NS-35-40-S2	59.4
#4-NS-50-40-S1	61.9
#4-NS-50-40-S2	60.9
#4-NS-40-60-S1	58.4
#4-NS-40-60-S2	59.8
#4-NS-50-60-S1	60.0
#4-NS-50-60-S2	59.2

As shown in Table 5.6, the values of the average modulus of elasticity are within 7.5 % to 1.4 % higher than the average modulus of elasticity measured from the statically loaded tests. These values are higher due to the high frequency with which the tests were applied.

5.6 Proposed fatigue life equation

In CSA S6 (2019), the fatigue stress limit on the steel rebars is a function of the stress range, where the stress range is a function of the minimum fatigue stress as a variable. In addition, AASHTO LRFD (2020) permitted a constant fatigue amplitude for straight reinforcement, which is also dependent on the minimum fatigue stress. However, the stress limits for GFRP bars in the codes and guidelines are only a percentage of the UTS of the bars.

It is crucial to establish fatigue limits for GFRP bars as a function of the stress ratio or the stress range, providing the flexibility to determine fatigue limits based on the minimum fatigue stress. Therefore, this study proposes an equation to limit the stress range as a function of the minimum fatigue stress and the UTS of GFRP bars.

Fig. 5.7 and 5.8 show the tested ribbed GFRP bars (failed and not failed), the 95% reliability levels estimated by the Sendeckyj model, and the stress range equation for codes CSA S6-19 (CSA 2019) and AASHTO LRFD (2020). Additionally, two proposed equations are shown limiting the stress range as a function of the minimum fatigue stress and the UTS.

Eq. 5.1 shows the proposed stress range equation, which uses the same linear form as CSA S6-19 (CSA 2019) and AASHTO LRFD (2020). Eq. 5.1 is formed based on the ribbed GFRP bars tested under fatigue, which survived for 2 million cycles and did not fail. The linear equation is clearly shown in Fig. 5.7. The proposed equation presents higher fatigue stress range limits compared to the equations used for steel rebars. On the other hand, the proposed linear equation has a higher

slope, which means that for higher values of minimum fatigue stress es, steel can sustain bigger values of stress range.

As shown in Fig. 5.8, the 95% confidence level shows a logarithmic trend. Eq. 5.2 presented a logarithmic trendline for the stress range. The logarithmic trendline has less conservative limits compared to the linear equation because the regression analysis was based on the 95% reliability levels, not the tested bars that did not fail.

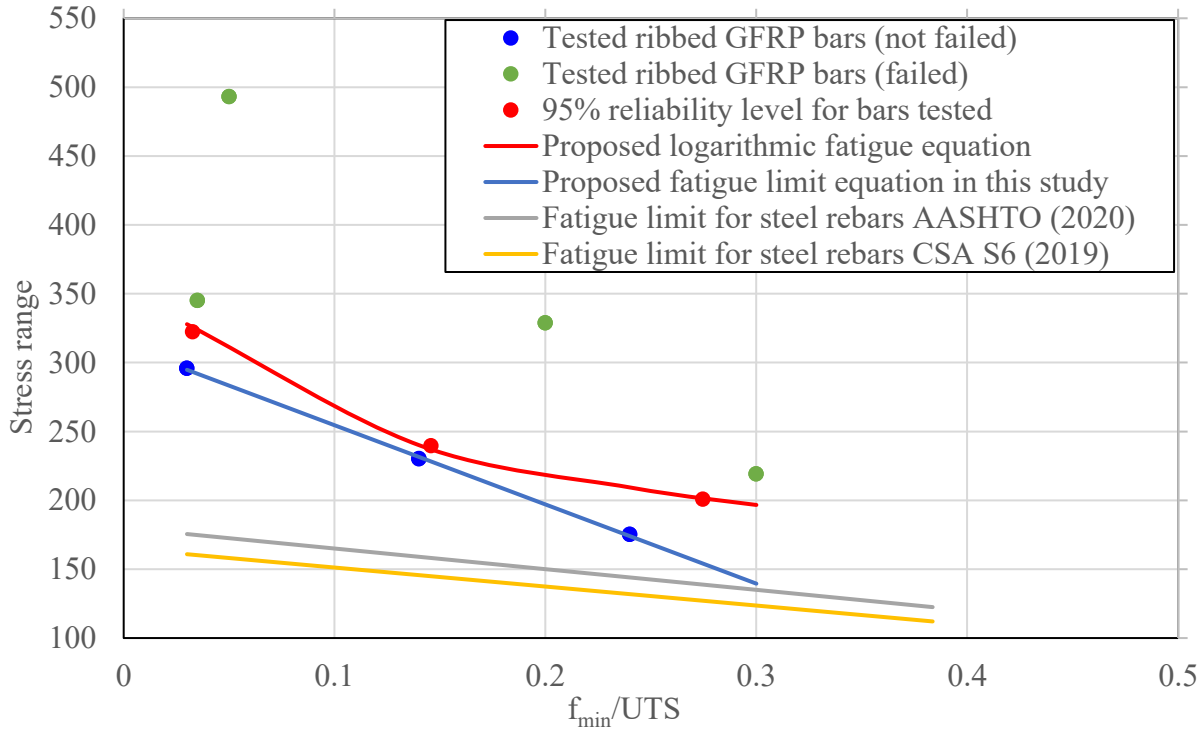

Fig. 5.7. Linear (f_{min}/UTS) with stress range curve of the tested ribbed GFRP bars.

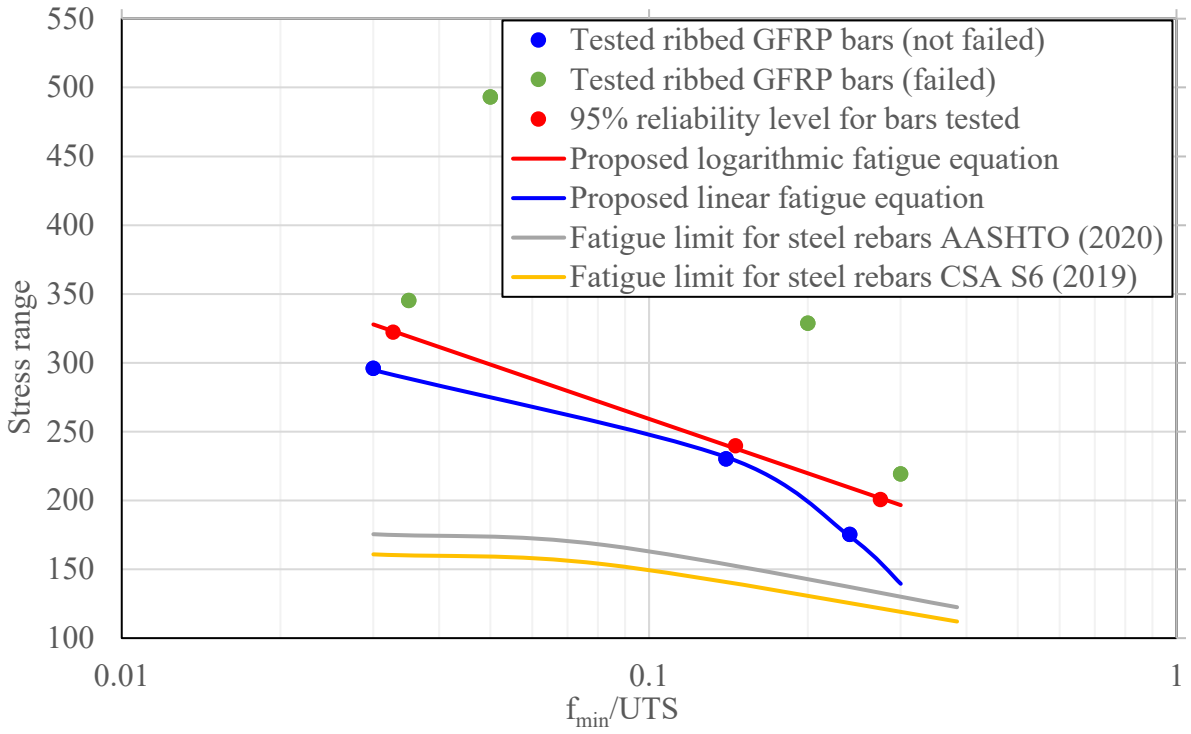

Fig. 5.8. Logarithmic (f_{min}/UTS) with stress range curve of the tested ribbed GFRP bars.

$$\text{stress range} = 312 - 575\left(\frac{f_{min}}{UTS}\right) \tag{5.1}$$

$$\text{stress range} = 128 - 57\ ln\left(\frac{f_{min}}{UTS}\right) \tag{5.2}$$

where stress range is the difference in amplitude between the maximum and minimum applied fatigue stresses in MPa, and min represents the unfactored sustained load stresses with minimum live fatigue stress in MPa. Eq. 5.1 and 5.2 are based on data with (fmin/UTS) ranging between 0.03 and 0.3 and fatigue stress range ranging between 140 and 500 MPa.

5.7 Summary and Conclusions

This study presents and analyses the findings of 19 ribbed GFRP bars. Among these, 5 bars underwent monotonic testing, 6 bars were tested at a stress ratio of 0.1, 4 bars at 0.4, and 4 bars at 0.6. This investigation represents the first known exploration of the stress ratio effect on the fatigue

life of ribbed GFRP bars. The results were utilized to establish the S-N curves for bars subjected to different stress ratios. The following conclusions were made:

- The fatigue testing results of the ribbed GFRP bars tested with a stress ratio of 0.1 are consistent with the findings of Noël and Soudki (2014) and surpass the findings of Janus et al. (2019). The variation can be ascribed to multiple factors, including but not limited to the gripping techniques, grinding processes, bar diameter, mechanical properties, and surface configurations.
- Stress ratio impacts the fatigue life of the ribbed GFRP bars. Increasing the stress ratio from 0.1 to 0.4 or 0.6 can increase the fatigue life by more than one order of magnitude. The data suggests that the bars tested with a stress ratio of 0.6 have an average fatigue life that is roughly 4000% greater than the bars tested with a stress ratio of 0.1. Furthermore, the bars subjected to a stress ratio of 0.4 exhibit a much longer fatigue life compared to those subjected to a stress ratio of 0.1, with an approximate increase of 420%.
- Performing fatigue testing at a stress ratio of 0.1 provides a conservative estimation of fatigue life for the GFRP bars. However, it is necessary to determine more realistic stress ratio values for bridges.
- The modulus of elasticity exhibited minimal variation across the whole fatigue lifespan, consistently measuring 7.5 % to 1.4 % higher than the statically determined modulus of elasticity.
- Two equations were proposed limiting the fatigue stress range as a function of the minimum fatigue stress and the UTS. Both proposed equations present conservative fatigue limits, but they show higher fatigue limits than steel rebars.
- The Sendeckyj model effectively represents the data, enabling the calculation and presentation of stress levels required to withstand one, two, and ten million cycles.

CHAPTER 6

Fitting Fatigue Life Data with a Normal Distribution Probabilistic Model

6.1 Abstract

The last few decades have witnessed many applications of fibre-reinforced polymer (FRP) bars as internal reinforcement in concrete structures, including buildings and bridges. Several codes and standards for designing FRP-reinforced concrete (RC) structures exist. Glass (GFRP), carbon (CFRP), and basalt (BFRP) fibre-reinforced polymers are used in many structural field applications. There is a wealth of research on the behaviour of FRP-RC flexural elements (beams and girders) subjected to static loading. However, there are very few studies on the behaviour of FRP-RC elements under fatigue loading, which arises from repeated loads, e.g., bridges. Fatigue life can be represented as a function of the applied stresses or strains by the S–N curve. By adding the probabilistic models, the resulting fatigue life curve is the S-N-P curve. Many models have been developed to capture and describe the reliability levels of fatigue life. The Sendeckyj model is a well-known model used to describe the probabilistic distribution of any set of fatigue data using the Weibull distribution. In the literature, studies apply the Sendeckyj model to FRP in the construction field. This study proposes a simpler model based on the Sendeckyj model by replacing the Weibull distribution with a normal distribution. A normal distribution applied with the Sendeckyj model is applied to the GFRP, CFRP, and BFRP fatigue data available in the literature. The resulting S-N-P curves are compared with the Sendeckyj model to verify the technique.

6.2 Introduction

Fibre-reinforced polymer (FRP) composite materials are used in many industries, such as aerospace, marine, and construction. FRP materials have high strength despite their low weight. It is also a corrosion-resistant material, making it a suitable replacement for steel reinforcing bars in harsh environmental conditions. The interest in the long-term properties of FRP materials and, thus, the experimental fatigue data are increasing. Glass FRPs are less expensive compared to other types of FRP, e.g., basalt FRP (BFRP), carbon FRP (CFRP) and aramid FRP (AFRP), which makes the GFRP bars more attractive for applications in the structural field.

Many probabilistic models have been developed to explain the fatigue behaviour of FRP materials. The curve that describes the fatigue life of any material relative to the applied stresses is called the S–N curve. The S–N curve is divided into three different regions in several studies, as explained by Noël (2019). Accurately modelling the three regions of S–N curves with adequate reliability is essential to have a realistic estimation of the fatigue life of civil engineering applications (Noël 2019). The resulting curve is called the S-N-P curve when reliability levels are added to the S–N curves.

ASTM E739 (2015) suggested a log-normal distribution to model the fatigue data with a well-explained data analysis procedure. The log-normal distribution model can accurately predict the fatigue life of the materials well in the tested range of stresses. However, using the log-normal distribution to predict the fatigue life in the untested range can be inaccurate (ASTM E739 2015). An accurate alternative to fit the fatigue data is the Sendeckyj model (Sendeckyj 1981), which uses the Weibull distribution model. This model was applied by Noël (2018, 2019) to fatigue data in the structure field and accurately represented life.

Normal distribution was used by (Vassilopoulos and Keller 2011) to analyze the fatigue data. (Vassilopoulos and Keller 2011) applied the normal distribution at each stress level to obtain different reliability levels and coefficients of variance (COVs). The Gaussian function, also called the normal distribution function, has been used by several studies and compared with the three-parameter Weibull distribution (Schijve 1993). The work done by Schijve (1993) concluded that the Weibull distribution agreed with or was even better than the normal distribution function. Schijve compared the 3-parameter Weibull, log-normal and 3-parameter $\log(N\text{-}N_0)$ normal distributions (Schijve 2005). Schijve (2005) concluded that all methods fit well with a skewed distribution for the data used. In a state-of-the-art study (Barbosa et al. 2019), both the Sendeckyj and Stussi models were concluded to be suited for composite materials. On the other hand, only the Stussi model gave a good fit for the experimental results in metallic materials. Vanhari et al. (2022) developed a new empirical fatigue model was developed to simplify the complex nonlinear optimization procedure in the Sendeckyj model. In this model, an exponential model was used in the low-cyclic region, and a power-law model was used in the high-cyclic region.

The primary goal of this study is to present a simpler technique to analyze fatigue data using a normal distribution. The base of the Sendeckyj method uses the power law function to apply the normal distribution. Instead of using the Weibull distribution, the normal distribution is used. The main advantage of using the power law function is the accuracy of modelling the low- and high-cyclic fatigue regions. The S–N curves drawn using the proposed technique are compared with the Sendeckyj model for verification.

The normalized data collected from the literature on fatigue tests performed on GFRP reinforcing rebars for structural engineering applications will be used in this study to verify the proposed technique (Adimi et al. 1997; D'Antino et al. 2022; Janus et al. 2019, 2021; Noël and Soudki 2014a; El Refai 2013).

Adimi et al. (1997) tested 13 GFRP-reinforced concrete prisms under fatigue. The maximum stress ranged between approximately 21% and 81% of the UTS. The stress ratio was 0.1, and the testing frequency was 4 Hz. Noël and Soudki (2014a) tested 12 beam-hinge specimens reinforced with GFRP bars under fatigue loading. The minimum stress was kept at approximately 4% of the UTS, while the maximum stress ranged between 23% and 57% of the UTS. The frequency was between 0.2 and 1 Hz. Janus et al. (2019) tested 12 concrete prisms reinforced with GFRP bars under fatigue loading with a frequency of 4 Hz. The stress ratio was 0.1, and the maximum stress was between 40% and 60% of the UTS. Janus et al. (2021) then tested five beams. One of the beams was tested monotonically, and four were tested under fatigue. Three beams were tested under varying loads until failure, while one beam was tested under a constant cycle of load to stress the GFRP bars with 20% of the UTS.

El Refai (2013) tested one set of 4 GFRP bars under fatigue loading. The minimum stress was 30% of the UTS, while the maximum stress was between 34% and 43% of the UTS. The frequency of the tests was 2 Hz. Noël and Soudki (2014a) tested 12 ground sand-coated GFRP bars where the fatigue tests were conducted under a frequency of 4 Hz. The minimum stress was approximately 4% of the UTS, while the maximum stress was between 32% and 45%. Janus et al. (2019) performed a study where they tested 15 GFRP bare bars. The stress ratio was 0.1, and the frequency was 4 Hz. The maximum stress ranged between 40% and 60% of the UTS. D'Antino et

al. (2022) performed a fatigue test on a bare GFRP bar for 5.1 million cycles, and the bar did not fail. The bar was stressed under approximately 20% of the UTS with a stress ratio of 0.1.

The fatigue data are separated into two groups. The first group is the GFRP bare bars tested in the air. The second group is the GFRP bars used as reinforcement in a concrete elements. The normal distribution method is then used on carbon (CFRP) and basalt (BFRP) fibre-reinforced polymers. Adimi et al. (2000) presented a new method for testing CFRP rebars encased in concrete prisms. They tested 14 rebars with a stress ratio of 0.1 and maximum stress ranging from 34.5% to 62.1% of the UTS. El Refai (2013) studied the durability and fatigue of GFRP, BFRP, and CFRP bars. Eighteen BFRP bars were tested under fatigue for unconditioned and conditioned specimens.

6.3 Fatigue models

For any material, the relationship between the number of cycles to failure and the applied stresses or strains is called the S–N curve, where S stands for the maximum stress (or strain), stress range, or stress amplitude, while N stands for the number of cycles to fatigue failure. If any statistical distribution is added to the S–N curve to give the probability of failure, the curve is named S-N-P.

Several equations are used to relate the stress (S) or strain (ε) with the number of cycles to failure (N). ASTM E739 (2015) mentioned Eq. 6.1 and Eq. 6.2.

$$\log N = A + B(S) \quad \text{or} \quad \log N = A + B(\varepsilon) \tag{6.1}$$

$$\log N = A + B\log(S) \quad \text{or} \quad \log N = A + B\log(\varepsilon) \tag{6.2}$$

Where S represents stress, ε is the strain, and A and B are parameters calibrated by the experimental data. The original form of the wear-out model is a factor of equivalent, maximum applied stress, residual strength, and the number of cycles. When assuming fatigue failure, Eq. 6.1 and Eq. 6.2 reduces to Eq. 6.3.

$$\sigma_e = \sigma_a * (1 - C + CN)^S \tag{6.3}$$

where σ_e is the effective static strength, σ_a is the maximum applied stress, N is the number of fatigue cycles to failure, and C and S are coefficients that measure the extent of the flat part and the slope of the S–N curve, respectively. For the case where $C > 1$, the S–N curve is steeper at the low-cyclic fatigue region, $C = 1$ means that the S–N curve is a line, and if $C < 1$, the S–N curve will flatten at the low-cyclic fatigue region. For $C = 1$, Eq. 6.3 becomes the traditional power law equation shown in Eq. 6.4.

$$S = A\,N^{B} \tag{6.4}$$

The difference between the power law equation Eq. 6.4 and the linear-logarithmic equation shown in Eq. 6.5 is elaborated by Noël (2019). The power law function can flatten to catch the low cyclic fatigue range, which makes it more suitable for describing composite materials (Noël 2019).

$$S = A\,ln(N) + B \tag{6.5}$$

ACI 440.3R (2012) refers to ASTM-E739 for drawing the S–N curve and defining the equations. After defining the S–N, the reliability bands of 95% are used to identify the range in which the failure can happen. For CSA S806 (2021), the S–N curve can be drawn between the log scale of the number of cycles to failure and the normal arithmetic scale of the maximum applied stress. The maximum applied stress can also be replaced by the stress range or stress amplitude.

6.4 Probabilistic fatigue models

Due to the wide scatter of data in fatigue tests, using deterministic equations is not preferred (Noël 2019). There is a need for statistical distributions to capture the variability of the tested data. Normal, log-normal, and Weibull distributions were used to explain the fatigue data. Each distribution model has different parameters that are calibrated by the experimental data. The normal distribution was used by Vassilopoulos and Keller (2011) at each stress level, while Schijve (1993) used the normal distribution function. The normal distribution function used to draw the S–N curves agreed with those drawn with the Weibull distribution model (Schijve 1993).

6.4.1 Log-normal distribution

ASTM E739 (2015) suggests the log-normal distribution to model the fatigue data. The main assumptions to apply the statistical analysis are as follows: (a) the fatigue life is related to a random

sample, (b) all run-outs or suspended tests are not used in the analysis, (c) the linear model shown in Eq. 6.6 describes the fatigue data, (d) two parameters, log-normal distribution, are used for the fatigue life model, and (e) a constant variance is assumed for the log-normal distribution.

$$logN = A + B\sigma \qquad logN = A + B\ log\sigma \tag{6.6}$$

where N is the number of cycles to failure, σ is the maximum applied stress, and A and B are the maximum likelihood estimators. ASTM E739–10, (2015) uses Eq. 6.7 to calculate the reliability band.

$$logN = A + B\sigma \pm \sqrt{2F_p}\hat{\mu}\left(\frac{1}{k} + \frac{(\sigma-\bar{\sigma})^2}{\sum(\sigma_i-\bar{\sigma})^2}\right)^{1/2} \tag{6.7}$$

where F_p is a reliability level coefficient, $\hat{\mu}$ is the variance, k is the number of specimens, and sigma is the average of the maximum applied stress. In this study, Eq. 6.7 is used to describe the fatigue data of the GFRP bars. The resulting S-N-P curve is shown in Fig. 6.1.

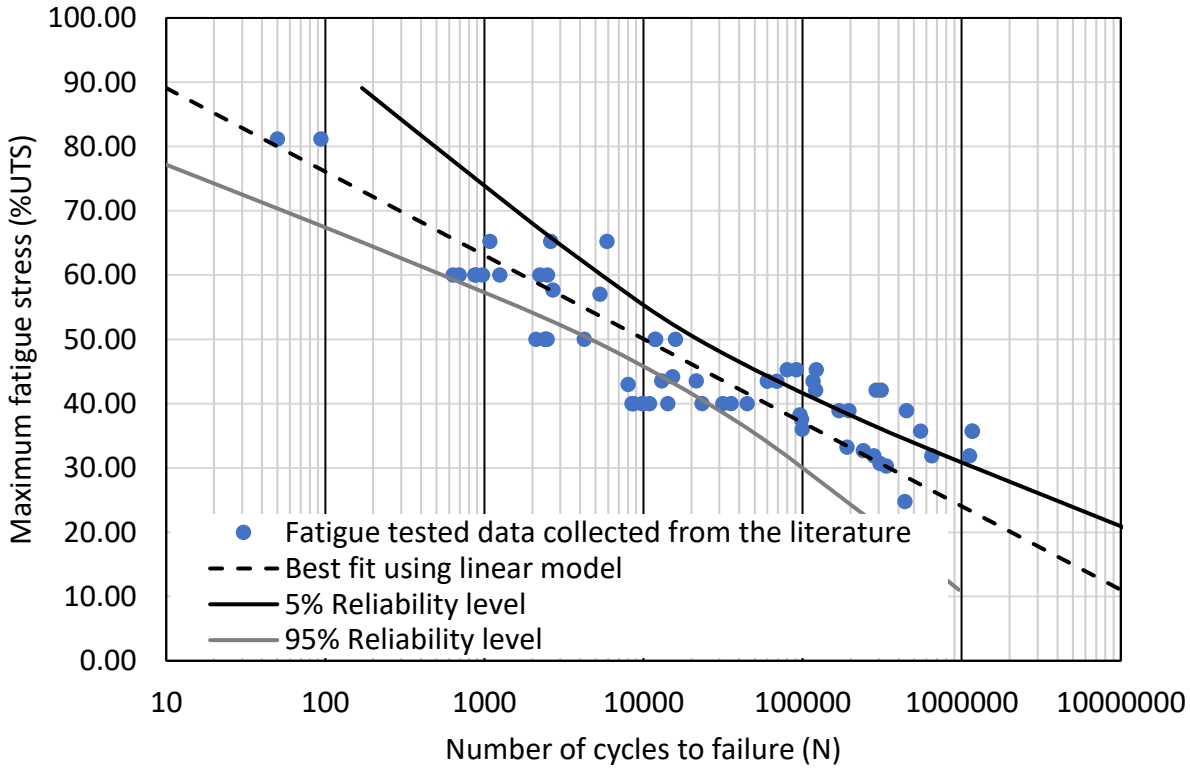

Fig. 6.1. S-N-P curve of GFRP bars (log-normal distribution)

It is evident from Fig. 6.1. that the log-normal distribution cannot describe the fatigue data of GFRP bars. As shown, there are several fatigue data points out of the 5 and 95% reliability ranges. The fatigue data do not follow the *F* distribution used in ASTM E739 (2015) because of the large variation. Thus, the assumption of the linear model is inaccurate based on ASTM E739 (2015), which can be solved by using a nonlinear model to describe the fatigue data. The nonlinear model is more complicated than the linear model, which will not be discussed because a simple model is the main target of this study.

To identify the reason for the scatter, the data were divided into two groups. The first group contained the fatigue test data of the GFRP bars tested under fatigue when embedded in concrete, while the second group was the bare bars fatigue tests. The S-N-P of the GFRP bars tested in concrete is shown in Fig. 6.2.

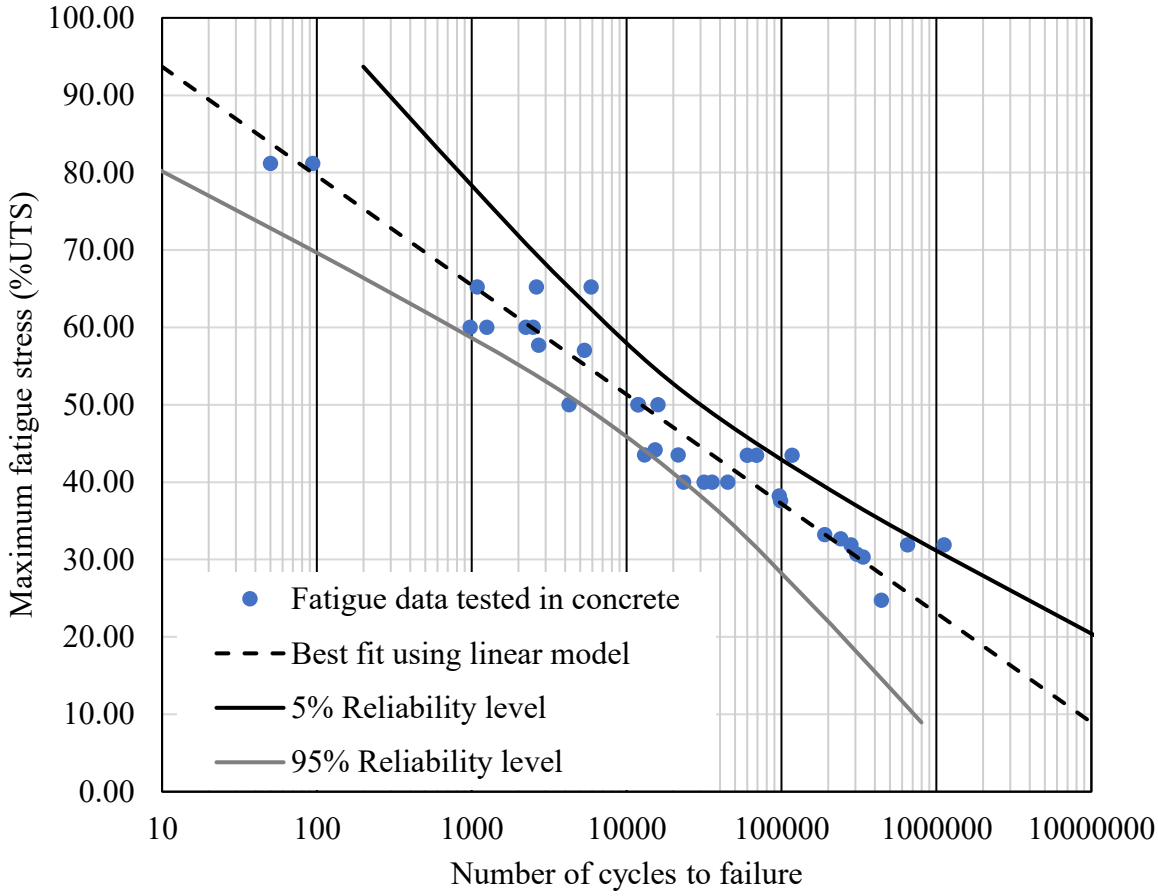

Fig. 6.2. S-N-P curve of GFRP bars tested in concrete (log-normal distribution).

As shown in Fig. 6.2, the log-normal distribution can describe the data well in the tested stress range. However, the model is inaccurate in the range outside the experimental data. The same procedure is applied to the fatigue data of the bare bars. Fig. 6.3 shows the resulting S-N-P curve. As shown, the log-normal distribution linear model could not model the GFRP bare bars fatigue data because of the large scatter.

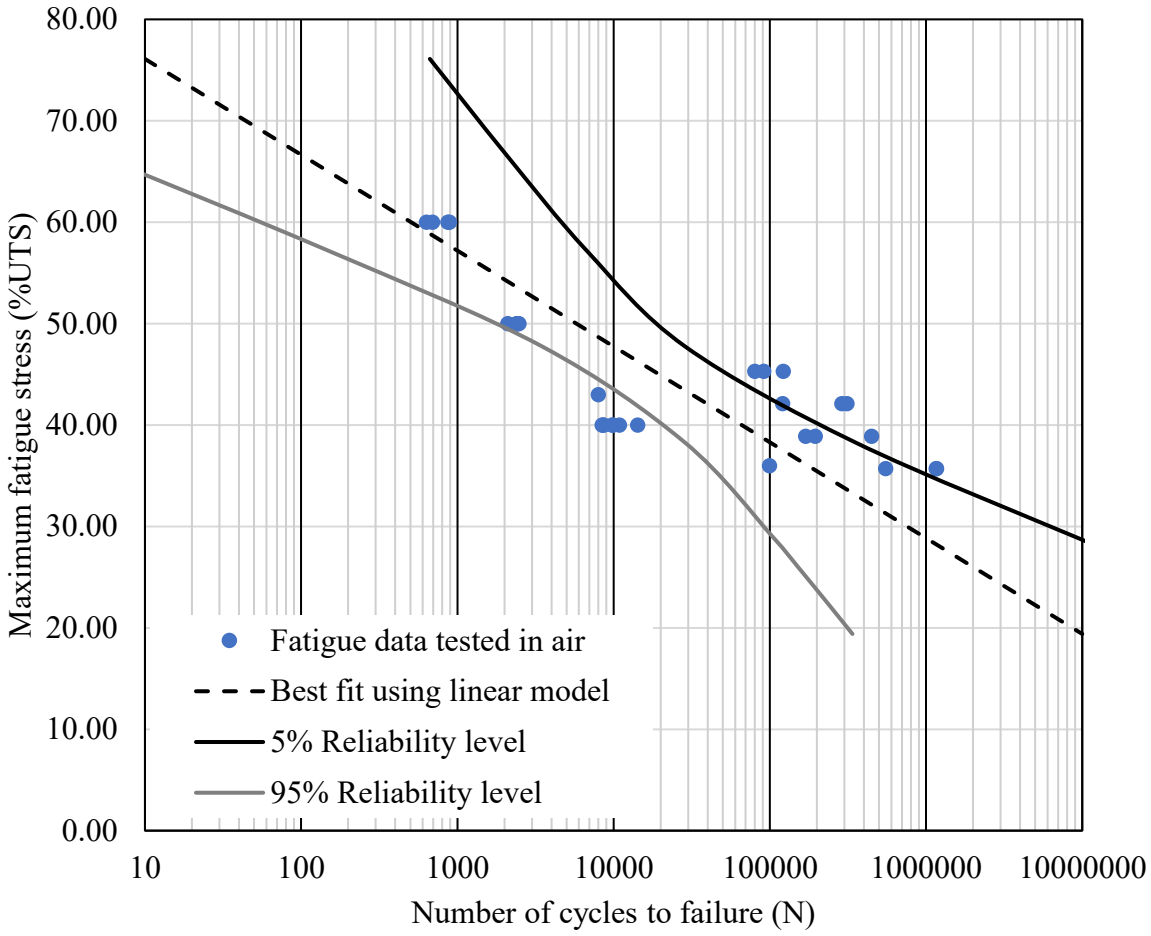

Fig. 6.3. S-N-P curve of GFRP bare bars (log-normal distribution).

6.4.2 Sendeckyj fatigue model

The Sendeckyj model is a fitting procedure for fatigue data using a probabilistic description (Sendeckyj 1981). This model is based on three main assumptions: (a) a deterministic equation should be able to describe the S–N behaviour of the data available, (b) the static strength is directly

related to the fatigue life, which means that the strongest specimen should have the longest fatigue life, and (c) the two-parameter Weibull distribution can describe the static strength data.

Three main steps are needed to fit the fatigue data. First, a deterministic equation is utilized to transform all fatigue data into equivalent static strength. Second, the two-parameter Weibull distribution is used to describe the equivalent static strength. The second step can use the maximum-likelihood estimates for the two Weibull distribution parameters. Finally, the first two steps are repeated until the maximum shape parameter of the Weibull distribution is reached.

Using the two-parameter Weibull equation, the S–N curve can be drawn for any reliability level using Eq. 6.8 and Eq. 6.9.

$$\sigma_a = \beta\{-\ln\big(P(N)\big)^{\frac{1}{\alpha}}\}[(N-A)C]^{-S} \tag{6.8}$$

$$A = -\frac{1-C}{\mathrm{C}} \tag{6.9}$$

where *P(N)* is the probability of survival after *N* cycles and α and β are Weibull distribution calibrated coefficients. Noël (2018, 2019) applied Sendeckyj equations and drew the 5 and 95% reliability level S–N curves for the data from Noël and Soudki (2014a). The model showed good agreement and described the fatigue data well.

In this study, the procedure to fit the fatigue data is applied to the fatigue data in the literature. The factors *S*, *C*, α, and β were 0.082, 0.3, 10.23, and 98.01, respectively. The resulting S-N-P curve is shown in Fig. 6.4. As shown, the Sendeckyj model can describe the fatigue data. Unlike the log-normal model, the large scattered data can be caught, giving wider variance.

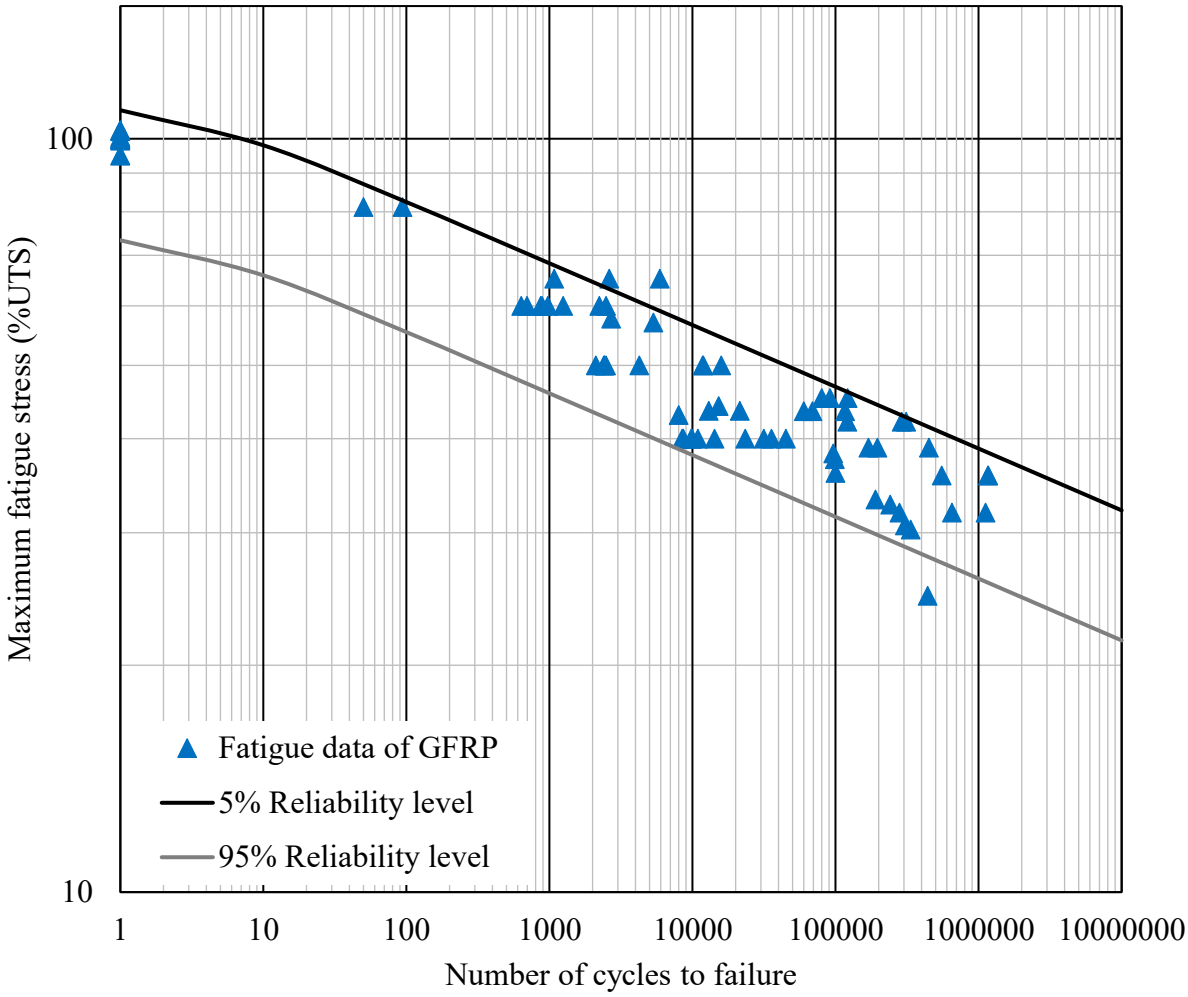

Fig. 6.4. S-N-P curve of GFRP bar in concrete and bare bars (Sendeckyj model).

6.5 The proposed normal distribution fatigue techniques

Similar to the normal distribution, the Weibull distribution can describe reliability levels for a data set. Although the Weibull distribution is much more flexible when modelling skewed data, the normal distribution is well-known and easy to apply in structural applications.

In order to simplify the procedure, the Sendeckyj model is used as a base, and the same technique is used but with a normal distribution. The main assumptions used are as follows: (a) the S–N data can be described with a deterministic equation, (b) fatigue life is directly proportional to the static strength of the specimens, and (c) normal distribution can describe the static strength of the tested samples.

6.5.1 Fitting fatigue data with a normal distribution

The proposed technique uses the normal distribution to fit the fatigue data for the lowest standard deviation (SD). Minimizing SD is equivalent to maximizing the shape parameter in the Weibull distribution.

The purpose of proposing the normal distribution is to reduce the number of iterations to reach the target reliability levels. In theory, the normal distribution can describe the static and effective stress data. There is no need to depend on the tested data to obtain the shape of the Weibull distribution, which might be skewed and does not represent a larger sample of data.

Using the wear-out model in Eq. 6.8, the tested fatigue data are used to calculate effective static data. The main difference is the application of different distribution methods to describe the effective stress data. The application of the Weibull and normal distributions is shown in Fig. 6.5.

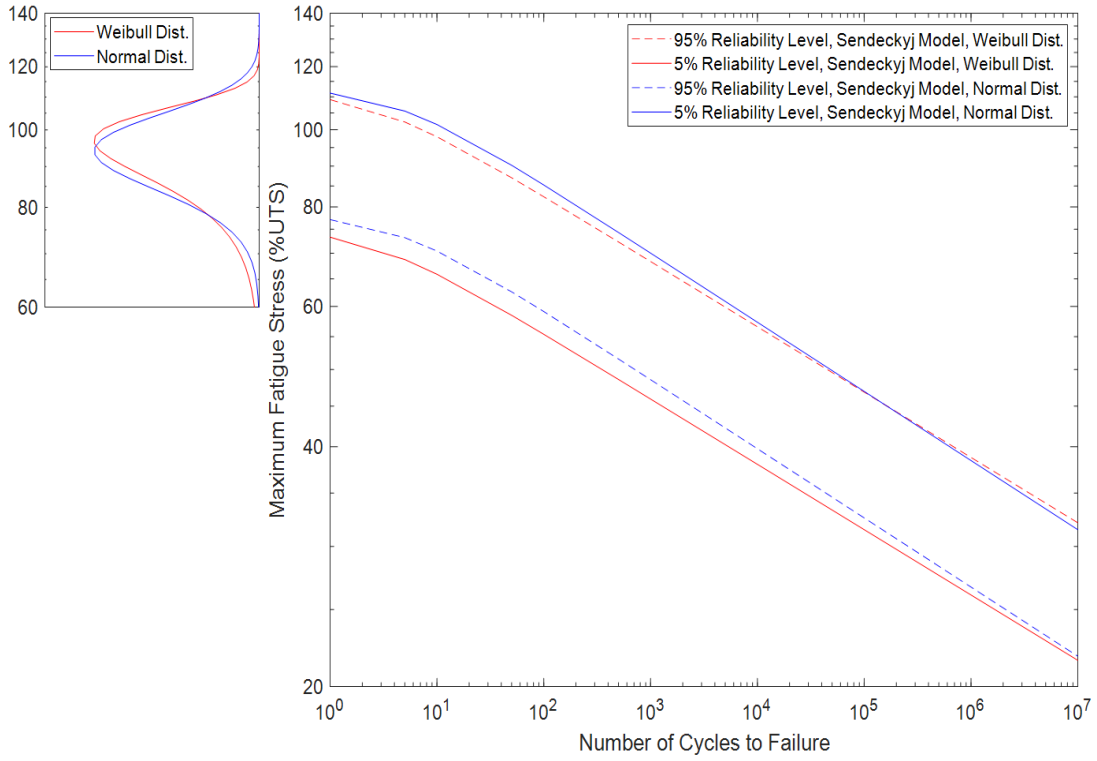

Fig. 6.5. *Application of Weibull and normal distribution on the effective static data of Sendeckyj model.*

The general procedure proposed to fit the fatigue data tested is as follows:

1- If more than a set of data needs to be fit, normalization can be used.
2- Assume values for *S* and *C* coefficients to be applied in Eq. 6.9. This is based on the wear-out model being used. The *C* coefficient is usually between 0 and 1 for GFRP.
3- Calculate the effective static stress for each data point.
4- Calculate the standard deviation of the normal distribution for the effective stresses calculated in step 3.
5- A trial and error procedure can be used on S and C parameters to reach the lowest standard deviation value.
6- The 95th percentile point can be calculated to identify the effective reliability stress (ERS), which can be calculated from the standard deviation.
7- The effective stress bands calculated for any reliability level can be used in Eq. 6.10 to obtain the S–N curve for any probability of failure.

$$\sigma_a = ERS * (1 - C + CN)^{-S} \tag{6.10}$$

6.5.2 GFRP reinforcing bars

The proposed procedure is used to draw the S-N-P with 95% reliability levels of the GFRP data available in the literature. The resulting S-N-P was drawn using the Sendeckyj model for comparison. After fitting the GFRP data with the Sendeckyj procedure, the factors *S*, *C*, α, and β equal 0.082, 0.3, 10.23, and 98.01, respectively. The S and C factors are equal to 0.086 and 0.21, respectively, when the data are fit using the normal distribution method proposed in this study. *S* values are relatively close, which means that the slope of the curves is almost the same. The *C* value of the Sendeckyj model is higher than that of the normal distribution method, which indicates that the flattened part in the normal distribution method is greater. The S-N-P for the overall GFRP fatigue data is drawn in Fig. 6.6.

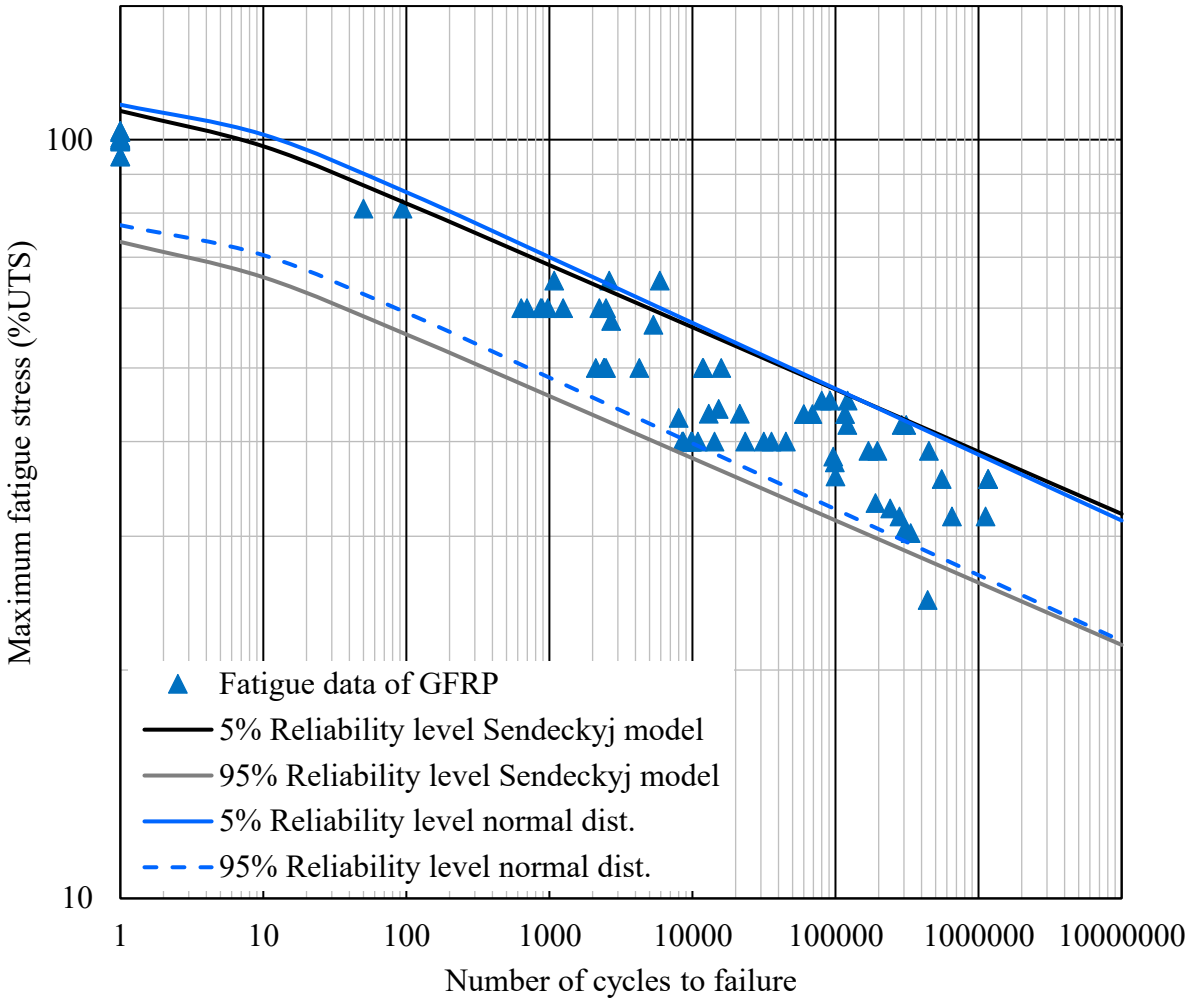

Fig. 6.6. S-N-P curve of GFRP bars in concrete and bare bars (proposed normal distribution method and Sendeckyj model).

As shown in Fig. 6.6, both proposed normal distribution methods for fitting the fatigue data, and the Sendeckyj model can describe the fatigue data well. Both techniques almost match the upper bounds for 5% reliability. In the lower bound, 95% reliability, however, the normal distribution assumes that the GFRP can withstand slightly higher stress under the same number of cycles. This shift is due to the shape of the normal distribution, which is symmetric, unlike the skewed shape of the Weibull distribution. Fig. 6.6 shows that the shifted 95% reliability did not include any more tested points, but it was close to the tested range.

To further analyze the data, the stress at which the GFRP has a 95% probability of failing before 2 million cycles (*P5*) and the stress at which the GFRP has a 5% (*P95*) probability of failure before 2 million cycles are extracted and shown in Table 6.1. .

Table 6.1. Maximum fatigue stress with 5% (P5) and 95% (P95) reliability for GFRP bar.

Distribution	P5 Max. stress	P95 Max. stress	P5/P95
	%UTS	%UTS	
Normal	36.2	25.1	1.44
Weibull	36.6	24.6	1.49

As shown in Table 6.1, the values for *P5* and *P95* are close. The Weibull distribution anticipates a 95% chance of specimen failure before 2 million cycles when tested under 36.6% of the UTS. This 36.6% is 0.4% higher than the normal distribution. According to the Weibull distribution, a specimen tested with stress of 24.6% of the UTS has a 5% chance that it will fail before 2 million cycles. The normal distribution predicted that 0.5% of the UTS had higher fatigue stress than the Weibull distribution. It can also be noticed that the normal distribution gives a lower *P5/P95*, which means a lower band difference.

The GFRP fatigue data are divided into two groups to check the efficiency of the proposed technique in describing different sets of data with different behaviours and parameters. The same comparison is made for the grouped fatigue tests performed in concrete and bare bars. Fitting the GFRP specimens tested in concrete with the Sendeckyj model resulted in the factors S, C, α, and β equal to 0.115, 0.033, 11.86, and 100.34, respectively. With the normal distribution method, the S and C factors equal 0.12 and 0.023, respectively. S and C are relatively equal, indicating similar slopes and flat regions. The difference will be in the bands calculated based on the different distributions. The GFRP bars tested in fatigue when encased in concrete are shown in Fig. 6.7.

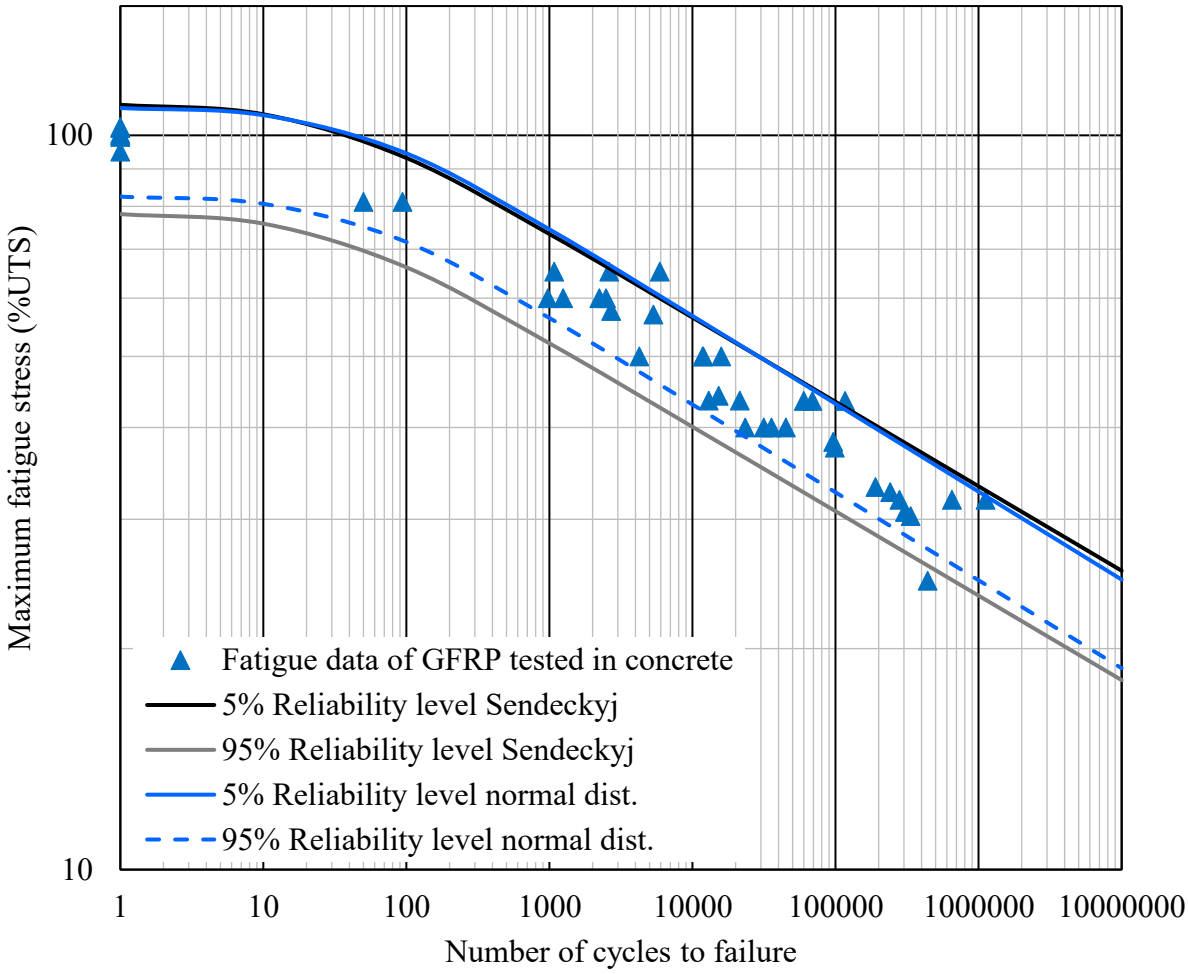

Fig. 6.7. The S-N-P curve of GFRP bars in concrete (the proposed normal distribution method and the Sendeckyj model).

Similar to Fig. 6.6, both models can describe the fatigue data well, as shown in Fig. 6.7. The same analysis can be concluded from both figures. There is a minimal difference in the 5% reliability level, which can be ignored. The 95% reliability level in a normal distribution is also shifted, giving less band range. P5, P95, and P5/P95 have reliability levels of 5% and 95%, and the ratio between them is shown in Table. 6.2.

Table 6.2. Maximum fatigue stress with 5% (P5) and 95% (P95) reliability for GFRP bars encased in concrete.

Distribution	P5 Max. stress	P95 Max. stress	P5/P95
	%UTS	%UTS	
Normal dist.	30.1	22.8	1.32
Weibull dist.	30.7	21.8	1.41

Table. 6.2 shows that the values of fatigue stress predicted by both Weibull and normal distributions are almost equal. There is a 0.6% UTS difference in the P5 value between the Weibull and normal distributions and a 1% UTS difference in P95. Similar to the GFRP overall data, the normal distribution offers lower reliability bands.

The GFRP bare bars are fit using the Sendeckyj model, resulting in the factors S, C, α, and β equal to 0.0725, 1, 12.66, and 96.93, respectively. The S and C factors calculated by the normal distribution method are equal to 0.0715 and 1, respectively. The C value in both curves equals 1, which means there is no flat part in the S–N curve, and the S–N is a line on the log scale. The S value in both curves is also very close, which means a close slope. For the fatigue tests of bare bars, the S-N-P is as shown in Fig. 6.8.

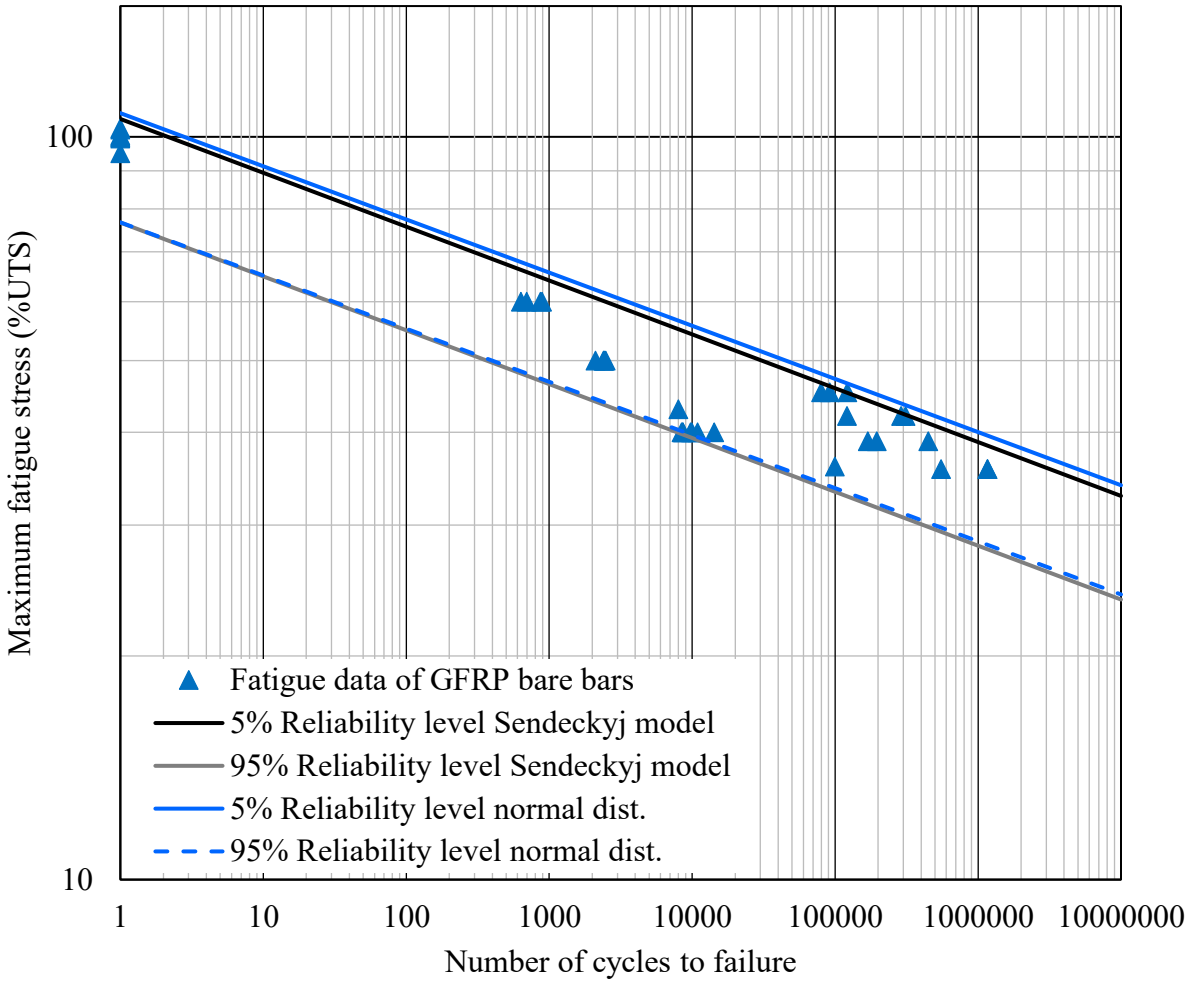

Fig. 6.8. *The S-N-P curve of GFRP bare bars (the proposed normal distribution method and the Sendeckyj model).*

In Fig. 6.8, it can be noted that the S–N curve does not flatten in the initial range. The S–N curve is fitted with a line on the log scale. The reason might be the large scatter of data, which might add over- or underestimated fatigue life data. It can also be noticed that the 95% reliability levels almost match. When describing this data set, the Weibull distribution did not have a skew in the distribution. 5% and 95% match with a minor difference using Weibull and normal distribution. The P5, P95 and P5/P95 are shown in Table. 6.3.

Table 6.3. Maximum fatigue stress with 5% (P5) and 95% (P95) reliability for GFRP bare bars.

Distribution	P5 Max. stress	P95 Max. stress	P5/P95
	%UTS	%UTS	
Normal dist.	38.1	27.2	1.4
Weibull dist.	36.9	26.8	1.38

In Table. 6.3, the difference in P5 is 1.2% of the UTS, while the difference is 0.3% of the UTS. The ratio between P5/P95 of the normal distribution is higher than that of the Weibull distribution. However, P5/P95 is almost equal.

6.5.3 CFRP reinforcing bars

Adimi et al. (2000) tested carbon fibre-reinforced polymer (CFRP) rods fully encased with concrete under tension-tension cyclic loading. Their experimental results suggested a maximum fatigue stress limit of 35% of the tensile strength with a stress ratio of 0.1 to reach a 4 million fatigue life cycle. Moreover, they concluded that the testing frequency considerably affects the results; the specimen life could decrease ten times if the frequency increased from 1 Hz to 5 Hz. This reduction in life was attributed to the high temperatures induced in the rebar at higher frequencies. Rahman and Kingsley (1997) concluded that the endurance limit of CFRP rebars could be reduced by increasing the mean stress and reducing the stress ratio.

The Sendeckyj model was applied to CFRP-tested specimens by Noël (2019). The factors S, C, α, and β equal 0.067, 2.7, 44.2, and 99.51, respectively. Factor C is equal to 2.7, which is larger than one which suggests that the S–N curve steepens at the low-cyclic fatigue region, as shown in Fig. 6.9. The behaviour with a steep curve has not been observed for composite materials (Sendeckyj 1981). The same samples were fit, but considering that the maximum value of C is 1, the resulting factors are S, C, α, and β, equal to 0.072, 1, 38.7, and 98.76, respectively.

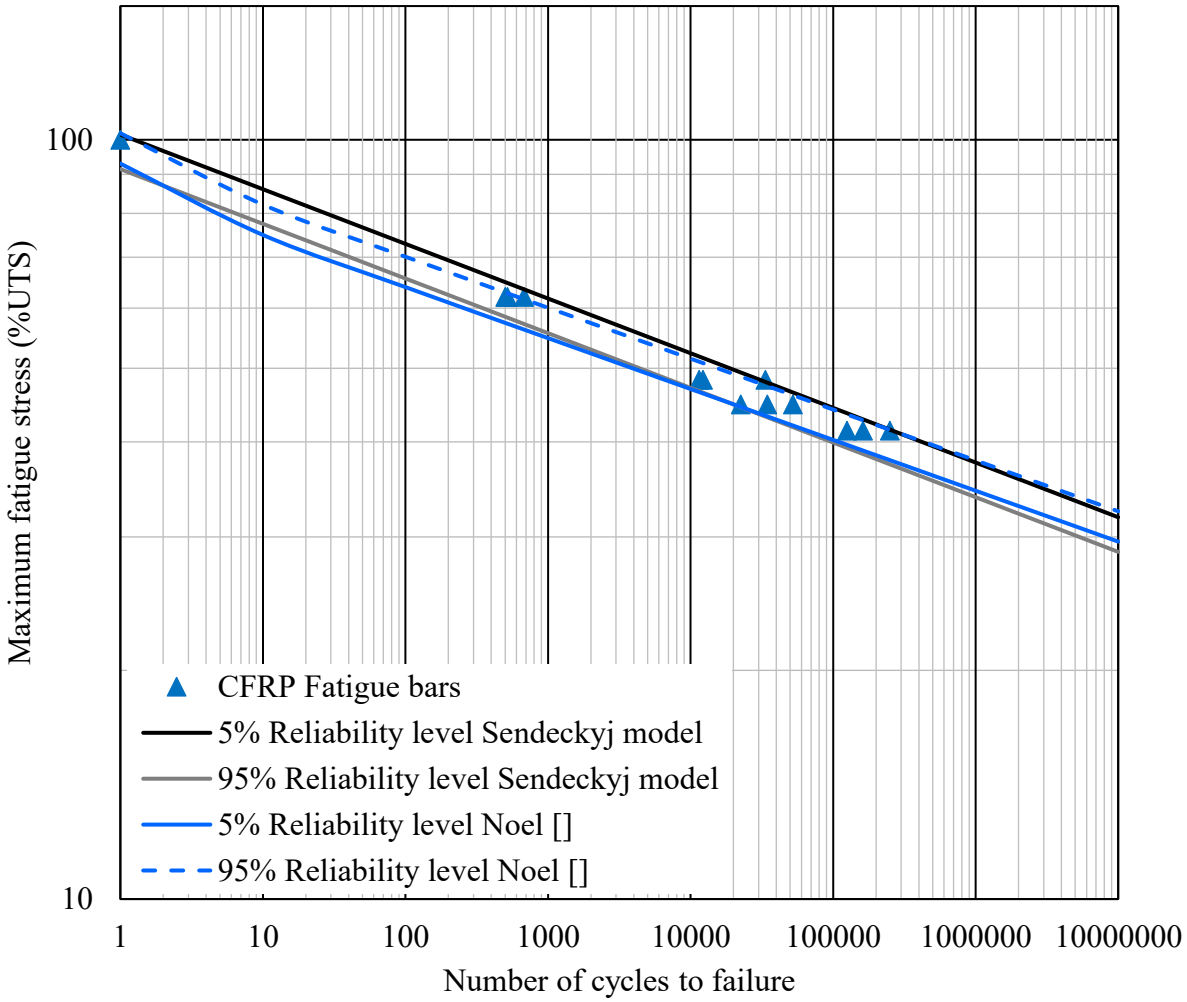

Fig. 6.9. *The S-N-P curve of CFRP rebar (Sendeckyj model).*

The proposed Sendeckyj model applies a normal distribution and describes the same CFRP rebars. S and C are 0.0725 and 1, respectively. The values of S calculated by the Sendeckyj model and normal distribution are close, and the C value is equal to 1. The two curves of the Sendeckyj model and normal distribution technique are shown in Fig. 6.10, with almost matching reliability levels.

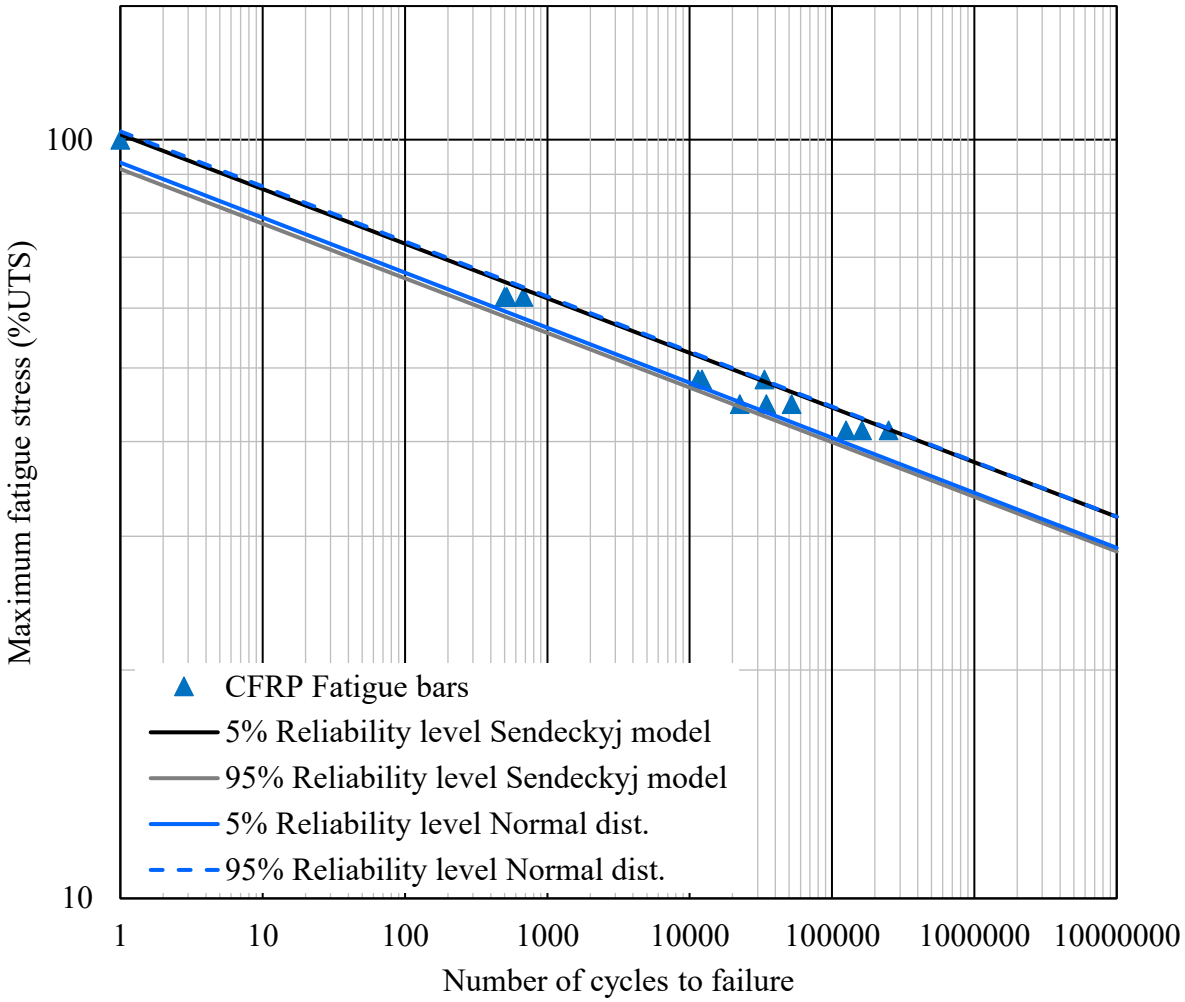

Fig. 6.10. *The S-N-P curve of CFRP rebar (the proposed normal distribution method and the Sendeckyj model).*

6.5.4 BFRP reinforcing bars

El Refai (2013) tested three groups of basalt fibre-reinforced polymers (BFRPs). One group consisted of unconditioned specimens, and the other two consisted of NaCl-conditioned specimens. In total, three static bars were tested, and eighteen fatigue-tested bars, seven of which were unconditioned, and the rest were NaCl-conditioned. The minimum stress was between 34% and 37% of the UTS. The maximum stress was between 38% and 49% of the UTS. All fatigue-tested bars failed to split either in the bar or in the anchor. The failure mode in the static bars was broom-shaped.

The fatigue results were used to draw the S-N-P curve. S, C, α, and β equal 0.066, 1, 20.76, and 97.86, respectively, for the Sendeckyj model parameters. The normal distributions S and C are 0.066 and 1, respectively. The resulting S-N-P is shown in Fig. 6.11.

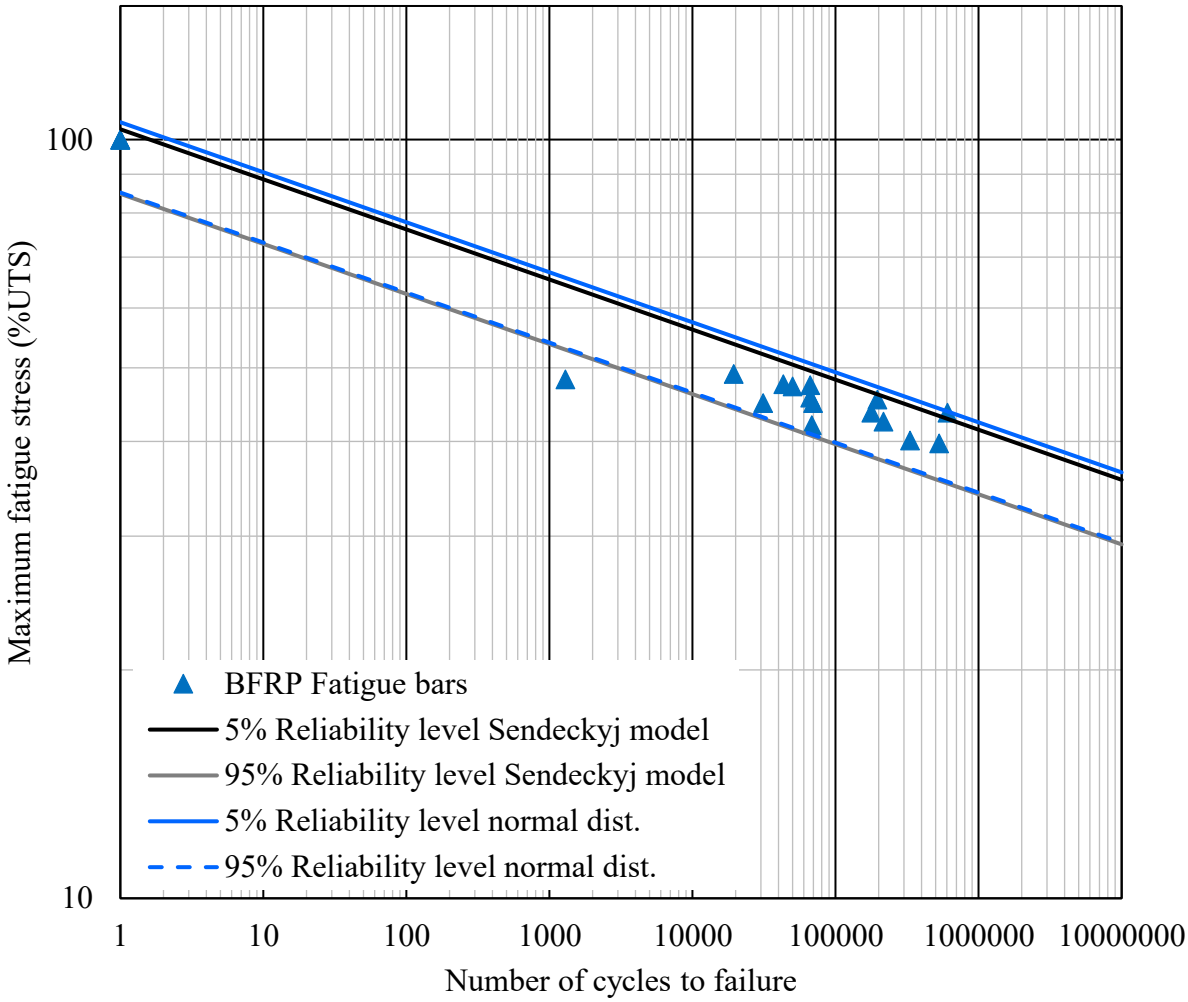

Fig. 6.11. *The S-N-P curve of BFRP bars (the proposed normal distribution method and the Sendeckyj model).*

The normal distribution shows a good fit to the data with small variation with the Weibull distribution. The skewed effect of the Weibull distribution is shown more at the 5% reliability level, while the 95% reliability levels almost match.

6.6 Conclusions

FRP composites are widely used in the structural field, which requires continuous research and improvements to the current studies. The fatigue life of FRP is essential to understand the behaviour of the material used in construction. Probabilistic fatigue models need to be introduced to obtain a better estimation of fatigue life. The probabilistic models describe the fatigue life with different probabilities of failure and reliability levels. This paper continues by discussing the work done before introducing probabilistic fatigue life models.

A new technique is illustrated and verified using a normal distribution instead of the Weibull distribution on the Sendeckyj model. The normal distribution is used widely in structural applications and can describe different types of tests. The technique shown is compared with the Sendeckyj model to better understand FRP fatigue behaviour. The resulting curves and analysis show that the normal distribution can describe the fatigue data. The results are close to those calculated using the Sendeckyj model. On the other hand, the procedure is simpler and less complex. The straightforward and easy procedure of applying the normal distribution can be used widely with efficient results.

The normalized fatigue data of the GFRP are used to draw the S-N-P curves with reliability levels of 5% and 95% using the Sendeckyj model with Weibull and normal distributions. The results showed a good fit, and a normal distribution can describe the fatigue results well. The separated data showed different results and behaviour, which shows the importance of continuing the fatigue tests in this field to study the effect of different parameters. Attempts have yet to be made to propose code limits for the codes due to the need to study many parameters not discussed in this research. The drawn S-N-P curves of the separated data of GFRP bars inside concrete elements and bare bars are discussed.

The fatigue life data of CFRP and BFRP are also shown and compared using normal and Weibull distributions. The results show a good match and that the normal distribution can fit any FRP composite data set.

CHAPTER 7

Summary and Conclusions

7.1 Summary

This study investigated the fatigue performance of concrete beams reinforced with ribbed GFRP bars. The experimental results reveal key insights into the cracking behaviour, deflection, and fatigue life of GFRP-RC beams. In addition, this research presents and discusses the results for 37 ribbed GFRP bars: 5 tested monotonically, 14 tested under low frequencies ranging from 0.03 to 0.04 Hz, 10 tested under a higher frequency of 4 Hz at a stress ratio of 0.1, 4 ribbed GFRP bars were tested with a stress ratio of 0.4, and 4 ribbed GFRP bars were tested at a stress ratio of 0.6. This is the first known study to investigate low-frequency testing and the first known study to investigate the effect of stress ratio on the fatigue life of ribbed GFRP bars. The results were used to establish the S-N curves for bars tested under low and higher frequencies. Additionally, the results were utilized to establish the S-N curves for the bars subjected to both different stress ratios.

The fatigue life of FRP is essential to understand the behaviour of the material used in construction. Probabilistic fatigue models need to be introduced to obtain a better estimation of fatigue life. The probabilistic models describe the fatigue life with different probabilities of failure and reliability levels. This study continues to discuss the work done before introducing probabilistic fatigue life models. Furthermore, a new methodology is demonstrated and validated by employing Normal distribution instead of the Weibull distribution for the Sendeckyj model. Normal distribution is commonly employed in structural applications and can be used to define several types of tests. The presented technique is compared to the Sendeckyj model to gain a deeper understanding of the fatigue behaviour of FRP materials.

7.2 Conclusions

- The displacement-control scheme, wherein the target forces are kept within the desired range, proved to be the most suitable for conducting the fatigue testing of GFRP RC beams. In contrast, the force-control scheme exhibited instabilities attributed to sudden changes in beam stiffness due to cracking during fatigue testing.

- The available GFRP codes and standards do not impose limits on the concrete compression stress under fatigue loading. However, the failure of beam B1-F-DC-35 in compression emphasizes the need to consider concrete stress limits for RC elements under fatigue loading. Although no concrete compression fatigue stress limit is observed in this study, further investigation is recommended.
- The ribbed GFRP bars used as reinforcement in the RC beams sustained 2 million cycles under maximum fatigue stresses of 30% and 35% at a stress ratio of 0.4. This suggests a potential for revising the fatigue stress limits recommended by AASHTO LRFD for GFRP and CSA S6-19. Further experimental data is required to confirm this conclusion for other types of GFRP bars available in the market.
- The ribbed GFRP bars used as reinforcement in the beams exhibited a higher fatigue life compared to other types reported in the literature. This difference could be attributed to the effect of surface profile, ribbed versus sand-coated, despite that stress ratio of 0.4 deviating from the more common 0.1 ratio found in the majority of available experimental data in the literature.
- Multiple trials have been undertaken to determine the most effective gripping system for enduring fatigue loading. From the results, it was shown that non-shrink grout outperformed other methods in sustaining fatigue loading and effectively transferring loads to the GFRP bars; out of 11 specimens tested with non-shrink grout, only one had premature failure, which was due to a power outage. In contrast, out of the 13 GFRP bars gripped with expansive grout or epoxy, 11 experienced premature failure, occurring either within or in close proximity to the grip.
- The fatigue testing results of the ribbed GFRP bars tested with a stress ratio of 0.1 are consistent with the findings of Noël and Soudki (2014) and surpass the findings of Janus et al. (2019). The variation can be ascribed to multiple factors, including but not limited to the gripping, grinding, bar diameter, mechanical properties, and surface configuration.
- Although performing fatigue tests at a stress ratio of 0.1 does offer conservative fatigue life for the GFRP bars, a more representative stress ratio that reflects the actual loading conditions of bridges and still can result in conservative fatigue life data is needed. This study recommends a stress ratio of 0.4 for the fatigue tests.

- Stress ratio does affect the fatigue life of the ribbed GFRP bars. Increasing the stress ratio from 0.1 to 0.4 or 0.6 can increase the fatigue life by more than one order of magnitude. The data suggests that the bars tested with a stress ratio of 0.6 have an average fatigue life that is roughly 4000% greater than the bars tested with a stress ratio of 0.1. Furthermore, the bars subjected to a stress ratio of 0.4 exhibit a much longer fatigue life compared to those subjected to a stress ratio of 0.1, with an approximate increase of 420%.
- Two equations were proposed limiting the fatigue stress range as a function of the minimum fatigue stress and the UTS. Both proposed equations present conservative fatigue limits, but they show higher fatigue limits than steel rebars.
- The low-frequency testing provided accurate and conservative values for fatigue design purposes. Most testing to date has been performed at significantly higher frequencies, but the good results achieved at low frequencies are attractive as they can be performed on standard universal testing machines and do not require specialized and expensive equipment.
- The modulus of elasticity remained relatively constant throughout the fatigue life, ranging between 2% and 3.5% higher than the statically measured modulus of elasticity. However, both the maximum and minimum strains increased progressively until failure. Specifically, bars H-NS-#4-35-S1, H-NS-#4-35-S2, H-NS-#4-50-S1, and H-NS-#4-50-S2 exhibited increases in maximum strain of 7.5%, 7.4%, 37%, and 3%, respectively.
- The Sendeckyj model effectively represents the data, enabling the calculation and presentation of stress levels needed to withstand one, two, and ten million cycles with reliability.
- A new technique is illustrated and verified using a normal distribution instead of the Weibull distribution on the Sendeckyj model. The normal distribution is used widely in structural applications and can describe different types of tests. The technique shown is compared with the Sendeckyj model to better understand FRP fatigue behaviour. The resulting curves and analysis show that the normal distribution can describe the fatigue data. The results are close to those calculated using the Sendeckyj model. On the other hand, the procedure is simpler and less complex. The straightforward and easy procedure of applying the normal distribution can be used widely with efficient results.
- The normalized fatigue data of the GFRP are used to draw the S-N-P curves with reliability levels of 5% and 95% using the Sendeckyj model with Weibull and normal distributions. The results showed a good fit, and a normal distribution can describe the fatigue results well. The

separated data showed different results and behaviour, which shows the importance of continuing the fatigue tests in this field to study the effect of different parameters. Attempts have yet to be made to propose code limits for the codes due to the need to study many parameters not discussed in this research. The drawn S-N-P curves of the separated data of GFRP bars inside concrete elements and bare bars are discussed.

7.3 Recommendations for future work

Despite the contribution made by this study, further research is recommended to investigate the effects of several other influential parameters, such as the GFRP bars surface types, stress ratio, stress range, surface type, bar diameter, fibre content, testing frequency, temperature, and presence of concrete on the fatigue life of GFRP bars.

References:

AASHTO LRFD. 2020. *American Association of State Highway and Transportation Officials LRFD Bridge Design Specifications*. *AASHTO*.

AASHTO LRFD for GFRP. 2018. "AASHTO LFRD Bridge Design Guide Specifications for GFRP-Reinforced Concrete." *AASHTO*.

Accornero, F., R. Cafarelli, and A. Carpinteri. 2021. "Cracking and Crushing in Prestressed Concrete Beams." *ACI Struct. J.*, 118 (2): 101–109. https://doi.org/10.14359/51728184.

Accornero, F., R. Cafarelli, and A. Carpinteri. 2022. "The cohesive/overlapping Crack Model for plain and RC beams: Scale effects on cracking and crushing failures." *Mag. Concr. Res.*, 74 (9): 433–450. https://doi.org/10.1680/jmacr.20.00260.

ACI 440.11. 2022. *Building Code Requirements for Structural Concrete Reinforced with Glass FiberReinforced Polymer (GFRP) Bars-Code and Commentary. ACI 440.11*. *ACI Comm. 440*.

ACI 440.1R. 2015a. "Guide for the Design and Construction of Structural Concrete Reinforced with Firber-Reinforced Polymer (FRP) Bars (ACI 440.1R-15)." *Am. Concr. Inst.* Farmington Hills, Michigan, USA: American Concrete Institute.

ACI 440.1R. 2015b. "Guide for the Design and Construction of Structural Concrete Reinforced with Fiber-Reinforced Polymer Bars. ACI 440.1R." *Am. Concr. Inst.* American Concrete Institute.

ACI 440.3R. 2012. "Guide Test Methods for Fiber-Reinforced Polymers (FRPs) for Reinforcing or Strengthening Concrete Structures. ACI 440.3R-12." *Am. Concr. Inst.* American Concrete Institute.

ACI PRC-215. 2021. "Concrete Structure Design for Fatigue Loading-Report. ACI PRC-215-21." *ACI PRC-215-21*. American Concrete Institute.

Adimi, M. R., A. H. Rahman, and B. Benmokrane. 1997. "Fatigue behaviour of GFRP bars embedded in concrete." *CSCE Annu. Conf.*, 121–130. Sherbrooke, Qu´ebec: Proc. Annu. Conf. Can. Soc. Civ. Eng.

Adimi, M. R., A. H. Rahman, and B. Benmokrane. 2000. "New Method for Testing Fiber-Reinforced Polymer Rods under Fatigue." *J. Compos. Constr.*, 4 (4): 206–213. https://doi.org/10.1061/(ASCE)1090-0268(2000)4:4(206).

Alsayed, S., Y. Al-Salloum, T. Almusallam, S. El-Gamal, and M. Aqel. 2012. "Performance of glass fiber reinforced polymer bars under elevated temperatures." *Compos. Part B Eng.*, 43 (5): 2265–2271. Elsevier. https://doi.org/10.1016/J.COMPOSITESB.2012.01.034.

ASTM-C39 / C39M. 2021. "Standard Test Method for Compressive Strength of Cylindrical Concrete. ASTM-C39 / C39M." *Annu B ASTM Stand 20211–8*. https://doi.org/https://doi.org/10.1520/ C0039.

ASTM C496 / C496M. 2017. "Standard Test Method for Splitting Tensile Strength of Cylindrical Concrete

Specimens. ASTM C496 / C496M-17." *ASTM Int 20171–5*. https://doi.org/https://doi.org/10.1520/mnl10881m.

ASTM C78 / C78M. 2021. "Standard Test Method for Flexural Strength of Concrete (Using Simple Beam with Third-Point Loading). ASTM C78 / C78M." *ASTM Int 20211–5*. https://doi.org/https://doi.org/10.1520/C0078.

ASTM D3479/D3479M. 2012. "Standard Test Method for Tension-Tension Fatigue of Polymer Matrix Composite Materials. ASTM D3479/D3479M." *Annu. B. ASTM Stand.*, 96 (August): 6. https://doi.org/10.1520/D3479.

ASTM D7205/D7205M. 2021. "Standard Test Method for Tensile Properties of Fiber Reinforced Polymer Matrix Composite Bars 1. ASTM D7205/D7205M." *ASTM Int.*

ASTM D7957/D7957M. 2017. "Standard Specification for Solid Round Glass Fiber Reinforced Polymer Bars for Concrete Reinforcement. ASTM D7957/D7957M." *ASTM Stand.* https://doi.org/10.1520/D7957.

ASTM E739. 2015. "Standard Practice for Statistical Analysis of Linear or Linearized Stress-Life (S-N) and Strain-Life (e-N) Fatigue Data. ASTM E739." *ASTM Int.*

Barbosa, J. F., J. A. F. O. Correia, R. C. S. Freire Júnior, S. P. Zhu, and A. M. P. De Jesus. 2019. "Probabilistic S-N fields based on statistical distributions applied to metallic and composite materials: State of the art." *Adv. Mech. Eng.*, 11 (8): 1–22. https://doi.org/10.1177/1687814019870395.

Collins, M. P., and M. Denis. 1997. *Prestressed Concrete Structures*. Response Publications.

CSA S6. 2017. *Canadian Highway Bridge Design Code (CSA-S6-14-4) Reprinted July 2017*. *Can. Stand. Assoc.*

CSA S6. 2019. "Canadian Highway Bridge Design Code (CSA S6-19)." *Can. Stand. Assoc.* Toronto, Ontario, Canada: CSA Group.

CSA S806. 2012. "Design and construction of building structures with fiber reinforced polymers (CSA S806-12)." *Can. Stand. Assoc.* Toronto, Ontario, Canada: Canadian Standards Association.

CSA S806. 2021. "Design and Construction of Building Structures with Fibre-Reinforced Polymers. CSA S806:12-R21." *Can. Stand. Assoc.* Canadian Standards Association.

CSA S807. 2010. "Specification for Fibre-Reinforced Polymers. CSA S807." *Can. Stand. Assoc.* Toronto, Ontario, Canada: CSA Group.

CSA S807. 2019. "Specification for Fibre-Reinforced Polymers (CSA S807-19)." *Can. Stand. Assoc.* Ontario, Canada: Canadian Standards Association.

D'Antino, T., M. A. Pisani, and C. Poggi. 2022. "Fatigue tensile testing of glass fiber-reinforced polymer reinforcing bars." *Constr. Build. Mater.*, 346 (June): 128395. Elsevier Ltd. https://doi.org/10.1016/j.conbuildmat.2022.128395.

Dineshkumar, R., and S. Ramkumar. 2020. “Review paper on fatigue behavior of reinforced concrete beams.” *Mater. Today Proc.*, 21: 19–23. Elsevier Ltd. https://doi.org/10.1016/j.matpr.2019.05.353.

El-Ragaby, A. 2007. “Fatigue Behaviour of Concrete Bridge Deck Slabs Reinforced with Glass FRP Bars.” Universite De Sherbrooke.

Elsayed Nagy, I., Asadian, A., and Galal, K. (2022). “Stiffness Degradation of GFRP Reinforced Concrete Beam Under High-Cyclic Fatigue Loading” SHMII-11 Annual Conf., Montreal, Quebec, Canada.

Elsayed Nagy, I., Asadian, A., and Galal, K. (2023). “Fatigue of Glass Fibre-Reinforced Polymer Rebars: A Review” AToMech1, Conf., Al Khobar, Saudi Arabia.

Elsayed Nagy, I., Asadian, A., and Galal, K. (2023). “Low-Cyclic Tension-Tension Fatigue Behaviour of GFRP Reinforcing Bars” CSCE Annual Conf., Moncton, New Brunswick, Canada.

Elsayed Nagy, I., Asadian, A., and Galal, K. (2023). “GFRP Reinforcing Bars Behaviour Under Low Cyclic Fatigue” ICSGE-16 Conf., Cairo, Egypt.

Elsayed Nagy, I., Asadian, A., and Galal, K. (2024). “The Behaviour of Ribbed GFRP Reinforced Concrete Beam Under Fatigue” CSCE Annual Conf., Niagara, Ontario, Canada.

Ibrahim, M., A. Asadian, and K. Galal. 2023. “A simplified approach for design of steel-GFRP hybrid reinforced concrete sections.” Eng. Struct., 278 (March). https://doi.org/10.1016/j.engstruct.2022.115352.

Janus, O., F. Girgle, V. Kostiha, J. Prokes, and P. Stepanek. 2021. “Fatigue Behaviour of GFRP Reinforced Beams.” *Solid State Phenom.*, 163–169. Trans Tech Publications Ltd.

Janus, O., F. Girgle, I. Rozsypalova, V. Kostiha, L. Bodnarova, P. Stepanek, and J. Prokes. 2019. “The Fatigue Behaviour of GFRP Bars - Experimental Study.” *Acta Polytech. CTU Proc.*, 38–47. Czech Technical University in Prague.

Kim, Y. J., Y. Ji, W. T. Jung, J. Y. Kang, and J. S. Park. 2022. “Load Factors for Residual Capacity of Bridges Strengthened with Carbon Fiber-Reinforced Polymer.” *ACI Struct. J.*, 119 (5): 17–29. https://doi.org/10.14359/51732988.

Kuttagola, I., M. H. Prashanth, and A. Kumar. 2023. “Numerical study on the behavior of RC beams by using GFRP bars as an alternate to steel bars.” *Mater. Today Proc.*, 88: 66–70. Elsevier Ltd. https://doi.org/10.1016/j.matpr.2023.04.579.

Mindess, S., J. F. Young, and D. Darwin. 2003. *Concrete*. Upper Saddle River. NJ.: Prentice Hall, Upper Saddle River (New Jersey).

Miner, M. A. 1945. “Cumulative Damage in Fatigue.” *J. Appl. Mech.*, 12 (3): A159–A164.

Mivehchi, H., and A. Varvani-Farahani. 2010. “The effect of temperature on fatigue strength and cumulative fatigue damage of FRP composites.” *Procedia Eng.*, 2 (1): 2011–2020. Elsevier. https://doi.org/10.1016/j.proeng.2010.03.216.

Noël, M. 2018. “Probabilistic Fatigue Life Modelling of FRP Composites.” *4th Brazilian Conf. Compos. Mater. Rio Janeiro*.

Noël, M. 2019. “Probabilistic fatigue life modelling of FRP composites for construction.” *Constr. Build. Mater.*, 206: 279–286. https://doi.org/10.1016/j.conbuildmat.2019.02.082.

Noël, M., and K. Soudki. 2014a. “Fatigue Behavior of GFRP Reinforcing Bars in Air and in Concrete.” *J. Compos. Constr.*, 18 (5): 04014006. American Society of Civil Engineers (ASCE). https://doi.org/10.1061/(ASCE)CC.1943-5614.0000468.

Noël, M., and K. Soudki. 2014b. “Shear behavior of post-tensioned FRP-reinforced concrete slabs under static and fatigue loading.” *Constr. Build. Mater.*, 69: 186–195. Elsevier. https://doi.org/10.1016/J.CONBUILDMAT.2014.07.066.

Nowak, A. S. 1999. “Calibration of LRFD Bridge Design Code.” *NCHRP Rep. 368, Transp. Res. Board, Washington, DC*, 218.

Rahman, A. H., and C. Y. Kingsley. 1997. “Fatigue Behaviour of a Fibre-Reinforced-Plastic Grid as Reinforcement for Concrete.” *First Int. Conf. Compos. Infrastruct.*, 427–439.

Ramakrishnan, V., and N. Jayaraman. 1993. “Mechanistically Based Fatigue-damage Evolution Model for Brittle Matrix Fibre-reinforced Composites.” *J. Mater. Sci.*, 28 (20): 5592–5602. https://doi.org/10.1007/BF00367835.

El Refai, A. 2013. “Durability and Fatigue of Basalt Fiber-Reinforced Polymer Bars Gripped with Steel Wedge Anchors.” *J. Compos. Constr.*, 17 (6): 1–11. https://doi.org/10.1061/(asce)cc.1943-5614.0000417.

Rossi, R. J. 2018. *Mathematical Statistics: An Introduction to Likelihood Based Inference*.

Schijve, J. 1993. “A Normal Distribution or a Weibull Distribution for Fatigue Lives.” *Fatigue Fract. Eng. Mater. Struct.*, 16 (8): 851–859.

Schijve, J. 2005. “Statistical Distribution Functions and Fatigue of Structures.” *Int. J. Fatigue*, 27 (9): 1031–1039. https://doi.org/10.1016/j.ijfatigue.2005.03.001.

Sendeckyj, G. P. 1981. “Fitting Models to Composite Materials Fatigue Data.” *ASTM STP 734*, 245–260. https://doi.org/10.1520/STP29314S.

Shirazi, A., and A. Varvani-Farahani. 2010. “A stiffness degradation based fatigue damage model for FRP composites of (0/θ) laminate systems.” *Appl. Compos. Mater.*, 17 (2): 137–150. https://doi.org/10.1007/s10443-009-9099-1.

Tilly, G. P. 1979. “Fatigue of Steel Reinforcement Bars in Concrete: a Review.” *Fatigue Fract. Eng. Mater. Struct.*, 2 (3): 251–268. https://doi.org/10.1111/j.1460-2695.1979.tb01084.x.

Vanhari, A. K., E. Fagan, and J. Goggins. 2022. “A novel estimation method for fitting fatigue data in the composite wearout model.” *Compos. Struct.*

Varvani-Farahani, A., and A. Shirazi. 2007. “A fatigue damage model for (0/90) FRP composites based on stiffness degradation of 0° and 90° composite plies.” *J. Reinf. Plast. Compos.*, 26 (13): 1319–1336. https://doi.org/10.1177/0731684407079771.

Vassilopoulos, A. P., and T. Keller. 2011. “Fatigue of Fiber-Reinforced Composites.” *Eng. Mater. Process. Springer-Verlag, London Ltd.*, 238.

Wu, F., and W. X. Yao. 2010. “A fatigue damage model of composite materials.” *Int. J. Fatigue*, 32 (1): 134–138. Elsevier Ltd. https://doi.org/10.1016/j.ijfatigue.2009.02.027.

Zhao, J., G. Li, Z. Wang, and X. L. Zhao. 2019. “Fatigue Behavior of Concrete Beams Reinforced with Glass- and Carbon-Fiber Reinforced Polymer (GFRP/CFRP) Bars after Exposure to Elevated Temperatures.” *Compos. Struct.*, 229: 111427. Elsevier Ltd. https://doi.org/10.1016/j.compstruct.2019.111427.

Appendix A

A.1 General

This appendix provides some additional information on the experimental process presented in chapters 3, 4, and 5 of the thesis. These procedures cover some construction procedures.

A.2 Construction of the concrete beams and testing setup

Fig. A.1 Typical GFRP cages for concrete beams

Fig. A.2 Typical formwork for the concrete beams

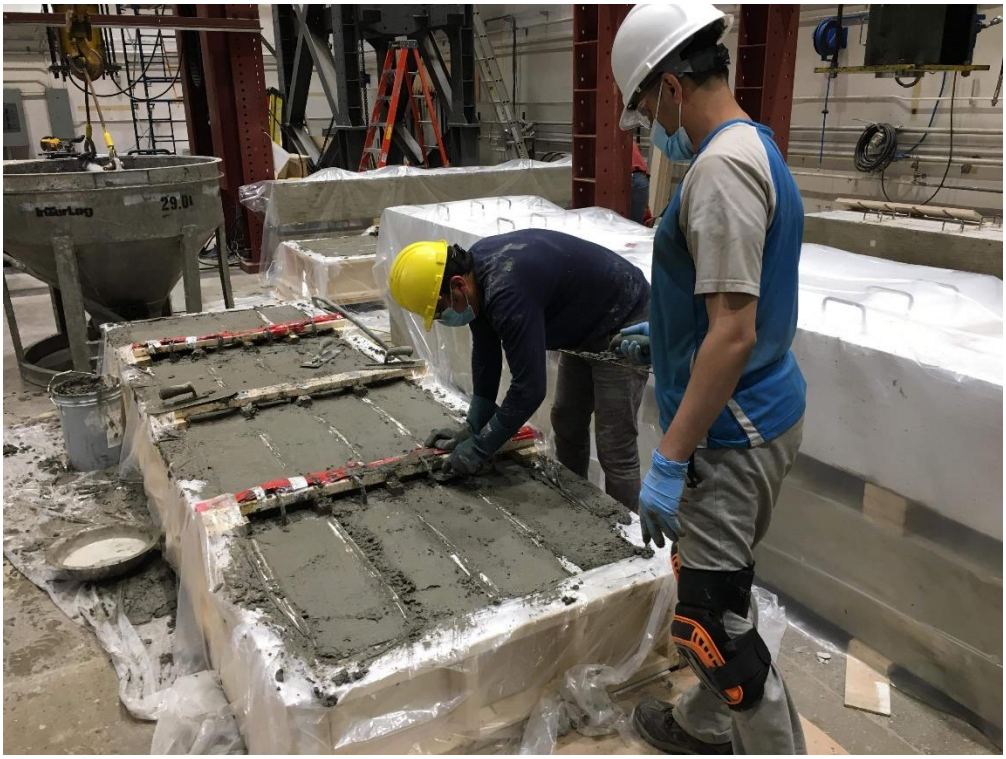

Fig. A.3 Finishing of the top concrete surface using trowels

Fig. A.4 Curing of the poured concrete

Fig. A.5 Construction of the testing frame

A.2 Pouring grout to grip the GFRP bars and testing GFRP bars under low cycle fatigue

Fig. A.6 Pouring grout to grip the GFRP bars.

Fig. A.7 Testing GFRP bar under low cycle fatigue